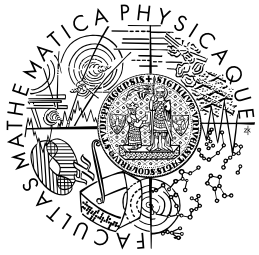

FACULTY
OF MATHEMATICS
AND PHYSICS
Charles University

DOCTORAL THESIS

Hana Jakoubková

Earthquake swarms in diverse tectonic environments: West Bohemia and Southwest Iceland

Department of Geophysics

Supervisor of the doctoral thesis: Ing. Josef Horálek, Csc.
Study programme: Physics
Study branch: Geophysics

Prague 2018

I declare that I carried out this doctoral thesis independently, and only with the cited sources, literature and other professional sources.

I understand that my work relates to the rights and obligations under the Act No. 121/2000 Sb., the Copyright Act, as amended, in particular the fact that the Charles University has the right to conclude a license agreement on the use of this work as a school work pursuant to Section 60 subsection 1 of the Copyright Act.

In Prague, May 22, 2018 .....

Acknowledgements

First of all I would like to thank my supervisor Josef Horálek for his consistent guidance, beneficial discussions and comments during the whole PhD. study. Further, I would like to thank all my colleagues from the Department of Seismology of the Institute of Geophysics CAS, namely Tomáš Fischer for many useful advices, Jana Doubravová for her taking care of WEBNET and REYKJANET database and putting the SeisMon package in commission, Alena Boušková for her help and support with processing WEBNET data, Václav Vavryčuk for specialized discussions, Bohuslav Růžek for discussions on event location, Zuzana Procházková and Martin Labuta for primary processing of the WEBNET and REYKJANET seismograms, and Jakub Klicpera, Petr Jedlička and Josef Kotek for keeping the WEBNET and REYKJANET seismic networks running in the best possible conditions. Last but not least, special thanks go to my family, especially to my husband, for his ability to create suitable conditions and extraordinary patience during the finalization of the thesis, and to my parents for their support during my studies.

The work was accomplished within the Grant Project P210–12–2336 of the Grant Agency of the Czech Republic, "Earthquake swarms and their triggering mechanisms in diverse tectonic environments (Bohemian Massif, Mid-Atlantic Ridge, Western Alps)." The monitoring system WEBNET providing earthquake data received considerable support from the Ministry of Education, Youth and Sport of the Czech Republic (Project LM201000), and the project LM2015079 CzechGeo/EPOS. The processing and management of the WEBNET data was supported by the project CzechGeo/EPOS-Sci (CZ.02.1.01/0.0/0.0/16_013/0001800) financed from Operational Programme Research, Development and Education.

Title: Earthquake swarms in diverse tectonic environments: West Bohemia and Southwest Iceland

Author: Hana Jakoubková

Department: Department of Geophysics

Supervisor: Ing. Josef Horálek, Csc., Institute of Geophysics CAS

Abstract: In my doctoral thesis I have investigated earthquake swarms from two completely different tectonic areas, West Bohemia/Vogtland and Southwest Iceland, with the aim of gaining a deeper insight into the nature of earthquake swarms in diverse tectonic environments. I analysed swarm-like activities from West Bohemia and Southwest Iceland from the perspective of statistical characteristics (magnitude-frequency distribution, interevent time distribution), seismic moment release, and space-time distribution of events. I found that the ratio of small to large events and the event rates are similar for all the activities in both areas, while the rate of the seismic moment release is significantly higher for the Southwest Icelandic swarms. Seismic moment released step by step is characterised for the West Bohemia swarms, whereas seismic moment released in one dominant short-term phase is typical of Southwest Icelandic earthquake swarms. All the West Bohemian swarms took place in a bounded focal zone Nový Kostel that is fairly complex, consisting of several fault segments. The Southwest Icelandic swarms are distributed at much larger area along the Mid Atlantic Ridge up to its branching in the Hengill triple junction, the individual swarms clearly reflect a tectonic structure of respective focal areas. I have concluded that most of the West Bohemia earthquake swarms were series of subswarms with one or more embedded mainshock-aftershock sequences, while the Southwest Iceland swarms, particularly those on the Reykjanes Peninsula, represent a transition between earthquake swarm and mainshock-aftershock sequence.

Keywords: earthquake swarms, West Bohemia/Vogtland, Southwest Iceland, mainshock-aftershock sequence, magnitude-time distribution, interevent time, seismic moment, earthquake localization, seismogenic tectonic fault

Název: Zemětřesné roje v různých tektonických prostředích: západní Čechy a jihozápadní Island

Autor: Hana Jakoubková

Katedra: Katedra Geofyziky MFF UK

Vedoucí: Ing. Josef Horálek, Csc., Geofyzikální ústav Akademie věd, v. v. i.

Abstrakt: Ve své doktorské práci jsem se zabývala zemětřesnými roji, které se vyskytují ve dvou tektonicky odlišných oblastech: v západních Čechách/Vogtlandu a na jihozápadním Islandu. Cílem mých výzkumů bylo hlubší pochopení samotné podstaty zemětřesných rojů, které vznikají v různých tektonických prostředích. Analyzovala jsem rojové aktivity ze západních Čech a jihozápadního Islandu z hlediska statistických charakteristik (magnitudo-četnostní rozložení, rozdělení mezijevových časů), uvolnění seismického momentu a časoprostorového rozložení ohnisek zemětřesení. Zjistila jsem, že rychlost, s jakou seismické jevy vznikají, a poměr výskytu slabých a silných seismických jevů jsou pro všechny analyzované zemětřesné aktivity ze západních Čech a jihozápadního Islandu stejné, zatímco rychlost uvolňování seismického momentu je v islandských rojích značně vyšší. Pro západočeské roje je charakteristické postupné uvolňování seismického momentu, kdežto v islandských rojích se seismický moment uvolňuje v jedné krátké hlavní fázi. Všechny západočeské zemětřesné roje se odehrály v jedné ohniskové zóně Nový Kostel, která sestává z několika různě orientovaných zlomů/zlomových segmentů. Islandské roje jsou lokalizované ve větší oblasti podél Středoatlantského hřbetu až k jeho rozvětvení v oblasti vulkanického komplexu Hengill. Jednotlivé roje zřetelně odrážejí tektonickou strukturu příslušných ohniskových oblastí. Na základě provedených analýz jsem dospěla k závěru, že zemětřesné roje v západních Čechách byly většinou řada dílčích rojů s jednou nebo několika fázemi typu hlavní otřes a série jeho dotřesů, zatímco roje na jihozápadním Islandu, zejména roje na poloostrově Reykjanes, reprezentují přechod mezi zemětřesným rojem a sekvencí hlavní otřes a jeho dotřesy.

Klíčová slova: zemětřesné roje, západní Čechy/Vogtland, jihozápadní Island, hlavní otřes - série dotřesů, magnitudo - četnostní rozdělení, časový odstup jednotlivých jevů, seismický moment, lokalizace zemětřesení, seismogenní tektonický zlom

Contents

Introduction

A seismic activity can be generally classified either as a common earthquake, called mainshock-aftershock sequence, or an earthquake swarm. In the mainshock-aftershock sequence a dominant earthquake (mainshock) is followed by a series of aftershocks with magnitudes usually by one or more magnitude units lower than that of the mainshock (Fig. 1a). An earthquake swarm is a series of earthquakes closely clustered in space and time, without a dominant event (Mogi, 1963). Similarly strong events occur throughout the whole swarm, several largest events are usually of similar magnitudes (Fig. 1b). The absence of a single dominant mainshock differentiates earthquake swarms from mainshock-aftershock sequences. The rate of swarm events usually varies a lot when compared with the rate of aftershocks in ordinary earthquakes; earthquake swarm activities are commonly composed of several phases of intense activity followed by periods of seismic calm, thus earthquake swarms are typically protracted, lasting for even several months.

Earthquake swarms occur worldwide both on the boundary of tectonic plates (interplate swarms) and inside plates (intraplate swarms). They are mostly related to volcanic areas (Hill, 1977; Pedersen et al., 2007; Farrell et al., 2009), geothermal fields and ocean ridges (e.g. Wyss et al., 1997; Lees, 1998). Quite frequent earthquake swarms occur in the Yellowstone volcanic field in the western United States, or in several areas in Japan. Other examples of swarm areas are Hawaiian Islands, Alaska, New Zealand and Canary Islands. The most intense interplate earthquake swarms in Europe occur probably in Iceland which is the onshore part of the mid-Atlantic plate boundary between the North America and Eurasia Plates. Further examples of European earthquake swarm areas somehow connected with the plate or microplate boundaries are few areas in Greece, western Alps (Ubaye valley), and also a few areas in Apennines. Intraplate earthquake swarms occur mainly in Quaternary-volcanism areas, which are often characterised by other phenomena as diffuse degassing or geothermal anomalies. A typical European intraplate swarm area is the western part of the Bohemian Massif (called the West Bohemia/Vogtland region), which is probably the most active intraplate earthquake swarm area in Europe.

Earthquake swarms are mostly originated in the Earth's crust. According to Horálek et al. (2015), depths of both interplate and intraplate swarm events range approximately between 2 and 20 km with the majority of around 10 km and shallower. The swarm earthquakes are usually of magnitudes $M < 5$, only occasionally reaching or exceeding $M \approx 6$ (e.g. volcanic earthquake swarm $M_{wmax}6.4$ on Miyakejima in Japan in 2000; Minson et al., 2007). Therefore, an amount of seismic energy released in earthquake swarms globally represents only a small fraction of that released in ordinary tectonic earthquakes.

Earthquake swarms have usually been considered to be an "exceptional phenomena" which differ from ordinary earthquakes at plate boundaries. It is assumed that a mainshock is triggered by plate motion loading and aftershocks are a consequence of stress redistribution after the mainshock. However, there is no such common knowledge of the origins of earthquake swarms yet. Prevalent hypotheses relate swarm-like activities to immediate influence of magma or crustal

fluids (e.g., intrusion to the fault). Accordingly, Hill (1977) proposed a model for volcanic earthquake swarms, and Yamashita (1999) created a model based on the interaction between the rupture process and migration of fluids. However, it should be noted that today the term earthquake swarm covers a wider range of seismicity all around the world and no particular characteristics being common for all of them are specified (e.g., Vidale and Shearer, 2006). Earthquake swarms in diverse tectonic environments in the world have been investigated by e.g., Pedersen et al. (2007), Hensch et al. (2008), Farrell et al. (2009), Kato et al. (2010), Daniel et al. (2011), Yukutake et al. (2011), Hainzl et al. (2012), Fischer et al. (2014) and Thouvenot et al. (2016).

The West Bohemia/Vogtland region is one of the best investigated earthquake swarm areas in the world. Earthquake swarms have been well documented since the beginning of the 19th century. I would note that the term "Erdbebenschwarm" (earthquake swarm) was very likely introduced by Credner (1876) and Knett (1899) who described the earthquake activity in West Bohemia and Vogtland in 1875 and 1824, respectively. A new stage of seismological observations based on continuous local observations was initiated by the M_L4.6 earthquake swarm in 1985/86. Since then the West Bohemia/Vogtland earthquake swarms have been thoroughly studied from various perspectives: the space-time distribution of events and the fault geometry in this zone (e.g., Fischer and Horálek, 2003; Horálek and Fischer, 2010; Fischer et al., 2010; Bouchaala et al., 2013; Čermáková and Horálek, 2015; Jakoubková et al., 2017); source mechanisms and stress field (Horálek et al., 2002; Vavryčuk, 2002, 2011; Horálek and Šílený, 2013); triggering mechanisms and driving forces (Hainzl, 2004; Hainzl and Ogata, 2005; Fischer and Horálek, 2005; Hainzl et al., 2012, 2016). Majority of the results has been summarised in Fischer et al. (2014).

In my doctoral thesis I utilise the results of the previous studies and analyse in detail recent West Bohemia earthquake activities in 2011, 2014 and 2017 together with interplate earthquake swarms from three tectonically different areas in Southwest Iceland lying on the boundary of two diverging tectonic plates. The aim of this thesis is better understanding of the nature of earthquake swarms in diverse tectonic environments.

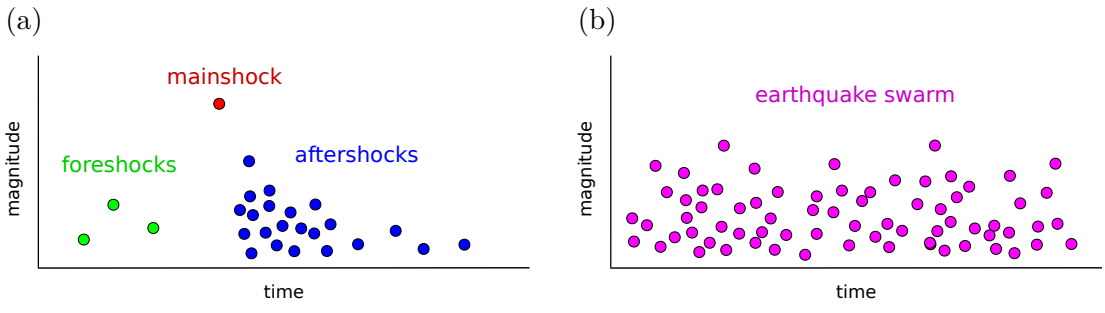

Figure 1: Schematic magnitude-time distribution of events in case of mainshock-aftershock sequence (a) and earthquake swarm (b). In (a), *red dot* - mainshock, *green dots* - foreshocks, *blue dots* - aftershocks. *Violet dots* in (b) - swarm-like events.

1. The areas of interest

1.1 West Bohemia/Vogtland region

West Bohemia/Vogtland (latitude $\approx 49.8-50.7$°N, longitude $\approx 12-13$°E) is well known for its geodynamic activity. Particularly, periodically recurring intraplate earthquake swarms and enormous emanations of CO_2 are the most striking features of the region which are usually attributed to subsiding Quaternary volcanism. The region is located in the western part of the Bohemian Massif, where three Variscan tectonic units: the Saxothuringian, the Teplá-Barrandian and the Moldanubian, merge (Bankwitz et al., 2003; Babuška et al., 2007). The West Bohemia/Vogtland region corresponds geographically to a border area of West Bohemia, SE Saxony and NW Bavaria roughly delimited by towns of Kraslice, Sokolov, Mariánské Lázně and Cheb on the Czech side, and Plauen, Selb and Marktredwitz on the German side (Fig. 1.1). The region is intersected by an NE-SW trending neotectonic structure, the Eger rift, and by the NNW-SSE striking Mariánské Lázně fault (ML fault, see Fig. 1.1). Another N-S trending fault system (so called Počátky-Plesná zone) was reported by Bankwitz et al. (2003).

In the Quaternary the region was affected by active volcanism which is nowadays manifested by two extinct volcanoes Komorní Hůrka and Železná Hůrka (estimated age 0.3 Ma, the latter maybe younger; Wagner et al., 2002) located only about 15 and 25 km apart from the main epicentral zone, and by two maar structures (Mrlina et al., 2009). Relating observable phenomena are crustal fluids represented by CO_2 degassing fields along the tectonic fault zones (e.g. Hartoušov, Soos) and numerous mineral springs. A source of the fluids is unknown, nevertheless it is believed that CO_2 is of a magmatic origin somewhere in depths between 30 and 50 km (Fischer et al., 2017).

In terms of seismicity, the West Bohemia/Vogtland region belongs to the N-S trending Leipzig-Regensburg seismoactive zone (see Fig. 2 in Korn et al., 2008). Earthquake swarms in the region in question have been well documented since the beginning of the 19th century. A significant increase of earthquake activity was observed at the turn of the 19th and 20th century when several larger swarms were observed by the local people. There were the earthquake swarms of 1897, 1900, 1903 and 1908. The only historical swarm with seismograph records of sufficient quality is that of 1908 having the strongest macroseismic observations corresponding to estimated intensity $I_0 = 7°$ MSK-64 (Leydecker, 2011). The swarm of 1908 was the strongest activity in the 20th century with $M_{Lmax} \approx 5$. Then, in the course of the 20th century, seismicity in West Bohemia/Vogtland was rather weak, only three more significant swarms with magnitudes $M_L < 3$ occurred in 1927, 1936/37 and 1962 (Neunhöfer and Meier, 2004; Neunhöfer and Hemmann, 2005).

Quite long, seismically calm period in the region was interrupted in 1985/86 when strong earthquake swarm with two fairly strong shocks having magnitudes of M_L4.6 and 4.2 hit the area. Macroseismic effects of the M_L4.6 event reached intensities $I_0 = 6°$ to $7°$ MSK-64 (Leydecker, 2011). This swarm represents a new revival of intense swarm activity and also initiation of a new stage of seismic observations and investigations in the region in question. Seismological, geologi-

cal, gas-hydrological and geodetic investigations have been in progress since the beginning of the nineties of the last century. Czech scientists in cooperation with German scientists carried out research based on continuous observations or regular measurements, particularly the seismic ones.

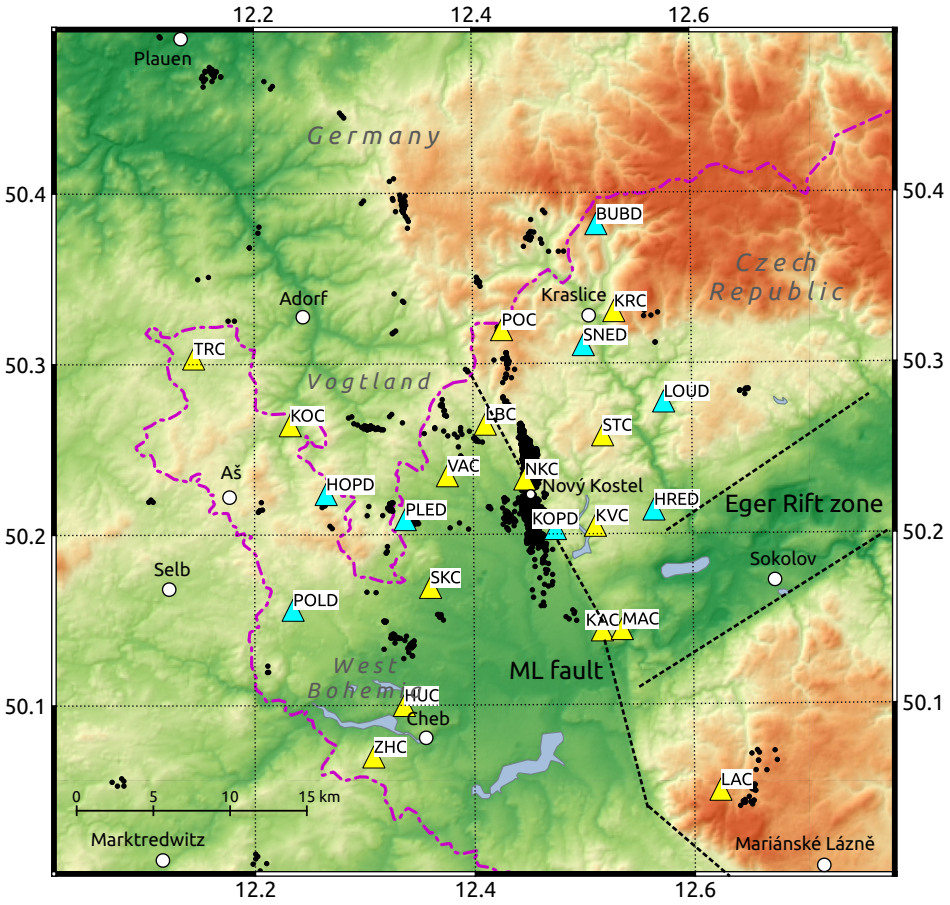

Figure 1.1: Map of the seismically active area in the West Bohemia/Vogtland region with stations of the WEBNET network. *Yellow triangles* - online stations, *light blue triangles* - offline stations. *Black dots* - seismic events of $M_L \geq 0$ from the time period 1997-2017. *Larger white circles* - towns. *Smaller white circle* - village of Nový Kostel. *Dashed lines* mark dominant tectonic structures in the region: the Mariánské-Lázně fault (ML) and the Eger Rift zone. *Dot-dashed violet line* denotes the Czech-German border. Note that station NKC is located in the middle of the main epicentral area of Nový Kostel (NK).

1.1.1 Local seismic network WEBNET

Practically immediately after ceasing of the 1985/86 swarm, a permanent digital station NKC was established just in the epicentral area of the swarm nearby the village of Nový Kostel (in 1986). In 1989 an analogue one-component station SKC (Skalná) was installed, upgraded to a digital station in 1994. The WEBNET network (WEBNET, 1991) has been operated since 1991 starting with four stations (NKC, KOC, KRC and LAC) having a telemetric transfer of data. The network was gradually complemented to the existing net of 23 stations covering an area of about 900 km^2 (Fig. 1.1). The network layout ensures a proper areal

and azimuthal coverage of the focal area, particularly with respect to the main focal zone Nový Kostel.

Currently, WEBNET consists of two subnets: (a) 15 broadband (BB) stations connected via Internet, and (b) 8 short period (SP) stations being autonomous ones. Stations of subnet (a) were originally equipped with passive seismometers SM-3 ($T_0 = 2\,\mathrm{s}$), and the Janus-Trident (by Nanometrics) or 5800 PCM data-acquisition systems. In 2015, these instruments were replaced by up-to-date BB seismometers CMG-3ESPC ($T_0 = 30\,\mathrm{s}$) by Guralp and new data-acquisition systems Centaur by Nanometrics. Hence, seismograms from these stations are proportional to the ground velocity in a frequency band of 0.5–80 Hz in the period 1992 to 2015, and 0.03–80 Hz since 2015. Stations of subnet (b) were established in 2001. They are equipped with the LE-3D Lite sensors ($T_0 = 1\,\mathrm{s}$) and data-acquisition systems Gaia (by VISTEC). The frequency response of these stations is proportional to the ground velocity in a band of 1.0–80 Hz. A storage capacity of the Gaia acquisition systems is about ten months, data are downloaded once in two months.

Subnets (a) and (b) have produced continual recordings since 2014, previously they operated in a triggered mode. The dynamic range of all the WEBNET stations is higher than 120 dB, the sampling rate of 250 Hz has been used for whole the observation period. The configuration and parameters of the WEBNET stations together with low seismic noise at the individual stations (Fischer and Bachura, 2014) guarantee high-quality recording of local events with local magnitudes $-0.5 \leq M_L \leq 5$ (magnitude of completeness $M_C = 0.5$).

1.1.2 Brief characteristics of the swarm-like seismicity in the region in the past years

The twenty-five-year observation showed that seismicity in the region is permanent, largely of swarm-like character on the micro-earthquake level. The seismic activity is typically of an episodic character with magnitudes M_L mostly lower than 4.0; stronger events are rather exceptional. Events are scattered within an area of about 3500 km^2 and several focal zones can be distinguished. Fig. 1.1 shows the distribution of hypocenters of events with magnitudes $M_L \geq 0$ from

Activity	Duration [days]	Num. of ev. ($M_L \geq 0$)	M_{Lmax}	Character	Num. of phases
1997	14	500	3.0	swarm	4
2000	71	3840	3.3	swarm	9
2008	28	4400	3.8	swarm	9
2011	12	5740	3.7	swarm	5
2013	33	270	2.3	mini-swarm	3
2014	12	2800	4.4	M-A sequence	3
2017	16	2500	3.1	swarm	3

Table 1.1: Basic characteristics of the West Bohemian activities. Duration of each activity indicates number of days during which 90% of events, which were recorded within three months, occurred.

the period of 1997–2015. It illustrates that the events largely cluster in seven focal zones which were already delineated by Horálek et al. (2000a). Seismicity in the region is relatively shallow having focal depths between 6 and 15 km; foci with a depth larger than 20 km are rather rare (Horálek and Fischer, 2010).

However, all larger swarms ($\sim M_L > 2.5$) are located in the focal zone Nový Kostel (NK) which dominates the seismicity of the whole region. According to rough estimations the NK zone accounts more than 90% of the total seismic moment released in the whole region in the past years (e.g., Horálek and Fischer, 2010; Fischer et al., 2014). Beside numerous microswarms ($M_L \leq 2.0$) all earthquake swarms which appeared after the 1985/86 activity were located in this zone. Notable swarms occurred there in 1997 (M_L3.0), 2000 (M_L3.3), 2008 (M_L3.8), 2011 (M_L3.7), 2013 (M_L2.3) and 2017 (M_L3.1). An exceptional non-swarm activity comprising three clearly separated earthquakes with magnitudes M_L 3.5, 4.4 and 3.6 occurred in 2014. A quite frequent recurrence of relatively intense seismic unrests starting with the 1985/86 swarm represents an extraordinary period of enhanced seismic activity in the West Bohemia/Vogtland region, especially in the NK zone, in the last 100 years. Brief characteristics of all significant seismic activities that have occurred in the NK zone since 1991 (beginning of the WEBNET observations) are given in Tab. 1.1.

1.2 Iceland - brief characteristics

Iceland is a volcanic island in the North Atlantic Ocean spanning a divergent Mid-Atlantic Ridge boundary between the Eurasian and North American tectonic plates. The Mid-Atlantic Ridge (MAR) is in fact a long (16000 km) and extensive submarine mountain range formed by plate tectonics. There are only a few places on the Earth where the MAR extends above sea level in the form of volcanic islands, Iceland is the largest island of such origin.

It is generally accepted that Iceland lies above a hotspot, the Iceland plume, which is partly responsible for the high volcanic activity and also has formed Iceland itself (Allen et al., 1999, 2002b,a). The interaction between the Iceland plume and the MAR has formed complex rifting zones and a series of volcanic and seismic transform zones that have developed over time. The MAR emerges on the surface at the southwest tip of the Reykjanes Peninsula (RP) and continues to the Hengill triple junction where it branches into the Western Volcanic Zone (WVZ) and South Iceland Seismic Zone (SISZ). Then it runs along the Eastern Volcanic Zone (EVZ) and the Northern Volcanic Zone (NVZ) to the northern coast of Iceland. Here, at the Tjörnes Fracture Zone (TFZ) the MAR leaves Iceland (Fig. 1.2) (Einarsson, 2008)

Volcanic activity in Iceland is very high. There are 30 active volcanic systems (Thordarson and Höskuldsson, 2008), the most active volcano in Iceland is Hekla, other active volcanos are Grímsvötn, Katla, Askja and Krafla. On average, Iceland experiences a major volcanic event once every 5 years, last two eruptions were those of Eyjafjallajökull volcano (2010) and Bárðarbunga volcano (2014/15).

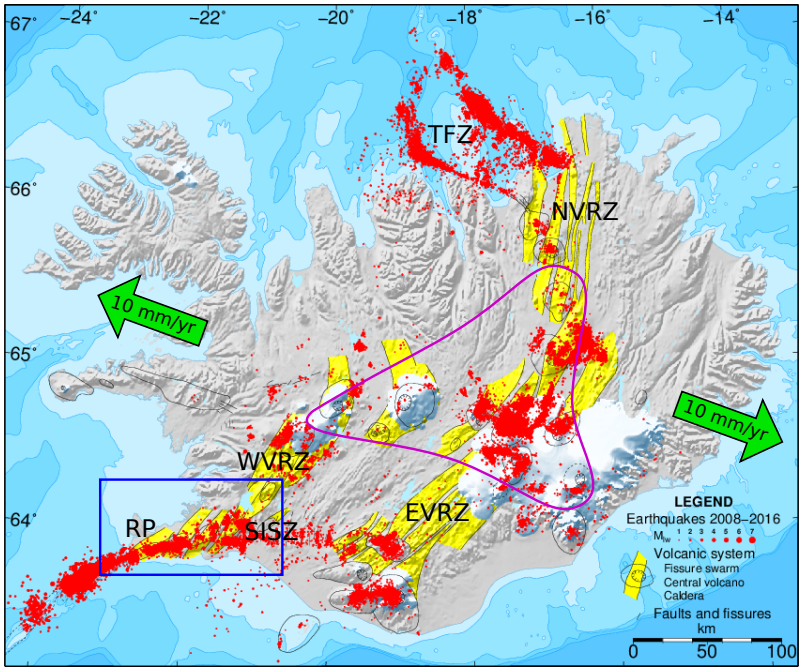

Figure 1.2: Distribution of seismic events in Iceland in the period 2008 – 2016 (*red dots*). The region of my interest is indicated by *blue rectangle*. RP - Reykjanes Peninsula, SISZ - South Iceland Seismic Zone, WVRZ - Western Volcanic Rift Zone, EVRZ - Eastern Volcanic Rift Zone, NVRZ - Northern Volcanic Rift Zone, TFZ - Tjörnes Fracture Zone. The *green arrows* indicate the plate motion. *Violet counter* - Iceland plume at 350 km depth.

The crustal structure in Iceland is fairly complex. The thickness of the Icelandic crust is very anomalous varying between 15 and 46 km, with the average of 29 km. The least thickness belongs to the rift zone offshore extensions (Reykjanes Peninsula and NE Iceland), contrarily, the greatest thickness is found in the SE-central Iceland where the postulated centre of the Iceland plume lies. The variations in the crust thickness can be explained in terms of the temporal variation in plume productivity over the last 20 Ma (Allen et al., 2002b).

Iceland is also well known for a high activity of crustal fluids which is mostly manifested by steam fields and hot springs. The steam field areas are directly linked to the active volcanic systems, there are about 20 high-temperature areas containing steam fields with underground temperatures reaching 200°C in 1 km-depth in Iceland. The low-temperature areas having temperature less than 150°C in the uppermost 1 km are located in the areas flanking the active zone (Arnórsson, 1995a,b).

Seismicity in Iceland is persistent. Usually about 150 to 400 earthquakes over the week are observed, most of them with magnitudes $M_L \leq 2.8$ (Jakobsdóttir et al., 2002; Jakobsdóttir, 2008). The seismicity in Iceland is mainly concentrated along the MAR plate boundary across the whole island and in two shear areas - the South Iceland Seismic Zone and Tjörnes Fracture Zone. The two areas (SISZ and TFZ) hosted all historic strong earthquakes of magnitude up to 7 or higher, in the SISZ also all stronger earthquakes in the recent past occurred (in 2000 two events of M_w6.6 and 6.5, and in 2008 event of M_w6.2) (Tryggvason, 1973; Björnsson and Einarsson, 1974; Einarsson, 1991; Decriem et al., 2010).

Several types of seismicity can be distinguished in Iceland. Ordinary earthquakes of the mainshock-aftershock type typically occur in the shear zones SISZ and TFZ. Earthquake swarms of magnitude up to 5 or higher are characteristic of the Reykjanes Peninsula, Hengill triple-junction area, and offshore areas of Iceland (e.g., on the Reykjanes Ridge and within the seismic zone north of Iceland). According to Hreinsdóttir et al. (2001) and Einarsson (2014) swarm-like seismicity on the Reykjanes Peninsula in the present magma-starved period is mostly due to stress loaded by the plate motion, while an interaction of the tectonic stress and magmatic activity may cause earthquake swarms in the Hengill area. Elsewhere in Iceland earthquake swarms are rare (Tryggvason, 1973). Swarm-like sequences of microearthquakes occur commonly along the whole plate boundary in the island. Earthquake swarms induced primarily by magmatic and volcanic activity occur quite often in the Western, Eastern and Northern Volcanic Zones. An exceptionally intense volcanic earthquake swarm accompanied the Bárðarbunga volcano eruption in August 2014 to February 2015. The largest earthquake reached magnitude M_w5.8 and more than 70 events had magnitudes $M_w > 5$ (Guðmundsson et al., 2016).

Seismicity on the Icelandic territory has been monitored by a regional network SIL (South Iceland Lowland) since 1990; the network has been operated by Icelandic Meteorological Office (IMO). Currently, the SIL network consists of 68 stations that are spread all over Iceland. The stations are equipped with the LE-3D/5s sensors (eigenperiod $T_0 = 5\,\mathrm{s}$) by Lennartz or with broadband seismometers Guralp CMG-3ESP $T_0 = 60\,\mathrm{s}$) and by digitizers Guralp CMG DM24. Sampling rate of 125 Hz is used (Gunnar B. Guðmundsson, IMO, personal communication). All the stations are networked and connected to the IMO data centre and processed automatically there.

1.2.1 Earthquake-swarm areas Reykjanes Peninsula and Hengill volcanic complex (Southwest Iceland)

In my thesis I focus on the Reykjanes Peninsula and adjacent Hengill volcanic complex which stretch along the Reykjanes Ridge (RR). It represents a belt roughly $80 \times 25\,\mathrm{km}$ delineated by latitude $\approx 63.8 - 64.15°$N, longitude $\approx 21.1 - 22.75°$W. The size of the area of the Reykjanes Peninsula and Hengill is comparable to a broader West Bohemia/Vogtland earthquake swarm region. Both Reykjanes Peninsula and Hengill are characterized by persistent seismicity mainly in the form of swarm-like sequences with magnitudes mostly of $M_L < 3$ and recurrent earthquake swarms with magnitudes $M_L > 4$ in some cases reaching even M_L6 (Jakobsdóttir et al., 2002; Jakobsdóttir, 2008; Einarsson, 2014).

Reykjanes Peninsula (RP)

The peninsula (latitude $\approx 63.8 - 64.05°$N, longitude $\approx 21.45 - 22.75°$W) exhibits the highest geodynamic activity in Iceland. The plate boundary extends there from the south-west to the east trending about N70 – 80°E and forms a pronounced oblique rift along the whole peninsula in length of about 65 km (Sæmundsson and Einarsson, 2014). The vector of the relative velocity of diverging plates is not perpendicular to the ridge direction but it is oblique to it at 25 –

30° (∼ N100°E) (Weir et al., 2001). The plate motion across the peninsula has a character of left-lateral shear spreading with the rate of about 17 – 19 mm/yr, having a significant component of opening with the rate of 7 – 9 mm/yr (Geirsson et al., 2010).

The plate boundary is flanked by a deformation zone of about 70 km width where strain is built up by the plate movements. Because the maximum width of the Reykjanes Peninsula is ∼ 40 km, the deformation zone is wider extending under the sea (Hreinsdóttir et al., 2001). There are two distinctly different fracture systems within the deformation zone. The first one, volcanic system, involves normal faults and systems of fissures. They trend highly oblique to the plate boundary and represent an extensional regime. The second system, fracture zone, consists of N-S trending strike-slip faults with a typical spacing of 1 km or less (Einarsson, 2008). According to Árnadóttir et al. (2004) this system appears to be responsible for most of recent larger earthquakes on the peninsula.

The Reykjanes Peninsula is highly complex geophysical structure with interaction between volcanic and tectonic activity. Most of the Reykjanes Peninsula surface is covered by lava. The magmatic activity occurred at intervals of about 1000 years. The last eruptive period ended in 1240 AD, when all the volcanic systems of the peninsula were active. After that, no eruption was observed (Einarsson, 2008).

The Reykjanes Peninsula is one of the most seismically active parts of Iceland, especially at the microearthquake level ($M_L < 3$), with events scattered along the whole plate boundary. A large $M_{Lw}5.9$ swarm took place in 2000, further larger swarms occurred in 2003 ($M_{Lw}5.2$) and in 2013 ($M_{Lw}5.2$) (Einarsson, 2014), a medium swarm of $M_{Lw}4.1$ appeared in 2017 (local moment magnitude M_{Lw} is defined in Section 4.1.2). The swarms occurred in a few zones showing considerably higher seismic activity compared to the other parts of the peninsula. Areas belonging to the zones are the Reykjanes and Svartsengi geothermal areas (SW tip of the peninsula), the Fagradalsfjall area or the Krísuvík geothermal area (volcano in the middle of the peninsula, the latest eruption in the 14th century) (Jakobsdóttir et al., 2002; Jakobsdóttir, 2008; Einarsson, 2014).

Hengill

The region (latitude ≈ 63.95 – 64.25°N, longitude ≈ 21.15 – 22.45°W) is a highly complex portion of the MAR plate boundary covering about 112 km^2 (Hardarson et al., 2009). It is located at the intersection of three tectonic systems: the Reykjanes Peninsula, the Western Volcanic Zone (both being rift zones), and the South Icelandic Seismic Zone (transform shear zone). The Hengill triple junction is named after the Hengill central volcano (64.084°N, 21.316°W, elevation 800 m) which is still active and produces numerous hot springs and fumaroles; several large high temperature geothermal fields are associated with the volcano. The last eruption occurred approximately 2000 years ago. The central volcano and its transecting fissure swarm form the Hengill volcanic system (Hardarson et al., 2009).

The complexity of the region contributes substantially to the seismic activity; the IMO has compiled more than 150,000 events ($M_L > 0$) in the last 25-year period (Gunnar B. Guðmundsson, IMO, personal communication). The series of earthquake swarms started with the activity beneath the Hengill in 1994 (M_L4)

which spread to the Ölfus area in 1995. The second strong activity started in 1997 near Hengill and also spread to the Ölfus area in 1998; the swarm culminated in two M_L4.7 and 4.5 earthquakes in June and November 1998 (Panzera et al., 2016). This unusual series of swarms lasted for about five years and over 90000 events were located altogether in this episode (Jakobsdóttir, 2008).

Ölfus

The region (latitude $\approx 63.92 - 63.97$°N, longitude $\approx 21.20 - 22.45$°W) is a transition area between the Hengill triple junction and SISZ situated about 15 km to the south from the Hengill central volcano. The area is characterized by lava fields, strong geothermal activity and frequent earthquakes. Both earthquake swarms and normal earthquakes (mainshock-aftershock sequences) occurred there (Jakobsdóttir, 2008). Besides earthquake-swarm activities in 1994/95 and 1997/98 one of the doublet M_w6.3 mainshocks and huge number of aftershocks of the 2008 activity were localized in the eastern part of the Ölfus epicentral zone which is attached to the SISZ (Decriem et al., 2010); a distance between the M_w6.3 mainshock of 2008 and the strongest event of the 1998 swarm is only about 10 km.

In my thesis I have investigated two individual earthquake swarms from the Hengill-Ölfus activity in 1997/98: the initial swarm episode in the Hengill in August-September 1997 and the culminating phases in Ölfus area in November-December 1998. Besides, I analyzed two short swarms from the Reykjanes Peninsula which occurred near Krísuvík in 2003 and 2017. Brief characteristics of the analysed Icelandic swarms are shown in Tab. 1.2, their mutual position in Fig. 1.3.

Activity	Duration [days]	Num. of ev. ($M_L \geq 0$)	M_{Lmax}	M_{Lw}
Hen 1997	54	4850	4.4	4.7
Ölf 1998	28	5130	4.9	5.1
Krí 2003	6	1160	4.3	5.0
Krí 2017	6	1660	3.9	4.1

Table 1.2: Basic characteristics of the swarms in Southwest Iceland. Hen - Hengill, Ölf - Ölfus, Krí - Krísuvík. Duration of each activity indicates number of days during which 90% of events, which were recorded within three months, occurred. Note significant difference between M_{Lmax} and M_{Lw} of the Krísuvík 2003 swarm.

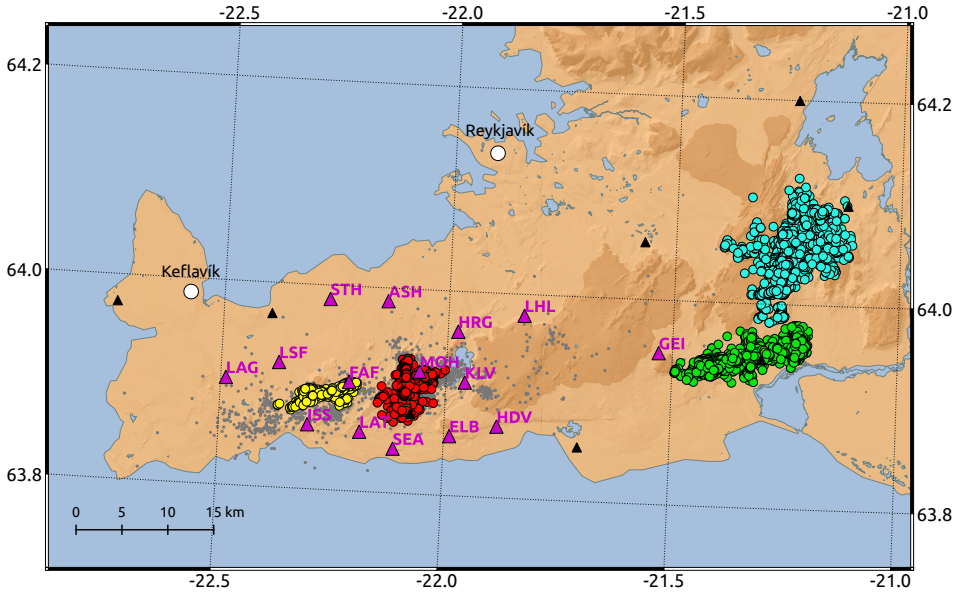

Figure 1.3: Map of Southwest Iceland with locations of the four earthquake swarms of my interest: the swarm of Hengill in 1997 (*light blue circles*), in Ölfus in 1998 (*green circles*), and the two swarms in the Krísuvík area in 2003 (*red circles*) and 2017 (*yellow circles*). The *gray dots* - seismicity in period 2013–2017 recorded by the REYKJANET stations. *Violet triangles* denote seismic stations of the local REYKJANET network, the smaller *black triangles* represent stations of the regional SIL network. *White circles* - towns.

1.2.2 Seismic network REYKJANET

The Institute of Geophysics and Institute of Rock Structure and Mechanics of the Czech Academy of Sciences have focused on the swarm-like seismicity on the Reykjanes Peninsula. For this purpose these institutions have operated seismic network REYKJANET on the Reykjanes Peninsula since 2013. REYKJANET comprises 15 autonomous broadband stations which cover the area roughly 60×20 km. Currently (after an upgrade in 2015), the stations are equipped with the Guralp CMG-40T ($T_0 = 30$ s) sensors, which are placed in special vaults on a concrete pillars being connected with bedrock, and with low-power GAIA data acquisition systems. All the stations operate in the continuous mode with the sampling rate of 250 Hz. A storage capacity of the GAIA is about ten months (32GB SD memory cards), data are downloaded once in three months. In the period before the upgrade (September 2013 to June 2016) nine stations were broadband equipped with the Guralp CMG-40T ($T_0 = 30$ s) and the remaining six were short-period equipped with the Lennartz LE-3D seismometers, $T_0 = 1$ s.

2. Data and velocity models

West Bohemia/Vogtland data used are solely from WEBNET. I created two datasets to analyse the activities of 1997, 2000, 2008, 2011, 2014 and 2017. The dataset I contains the origin time and magnitude of the individual events; it was used for determining the cumulative seismic moment, magnitude-frequency and interevent time distributions and rate of the activities. The 1997, 2000 and 2008 parts of this dataset had been created formerly by manual processing of triggered records and count about 500, 3850 and 4400 $M_L \geq 0$ events for the 1997, 2000 and 2008 swarm. The 2011, 2014 and 2017 parts of the dataset I were extracted from the continuous records using an automatic seismogram processing similar to that of Fischer (2003). In this way I obtained about 5740 events for the 2011, 2800 events for the 2014, and 2500 events for the 2017 activity (all $M_L \geq 0$).

The dataset II contains P- and S-arrival times which were picked manually with the accuracy of ± 4 ms for the P-wave onset and $\pm 8-12$ ms for the S-wave onset. The events belonging to this dataset have the arrival times on at least six stations from ten selected stations which ensure good azimuthal coverage. Six stations surround the NK focal zone at distances less than 10 km (NKC, KVC, SKC, VAC, LBC and STC), and four stations at distances from 13 to 24 km (KRC, KOC, POC and LAC). Number of $M_L \geq 0$ events for the individual activities was about 270 (1997 swarm), 1700 (2000 swarm), 3000 (2008 swarm), 2600 (2011 swarm), 1700 (2014 sequence) and 1000 (2017 swarm). Dataset II was used for location of events and afterwards for analysing their space-time distribution.

Southwest Iceland data which I used are of two types: (1) The catalogue data of Icelandic regional network SIL from the time period 1991 – 2009 provided by the Icelandic Meteorological Office, and (2) data of local seismicity on the Reykjanes Peninsula which were obtained from observation of our network REYKJANET in the time period 2013 – 2017.

(1) The SIL catalogue contains seismic events from the whole region of Southwest Iceland (the Reykjanes Peninsula and its offshore areas through Hengill up to SISZ). It gives the date, origin time, magnitude and relative location (obtained by a method similar to the master event, Dr. Gunnar B. Guðmundsson, IMO, personal communication) for each event included. Since the seismicity contained in the SIL catalogue is persistent and spread out over the whole region, I selected three groups of events meeting the following conditions: (i) clustered in space and time, (ii) showing significantly higher event rate than the long-term average one, and (ii) located in diverse tectonic areas. This way I created the dataset III that is in fact the catalogue of three earthquake swarms which occurred in the Krísuvík area in 2003 (Reykjanes Peninsula; 940 $M_L \geq 0$ events), in the Hengill volcanic complex in 1997 (3200 $M_L \geq 0$ events), and in the Ölfus area in 1998 (4300 $M_L \geq 0$ events).

(2) The data of local seismicity on the Reykjanes Peninsula in the time period 2013 – 2017 form the dataset IV that consists of 2139 events with magnitudes $M_L \geq 0$. This dataset was created by means of the automatic seismogram processing (similarly as the 2011 and 2014 part of the dataset I). Each event included is described by the date, origin time, magnitude, absolute location, and completed by the arrival time readings of the direct P and S waves for the individual stations.

Moreover, I selected data of the M_L3.1 earthquake swarm which occurred in the turn of July/August in 2017. All the swarm events with magnitudes $M_L \geq 0.5$ were reprocessed manually to obtain as accurate the P- and S-wave onsets as possible for a precise localization of hypocenters.

Velocity models

A precise localization of earthquake's hypocenters is one of the main tasks of my thesis. The P- and S-wave velocity structure, which determines the ray paths and hence travel times, and the P- and S-wave arrival times are crucial for locating an earthquake's hypocenter. Therefore, a proper seismic velocity model is a prerequisite for a correct locating of earthquakes. All the event locations, which are involved in this thesis, have been performed in 1-D models.

As regards the West Bohemia earthquake-swarm region, two relevant 1-D vertically inhomogeneous isotropic velocity models of the upper crust were published (Fig. 2.1a). The first one by Málek et al. (2005), termed WB2005, is composed of piecewise constant gradient layers, and was derived using the P-wave travel times of shots and P- and S-wave arrival times of local earthquakes. The second model by Růžek and Horálek (2013), termed WB2013, is an approximation of the authors' 3-D one, when the approximation was obtained by averaging the velocity fields along selected depth horizons. This model was derived, just as the WB2005 one, using both P-wave travel times of shots and P- and S-wave arrival times of local earthquakes.

The P-wave velocities in both models are nearly the same, while S-wave velocities are systematically lower in the WB2013 model. It results in lower hypocenter depths in this model by a few hundred of meters when compared to the depths in WB2005; the horizontal coordinates are practically identical (Růžek and Horálek, 2013). Since the location ability of both models are similar and for the sake of keeping compatibility with the previous event-location studies (e.g., Horálek and Šílený, 2013; Fischer et al., 2014) I used only the WB2005 model for locating the West Bohemia earthquake activities.

As for Southwest Iceland, there exist a few 1-D vertically inhomogeneous isotropic velocity models for this region which, however, fairly differ (Fig. 2.1b).

1. The Icelandic Meteorological Office (being responsible for monitoring local seismicity in Iceland) uses routinely a standard 1-D SIL velocity model with the ratio $v_P/v_S = 1.78$, which is identical for the whole territory of Iceland. The model was constructed by Stefánsson et al. (1993) on the basis of refraction/reflection profile measurements.

2. Vogfjörd et al. (2002) derived a 1-D model consisting of piecewise constant gradient layers with the ratio $v_P/v_S = 1.78$ for the Reykjanes Peninsula; they applied profile technique (utilizing the SIL stations) on swarm earthquakes from Hengill .

3. Tryggvason et al. (2002) derived a 1-D model for a region of $220 \times 110\,\mathrm{km}^2$ in Southwest Iceland (comprising Reykjanes Peninsula, Hengill volcanic complex and South Iceland Seismic Zone) by inversion of the P- and S-wave

arrival times of local earthquakes. This model exhibits significantly higher P- and S-wave velocities in the upper layers than the two previous ones.

4. Another 1-D model was extracted from a 2-D model of the Reykjanes Peninsula by averaging of the P-wave velocities and using a standard ratio $v_P/v_S = 1.78$. This model shows significantly lover velocities at shallower depths down to ~ 4.5 km and significantly higher velocities at depths $> \sim 5.0$ km compared to all the three previous models. The 2-D model (obtained from seismic-profile measurements along the Reykjanes Peninsula) was provided with Dr. Bryndís Brandsdóttir, University of Iceland (personal communication).

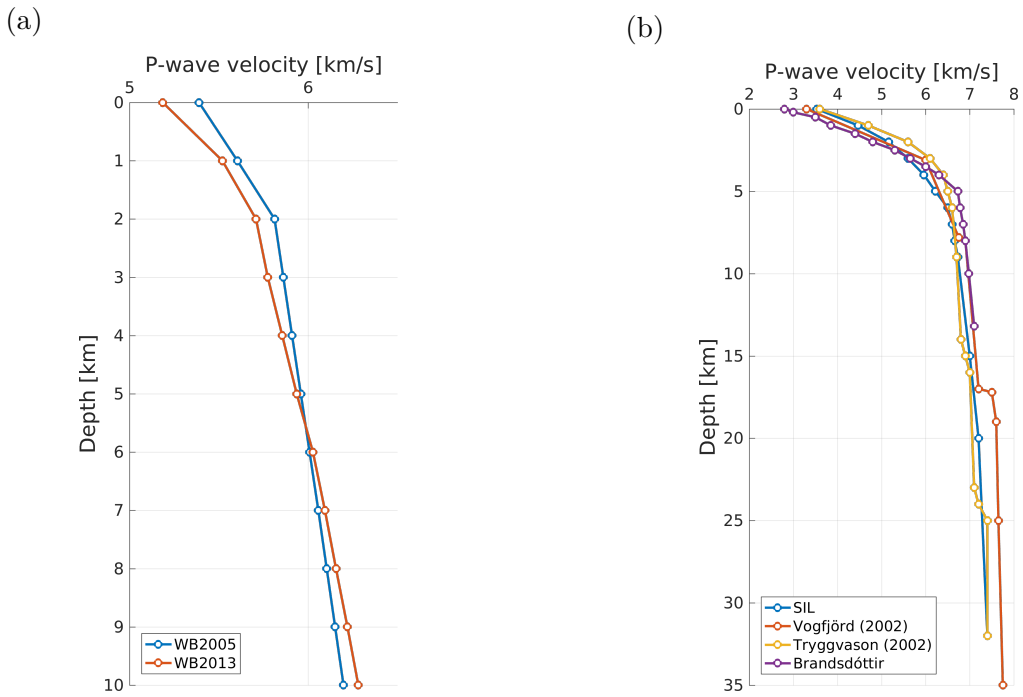

Figure 2.1: 1-D velocity models available for the West Bohemian region (a) and Southwest Iceland (b), represented by P-wave velocity. In (a), WB2005 denotes the model by Málek et al. (2005) (*blue line*), and WB2013 the model by Růžek and Horálek (2013) (*red line*). In (b), *blue line* represents the model used for locating events recorded by the regional network SIL, constructed by Stefánsson et al. (1993), *red* and *yellow line* denotes the models by Vogfjörd et al. (2002) and Tryggvason et al. (2002), and *violet line* shows the model provided with Dr. Bryndís Brandsdóttir, University of Iceland (personal communication).

As far as I know relevant 1-D velocity models of the Reykjanes Peninsula has not been summarised in literature yet. Therefore, the given models are presented by both plots and tables, which may be useful for future studies.

The choice of velocity model is essential for the event location. Therefore, I tried to locate events using every single Southwest Icelandic model to compare its influence to the location. For the locations I used events from dataset IV which are recorded by the REYKJANET network. I found that the SIL model has almost systematically higher depths than all the other models when the differences are mostly < 700 m; differences in horizontal coordinates are mainly < 200 m. Only

when compared the SIL model to the model of Tryggvason et al. (2002), prevailing differences on the edges of the event cluster are in horizontal coordinates ($<$ 500 m) while depth differences decrease to $<$ 200 m.

SIL	
Depth [km]	v_p [km/s]
0	3.53
1	4.47
2	5.16
3	5.60
4	5.96
5	6.22
6	6.50
7	6.60
8	6.66
9	6.73
15	7.00
20	7.20
32	7.40

(a)

Vogfjörd (2002)	
Depth [km]	v_p [km/s]
0	3.30
3.1	6.00
7.8	6.75
8.0	6.90
17.0	7.20
17.2	7.50
19.0	7.60
25.0	7.65
35.0	7.75

(b)

Tryggvason (2002)	
Depth [km]	v_p [km/s]
0	3.60
1	4.70
2	5.60
3	6.10
4	6.40
5	6.50
6	6.60
9	6.70
14	6.80
15	6.90
16	7.00
23	7.10
24	7.20
25	7.40
32	7.40

(c)

Brandsdóttir	
Depth [km]	v_p [km/s]
0.00	2.80
0.15	3.00
0.50	3.50
1.00	3.85
1.50	4.40
2.00	4.80
2.50	5.30
3.00	5.65
3.50	6.00
4.00	6.30
5.00	6.73
6.00	6.78
7.00	6.85
8.00	6.90
10.00	6.98
13.20	7.10

(d)

Table 2.1: 1-D velocity models available for Reykjanes Peninsula. (a) the model after Stefánsson et al. (1993) used for locating events recorded by the regional network SIL, (b) the model after Vogfjörd et al. (2002), (c) the model after Tryggvason et al. (2002), (d) the model provided with Dr. Bryndís Brandsdóttir, University of Iceland (personal communication).

3. Rationale and aims of the thesis

The West Bohemia/Vogtland earthquake swarms have been investigated since the M_L4.6 earthquake swarm of 1985/1986. The results obtained (being published in about 140 papers) have greatly contributed to a deeper understanding of nature of earthquake swarms and their underlying processes. However, each new earthquake activity changed substantially the ideas of the West Bohemia earthquake swarms; for example, even in 2010 (when I chose the topic of my doctoral thesis) it was thought that the main focal zone Nový Kostel was composed of only one fault plane (see Fischer et al., 2010; Horálek and Fischer, 2010). However, three following activities in 2011, 2014 and 2017 completely changed this idea (see Section 5.3.1, Fig. 5.4).

Although our knowledge of earthquake swarms has increased significantly in recent years (particularly of the West Bohemia/Vogtland ones) a fundamental question - what are the causes leading to seismic energy release in the form of earthquake swarms instead of common mainshock-aftershock sequences, remain, however, still unclear. A prerequisite for understanding of this is knowledge of the swarm characteristics which are dependent or vice-versa independent on the tectonic environment. A comparison of intraplate earthquake swarms from the West Bohemia/Vogtland with interplate earthquake swarms from Southwest Iceland presents a challenge to reveal their common features.

In my doctoral thesis I analyse earthquake swarms from these two completely different tectonic areas from the perspective of statistical characteristics (magnitude-frequency distribution, interevent time distribution), seismic moment release, space-time distribution of events and seismic moment released with the aim of finding the swarm characteristics which are dependent/independent on the tectonic environment and which differentiate earthquake swarms from mainshock-aftershock sequences. Namely I analysed the intraplate earthquake swarms from West Bohemia in 1997, 2000, 2008, 2011, 2017 together with the non-swarm activity in 2014, and the interplate swarms from the Krísuvík geothermal field (Reykjanes Peninsula) in 2003 and 2017, the Hengill volcanic complex in 1997, and the Ölfus area (the edge of the South Iceland Seismic Zone where typically mainshock-aftershock earthquakes occur) in 1998. Furthermore, I relocated all the $M_L \geq 0$ events of the West Bohemian earthquake swarms in question by the hypoDD, and derived 3D structure of the main focal zone Nový Kostel which is complex, comprising several differently oriented fault segments. I also retrieved prevailing focal mechanisms in the 2011 swarm and in the 2014 non-swarm sequence.

Prior to analyses I improved the estimation of local magnitude M_L by the WEBNET network and adapted the formula for computing M_L by network SIL for the M_L estimation by REYKJANET. Furthermore, I derived the scaling relation between local magnitude M_L by WEBNET and seismic moment M_0, and performed synthetic tests to evaluate location errors yielded by the hypoDD code when applied to the WEBNET data.

Most of the results regarding the West Bohemia earthquake activities, which

are presented in this thesis, have been published in the papers by Čermáková and Horálek (2015) and Jakoubková et al. (2017), the results concerning Southwest Icelandic swarms have not been published yet.

4. Investigations prior to analysis

4.1 WEBNET and REYKJANET magnitudes and their calibration

Calculating magnitudes of earthquakes is a basic and essential task of any seismic network. There are several different magnitude scales in use - different magnitude scales are suited for different epicentral distances and size of events. Magnitude estimation is mostly based on amplitudes of seismic waves. However, the amplitudes vary due to the station position with respect to the source radiation pattern, variation in attenuation or ground-motion site amplification, and a local structure beneath individual stations. It consequently leads to a significant variance in magnitude estimate at individual stations, especially those in local networks. But the use of reliable and homogeneous magnitudes is crucial in analyses of the magnitude-frequency distribution and seismic moment release (given in Sections 5.1.1 and 5.2). For that reason I calibrated the WEBNET magnitudes and improved their estimation, and introduced the magnitude estimation for the REYKJANET network.

4.1.1 WEBNET magnitudes

The WEBNET local magnitude has been calculated by the following formula (Horálek et al., 2000a):

$$M_{Li} = \log A_{Smax} - \log 2\pi + a \cdot \log R_i + C_i + K, \tag{4.1}$$

where M_{Li} is a local magnitude of the i-th station, A_{Smax} is the absolute value of the maximum total amplitude of the S-wave ground velocity measured in µm/s, a is a constant involving intrinsic attenuation and scattering of the S-wave, R_i is the hypocentral distance of the station in km, C_i is the station correction, and K is a calibration constant. The eventual local magnitude M_L of an event is calculated as the average of the station magnitudes M_{Li}. The formula (4.1) was introduced in 1993 when the WEBNET network comprised five stations only (NKC, KOC, KRC, SKC and TRC, see Fig. 1.1). In the original form of (4.1) the values of $a = 2.1$ and $K = -1.7$ were used, the corrections C_i for the individual stations are given in Horálek et al. (2000a). The constant $K = -1.7$ related magnitudes M_{Li} (at each station) to local magnitude determined at the station PRU of the Czech Regional Seismological Network.

Although the number of online stations of WEBNET increased step by step up to existing 15 ones, only the five of them (for which corrections C_i were known), were used to determine local magnitudes M_L until 2015. Moreover, the data from TRC, which was formerly an autonomous station, were usually available with some delay. Thus the magnitudes were usually determined using only four or even less stations (particularly in case of a failure of some of the stations). My primary task was to enhance the quality of the M_L estimation by including all the networked stations in the routine local magnitude determination, i.e. 13 stations which were operating in 2015. For this purpose, it was necessary to compute corrections C_i for all the stations and revise the original formula (4.1).

In order to determine the corrections C_i I selected a representative set of 445 $M_L \geq 0$ events uniformly distributed in the whole West Bohemia/Vogtland region, the criteria of the event selection are given in Čermáková and Horálek (2015). This set of events (m events hereinafter) was used for the following calculations. I applied the classical iterative approach. In the first iteration all station corrections were set to zero ($C_i = 0$) and for each event I calculated station magnitudes M_{Li} and their average value $M_L = \overline{M_{Li}}$. This way I obtained m differences $\Delta M_{Li} = M_L - M_{Li}$ for each station and their average value $\overline{\Delta M_{Li}}$. In the next iteration a new correction C_i^{new} for each station was determined by adding the average value $\overline{\Delta M_{Li}}$ to the previous correction C_i^{old} ($C_i^{new} = C_i^{old} + \overline{\Delta M_{Li}}$). This procedure was repeated by changing parameter a from 1.0 to 3.0 by steps of 0.1, and I searched for the parameter a and a set of corrections C_i for which the mean of m differences ΔM_{Li} is minimal. The resulting C_i and their standard deviations σ_i are listed in Tab. 4.1 ($\sigma_i < 0.28$, for $i = 1$ to 13 stations). Further, I found that the optimum value of a was confirmed to be 2.1, even for the extended set of stations. A refined formula for the WEBNET local magnitude M_L is:

$$M_{Li} = \log A_{Smax} - \log 2\pi + 2.1 \cdot \log R_i + C_i - 1.2 \tag{4.2}$$

I redefined the calibration constant K as -1.2 to match M_L estimated by the former and new formula. Unlike Horálek et al. (2000a), I did not link the new M_L to any regional station explicitly because magnitudes over those stations are rather scattered. Nevertheless, the same link with the station PRU is implicitly preserved for the new formula.

To verify that none of the WEBNET stations had a predominant effect on the M_L estimation, I applied the jackknife test. I defined various station subsets where one or more stations were omitted. For each subset, I computed magnitudes M_L and the station corrections C_i, and checked their stability. I also tested the stability of M_L estimated using several combinations of only four or five stations, as this is common practice. The tests show that the maximum errors of M_L are of ± 0.2 of magnitude, even when only four or five stations are used. The corrections C_i are quite stable having variations on the order of only hundredths of a magnitude throughout all the events. Such errors are significantly lower than the errors of the M_L estimation itself and can be neglected. The problems of improving the WEBNET local magnitudes and results obtained have been published in Čermáková and Horálek (2015).

	KAC	KOC	KRC	KVC	LAC	LBC	NKC
C_i	-0.393	-0.013	-0.128	0.103	-0.132	0.133	0.093
σ_i	0.217	0.219	0.185	0.185	0.274	0.199	0.229
	POC	SKC	STC	TRC	VAC	ZHC	
C_i	0.038	0.081	0.107	0.135	0.017	-0.240	
σ_i	0.197	0.182	0.259	0.183	0.218	0.270	

Table 4.1: Station corrections (C_i) and standard deviations (σ_i) for 13 permanent WEBNET stations.

4.1.2 REYKJANET magnitudes

As it is mentioned above, the Icelandic Meteorological Office (IMO) has been operated the Icelandic regional network SIL since 1990 and is responsible for monitoring of seismicity in Iceland. IMO has used two types of magnitudes in the SIL network: a local magnitude M_L and a local moment magnitude, denoted M_{Lw} or $M_L(M_0)$. The SIL local magnitude has been calculated by the formula (Jakobsdóttir, 2008):

$$M_L = \log A_{Smax} + 2.1 \cdot \log D - 4.8, \tag{4.3}$$

where A_{Smax} is the maximum of the ground velocity amplitude of highpass (corner frequency 2 Hz) filtered waveforms in a 10 seconds interval around the S-wave and scaled to the response of seismometer and digitizer (by recalculating it corresponds to ground velocity measured in nm/s), D is a distance from the hypocenter to the station in km, and -4.8 is a calibration constant, which ensures similar magnitudes as the magnitudes calculated from the former analog regional network (Jakobsdóttir, 2008; Dr. Gunnar B. Guðmundsson, IMO, personal communication). Interestingly, the formula (4.3) is very similar to the formula (4.1) for a local magnitude by WEBNET, although the two formulas were derived fully independently.

The other SIL magnitude is a local moment magnitude, called M_{Lw} or $M_L(M_0)$, definition of which is not single but divided into parts as follows:

$$\begin{aligned}
M_{Lw} &= m, && M_{Lw} \leq 2.0 \\
M_{Lw} &= 2.0 + (m - a) \cdot 0.9, && 2.0 < M_{Lw} \leq 3.0 \\
M_{Lw} &= 3.0 + (m - a - b) \cdot 0.8, && 3.0 < M_{Lw} \leq 4.6 \\
M_{Lw} &= 4.6 + (m - a - b - c) \cdot 0.7, && 4.6 < M_{Lw} \leq 5.4 \\
M_{Lw} &= 5.4 + (m - a - b - c - d) \cdot 0.5, && 5.4 < M_{Lw} \leq 5.9 \\
M_{Lw} &= 5.9 + (m - a - b - c - d - e) \cdot 0.4, && 5.9 < M_{Lw} \leq 6.3 \\
M_{Lw} &= 6.3 + (m - a - b - c - d - e - f) \cdot 0.35, && 6.3 < M_{Lw}
\end{aligned}$$

$$m = \log_{10} M_0 - 10, \tag{4.4}$$

where M_0 is seismic moment in Nm, and $a = 2$, $b = 1/0.9$, $c = 1.6/0.8$, $d = 0.8/0.7$, $e = f = 1$ (Panzera et al., 2016; Dr. Gunnar B. Guðmundsson, IMO, personal communication). In the SIL catalogues the local magnitude M_L is mostly used. However, the SIL local magnitude scale saturates around $M_L 5.5$ (due to highpass filter with the corner frequency of 2 Hz), so the largest events are reported only with local moment magnitude M_{Lw} (Dr. Gunnar B. Guðmundsson, IMO, personal communication).

As regards estimation of local magnitudes from the REYKJANET network we benefit from similarity of the formulas for M_L by WEBNET (4.2) and by SIL (4.3) which allows us to determine M_L of events recorded by REYKJANET using our formula (4.2). For this purpose I calculated corrections C_i for all 15 REYKJANET stations (Tab. 4.2). I used a set of 274 $M_L \geq 0$ events uniformly distributed on the whole Reykjanes Peninsula and applied the same iterative approach as in case of the station corrections C_i for WEBNET. The only exception

was that the local magnitudes where linked with the SIL magnitudes by setting the constant $K = -1$, which ensures consistency of local magnitudes M_L determined by REYKJANET and SIL. So the formula used for the REYKJANET local magnitude determination is:

$$M_{Li} = \log A_{Smax} - \log 2\pi + 2.1 \cdot \log R_i + C_i - 1, \tag{4.5}$$

where C_i are corrections of the REYKJANET stations.

	ASH	ELB	FAF	GEI	HDV	HRG	ISS	KLV
C_i	0.561	0.102	-0.382	0.005	-0.528	0.158	0.104	-0.182
σ_i	0.276	0.212	0.211	0.378	0.297	0.347	0.164	0.204
	LAG	LAT	LHL	LSF	MOH	SEA	STH	
C_i	0.395	-0.062	0.144	-0.146	-0.241	-0.021	0.069	
σ_i	0.206	0.195	0.199	0.194	0.169	0.178	0.177	

Table 4.2: Station corrections (C_i) and standard deviations (σ_i) for 15 REYKJANET stations.

4.2 Scaling relation between local magnitude and seismic moment

Scalar seismic moment M_0 (seismic moment hereinafter) is a measure of an earthquake size defined as $M_0 = \mu AD$, where μ is the shear modulus (rigidity) in the source, A is the area of the rupture, and D is an average final displacement along the fault after the rupture. Seismic moment, as opposed to magnitude, is a physical quantity measured in Nm that gives a static strength of a seismic shear source, thus it is related to frequencies $f \to 0$ Hz of the radiated source spectrum. Seismic moment can be determined by spectral analysis of the P- and S-wave seismograms or moment tensor inversion. There is no direct relation between local magnitude M_L by WEBNET and seismic moment M_0; however, a reliable $M_L - M_0$ relation was a precondition for trustworthy seismic moment analyses performed within my thesis.

There are three completely different empirical $M_L - M_0$ scaling relations in West Bohemia. Hainzl and Fischer (2002) proposed the relation based on the moment tensors of the 1997 swarm events, Michálek and Fischer (2013) based on the source spectrum analysis of the 2000 and 2008 swarm events, and Horálek and Šílený (2013) based on the moment tensor retrieval of the 2000 swarm. Fig. 4.1 indicates that these scaling relations differ significantly when the seismic moments reported in the two former papers exceeds those by Horálek and Šílený (2013) by more than one order. This inconsistency may be due to a different methodology of determining the M_0 but it is not a subject of my thesis. Nevertheless, it was necessary to clarify this issue using independent data and method, and, if needed, to revise the $M_L - M_0$ scaling relation. For this purpose I used data from the 2014 non-swarm activity. I selected and processed 15 events in the M_L range of 2.0 – 4.4 for which Vavryčuk calculated scalar seismic moments (personal communication).

He applied the algorithm of Vavryčuk and Kühn (2012) which is based on the waveform inversion to P-wave displacement records in the time domain.

The resultant seismic moments M_0 of all the 15 events range between 2.0×10^{12} and 8.0×10^{14} Nm which correspond to moment magnitudes $M_w2.1$ ($\sim M_L2.0$) and 3.9 ($\sim M_L4.4$). An important finding is that the seismic moments by Vavryčuk are quite close to those estimated using the Horálek and Šílený (2013) relation $\log_{10} M_0 = 1.12 \cdot M_L + 9.78$. Although they slightly differ in the absolute level (M_0 by Vavryčuk are larger in all but two cases), the slopes of the $\log_{10} M_0$ vs. M_L dependences are quite similar (see Fig. 4.1).

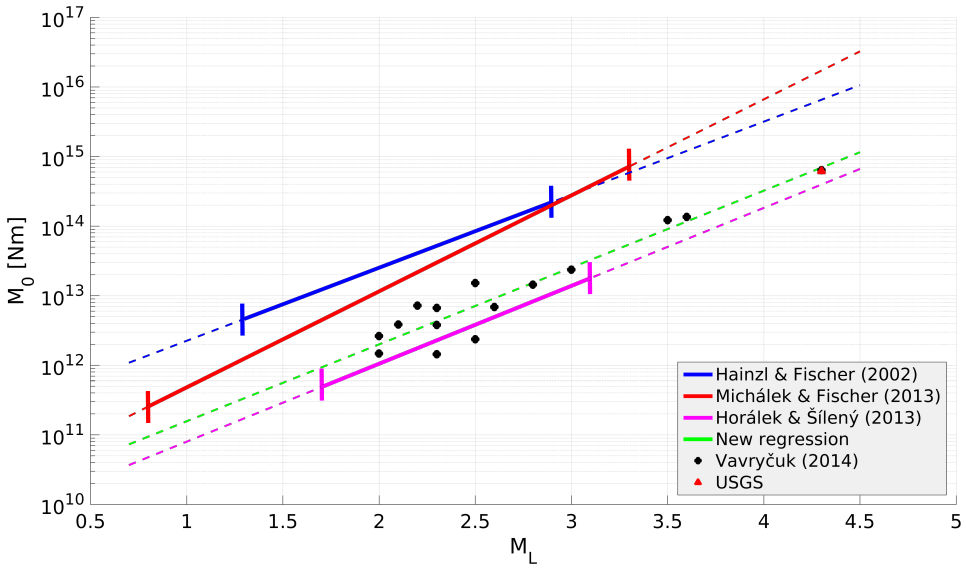

Figure 4.1: Scalar seismic moment M_0 versus the WEBNET local magnitude M_L for the scaling relation based on the 2014 events (*dashed green line*), and for the prior relations by Horálek and Šílený (2013) (*violet line*), Michálek and Fischer (2013) (*red line*), and Hainzl and Fischer (2002) (*blue line*). *Black dots*: M_0-M_L relation of 2014 events used for the M_0–M_L linear regression. *Red triangle*: $M_0 = 6.16\times10^{14}$ Nm ($\sim M_w = 3.8$) reported by USGS for the $M_L4.4$ mainshock. *Solid parts* of the blue, red and violet lines indicate the magnitude range of the events used to derive the corresponding relations.

Moment magnitude of the $M_L4.4$ event determined by Vavryčuk, $M_w3.9$, is quite similar to moment magnitude reported by U.S. Geological Survey (USGS), $M_w3.8$ ($M_0 = 6.16\times10^{14}$ Nm), being based on regional stations. The Horálek and Šílený (2013) relation gives $M_0 = 3.9\times10^{14}$ Nm, corresponding to $M_w3.7$, which is a bit smaller than that determined by USGS.

Since the Horálek and Šílený (2013) relation is based on a rather narrow M_L range between 1.7 and 3.1, I modified this scaling relation to fit data of the 2014 activity, in particular those of stronger events ($M_L \geq 2.5$, Fig. 4.1). Linear regression of the $\log_{10} M_0$ vs. M_L data yields a relation between the WEBNET local magnitude M_L and the seismic moment M_0:

$$\log_{10} M_0 = 1.10 \cdot M_L + 10.09, \tag{4.6}$$

where M_0 is measured in Nm.

All the seismic moment studies involved in my thesis are based on formula (4.6). The problems of the relation between the WEBNET local magnitude M_L and the seismic moment M_0 has been published in Jakoubková et al. (2017). As regards the seismic moment estimation of events form Southwest Iceland I used the local moment magnitude M_{Lw} provided by IMO (Dr. Gunnar B. Guðmundsson, IMO, personal communication).

4.3 Locating earthquakes

4.3.1 Earthquake hypocenter location

The exact location of an earthquake source is one of most important tasks in practical seismology. The source location is defined by its hypocenter coordinates (x_0, y_0, z_0) and the origin time T_0. Basically, the earthquake hypocenter localization is defined as a search for four parameters: the hypocenter coordinates x_0, y_0, z_0 and the origin time T_0; these parameters can be arranged into a vector $\boldsymbol{m}$:

$$\boldsymbol{m} = (x_0, y_0, z_0, T_0) \tag{4.7}$$

which is to be determined. There is a number of ways of how to search $\boldsymbol{m}$, but always measured and location-dependent quantities are fitted. A standard method is fitting measured and predicted (calculated) onset times:

$$T_i^{obs} \approx T_i^{calc}(\boldsymbol{m}), i = 1, 2, ..., n, \tag{4.8}$$

where n is a number of observations and T_i^{obs} is the observed onset time; the calculated onset time T_i^{calc} is the required hypocenter-dependent quantity. Usually, the equations (4.8) are solved in a least-squares context, i.e. by minimizing:

$$\sum_{i=1}^{n} (T_i^{obs} - T_i^{calc})^2 = \min(\boldsymbol{m}) \tag{4.9}$$

or, more rigorously, taking into account individual onset time uncertainties σ:

$$\sum_{i=1}^{n} \left(\frac{T_i^{obs} - T_i^{calc}}{\sigma_i} \right)^2 = \min(\boldsymbol{m}). \tag{4.10}$$

Calculated onset time is evaluated by adding travel time t^{calc} to the origin time ($T^{calc} = T_0 + t^{calc}$), so correct velocity model of the medium must be known. Generally, different seismic phases arriving to different seismic stations can be included in equation (4.10). Since solution of (4.10) for $\boldsymbol{m}$ represents nonlinear problem, appropriate algorithm must be selected to achieve good result.

The well-known localization program Fasthypo (Herrmann, 1979) uses linearization and an iterative search of the hypocenter. Similarly as all nonlinear problems solved by linearization, success of the localization depends strongly on proper starting hypocenter close to the true position. Moreover, since derivatives of travel times with respect to four hypocenter coordinates are needed inside the algorithm, Fasthypo's performance degrades quickly if the true hypocenter is close e.g. to some velocity discontinuity across which the derivative does not exist. In addition to that, the error function in Fasthypo is strongly dependent on the

number of stations and their configurations. Too flat or reversely more complex error function often results in an imperfect finding of its absolute minimum, thus in erroneous hypocenter location.

However, concurrently with improvement of computational capabilities, the numerical efficiency became commonly available and robust techniques dominated the seismological scene. Nowadays, the NonLinLoc (NLLoc; Lomax et al., 2000, 2009) represents a robust, widely used localization program. The hypocenter is searched by combining direct search in a rectangular grid and random sampling around candidate solution (final hypocenter). Robustness of such kind of localization consists in exhaustive search through the whole allowed search space, thus reducing the risk of trapping into local minima, and in the use of only travel times without their derivatives. Travel times in NLLoc are calculated from all points of a dense grid to each station used. Once the travel times are pre-calculated and stored for a fixed stations configuration, the localization can be efficiently run for a voluminous list of seismic events.

The advantage of the code is that the arrival times from each cell in the area of interest is calculated only once and the event location itself is only comparing these already calculated arrival times with those observed. Moreover, the code does not search the right solution over all the cells but it utilizes the oct-tree method. First, it is searching over initial cells having the largest dimension, then the cells with the highest PDF values in their centers are sampled into smaller cells through which the searching process is done again. When the cells with a required smallest size are reached, the cell with the highest PDF is considered to be the solution. The program NLLoc was implemented in the SeisMon software package (Doubravová and Horálek, 2013), and now it is routinely used for processing the WEBNET and REYKJANET data. In the current version NonLinLoc is limited to invert only direct P and S waves on a local scale.

Although the localization using NLLoc or similar software is fairly robust, the event locations may be imperfect due to inexact velocity model. However, there are ingenious methods enabling at least good relative locations for clustered events like seismic swarms or aftershock sequences even if the velocity model is imperfect.

First kind of such approach is 'Master event localization' (ME; Stoddard and Woods, 1990). Once the master event was at least approximately localized, travel times from the master hypocenter to all stations serve as a reference for locating 'target' events relatively to the master. Since ray paths from the master and target events to any station are nearly the same, inhomogeneities along these paths do not affect the relative positions between the master and target events. Only the P- and S-wave velocities in a close surroundings of the master event hypocenter play a role.

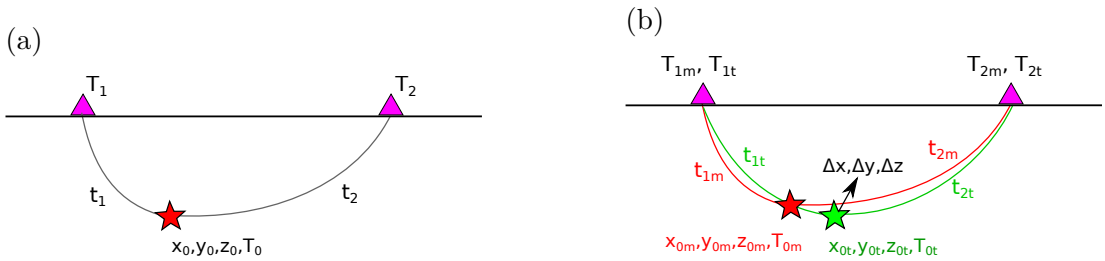

Figure 4.2: Illustration of absolute location (a) and relative location based on Master event approach (b). In both (a) and (b): *violet triangles* - stations, x_0, y_0, z_0 - hypocenter coordinates, T_0 - origin time of the event, t - travel time, T - onset time. Indexes 1 and 2 indicate number of station. *Gray, red and green line* - ray paths from sources to stations. *Red star* in (a) - location of the event. In (b): *red star* - master event, *green star* - target event. Index m indicates value valid for the master event, index t for the target event. $\Delta x, \Delta y, \Delta z$ together with the *thick arrow* depict the relocation vector for the target event.

Further generalization of the ME is 'Double difference localization' method (hypoDD; Waldhauser and Ellsworth, 2000; Waldhauser, 2001), where no preferred master event is selected, but all 'target' events become to be 'master' in a cyclic arrangement. So in hypoDD all localized events are both 'masters' and 'targets' when all the clustered events are localized simultaneously. The code represents an efficient technique allowing to relocate large numbers of earthquakes over large distances. Instead of travel times the code makes use of P- and S-wave travel time differences between two events in a pair. The differences can be obtained either from catalogue data or derived from cross-correlation of the two events waveforms; the differences obtained by both sources can be combined. The hypoDD program consists of two packages. The first one, *ph2dt*, generates the network of event pairs within an earthquake cluster, for which a sufficient accuracy of the input locations is essential. The second package, *hypoDD*, iteratively relocates events in the cluster. Here, a sufficient precision of P- and S-wave arrival times represents a basic precondition for acceptable results.

4.3.2 Locating methods used

Until recently the West Bohemian/Vogtland earthquakes were routinely located by the Fasthypo code. Refined relative event locations were performed by the Master event technique. The Fasthypo code was introduced in the beginning of the WEBNET observations because of its simplicity and low demands on a computer technology and computing speed. The weak points of Fasthypo are stated in the previous section. As mentioned there, the algorithm is quite sensitive to the number and configuration of the stations used, when only one excluded station can cause a significant change in an event location. However, a substantial part of the single event locations in the period 1991 – 2013 might have been inconsistent because both number of the WEBNET stations and their configuration changed over time (owing to establishing new stations or due to failures on some station(s)).

Therefore, I localized all the West Bohemia/Vogtland events from the period

1991 – 2013 again by the NLLoc code that is much less sensitive to excluded stations. Besides, I had the use of a set of stations as much consistent as possible throughout the whole analysed time period.

The Master event (ME) technique enables high-quality relative event locations, nevertheless there are some weaknesses and limitations which should be taken into consideration: (i) accuracy of the event locations strongly depend on the precision of the absolute location of the ME; (ii) location errors fairly increase with increasing distance of events from the ME; this, together with a precondition for the distance between the ME and a near event to be much smaller than the distance between the event and each station, limit the application of the ME method only to a rather small event cloud, for a larger event cloud a combination of multiple MEs must be used; (iii) only the stations used in localization of the ME can be used for locating other events.

Because of that I moved from the relative event locations using ME method to the hypoDD method where these shortcomings are overcome. However, proper hypoDD localization requires an experienced approach not only to the method but also to data used. Because the hypoDD code relates all sufficiently close event pairs regardless the data quality, it is appropriate to filter out all the input events having location errors larger than given threshold throughout the event cloud. Since I work with manually picked arrival times which are of sufficient precision to get satisfactory event locations, I used only catalogue data to get the P- and S-wave travel time differences.

Optimization of the hypoDD parameters

In the hypoDD code the input parameters MAXNGH, MAXSEP and MINLNK are used to constrain neighbours of each event for which the travel time differences are calculated. Optimum values of these parameters depend on the size of a particular focal cloud, on the number and density of events, and on the distribution of stations; unsuitable values of the parameters lead to loss of events and false outliers. I performed a number of tests to optimize these parameters to be identical for most of West Bohemia/Vogtland and Southwest Iceland activities. The optimum parameters that I found associate each event with the 20 nearest neighbours within a distance of 1 km. For each event and its neighbours, at least 8 phase pairs (P and S) at common stations are necessary. These parameters ensured a stable solution without outliers and with a negligible number of lost events for the whole NK zone in West Bohemia and an area of the Reykjanes Peninsula covered by REYKJANET network.

4.3.3 Evaluation of the location errors - synthetic tests

A direct evaluation of the location errors yielded by the hypoDD code is not simply accomplishable. Therefore, I performed synthetic tests to get an idea of the accuracy of the event locations when the hypoDD code is used for relocating the West Bohemia/Vogtland events. In the area covered by the WEBNET network I created 750 synthetic events with coordinates x_s, y_s, z_s and origin times t_{0s}. The events were grouped in six clusters which varied in number of events, shape, depth, and position relative to the WEBNET stations. The basic characteristics of each cluster are shown in Tab. 4.3, their positions in Fig. 4.3.

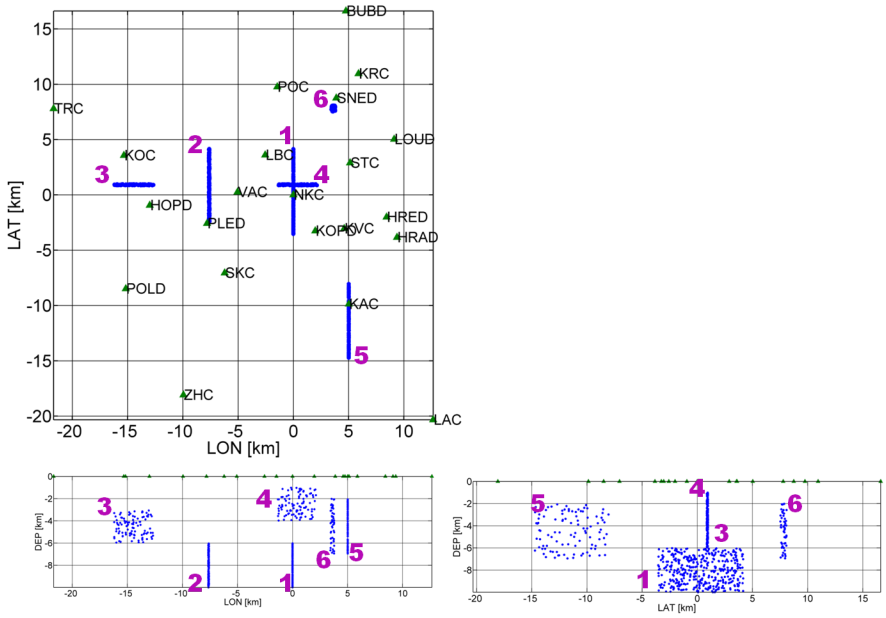

Figure 4.3: Space distribution of synthetic clusters used for tests of the event location accuracy obtained by the hypoDD code, in relation to stations of the WEBNET network. Note small depths of cluster 4.

For all the events I calculated arrival times of the P and S waves, t_{Ps} and t_{Ss}, to all the WEBNET stations in the 1-D WB2005 velocity model for the ratio $v_P/v_S = 1.71$. First of all I relocated all the 750 synthetic events using the arrival times t_{Ps} and t_{Ss} for each event in the same velocity model to check whether the hypoDD locations coincide with the synthetic ones. I found that the difference in all coordinates are smaller than 10 m which is negligible.

Then I perturbed the locations x_s, y_s, z_s of the synthetic events by random errors, so I obtained perturbed coordinates x_p, y_p, z_p for each event. This way I simulated imperfect results of an absolute single localization. Finally, I relocated the perturbed events (with coordinates x_p, y_p, z_p) by the hypoDD package using synthetic arrival times of P waves t_{Ps} and the ratio $v_P/v_S = 1.71$. I made a number of perturbations with various size of the random errors (maximum errors were ±300 m in horizontal coordinates and ±500 m in depth) and tested their effect on the location results. Furthermore, I created various sets of the WEBNET stations and analyzed an influence of the number of the stations and their configuration on the locations.

Cluster	Num. of ev.	Shape	Position	Orientation
1	200	plane	center	northsouth
2	200	plane	center	northsouth
3	100	plane	west	eastwest
4	100	plane	center	eastwest
5	100	plane	southeast	northsouth
6	50	pipe	northeast	-

Table 4.3: Basic characteristics of synthetic clusters used for evaluating the event location accuracy obtained by the hypoDD code.

The tests showed that shapes of the event clusters situated within the network are well constrained. When a cluster is situated at the edge or outside the network, the cluster shape is slightly deformed and elongated towards the network center. Location errors are comparable for all events both in the center and on the edge of the seismic network, nevertheless, the biggest location errors were found for events situated in the smallest depths even in the network center. For horizontal components, the resulting errors are on the order of tens of meters, usually lower than 30 m. Regarding focal depths, the errors are slightly higher but still lower than 50 m. The maximum location errors for events situated in the smallest depths (< 3 km) were below ~ 70 m in horizontal and below ~ 150 m in vertical axes, which is quite satisfying. Besides, I found that the event locations by hypoDD were stable showing very low errors even if only four suitably distributed stations along the edge of the network were used. I also examined a response of the hypoDD code on a systematic shift in the absolute locations of clustered events and found that the systematic shift in the absolute locations is retained in the hypoDD relocation.

5. Analysis

5.1 Statistical characteristics

5.1.1 Magnitude-frequency distribution

A magnitude-frequency distribution (MFD) is a function that describes the ratio of earthquakes in a given activity or region and time period over all magnitudes. MFD of both aftershock sequences and earthquake swarms typically follow the Gutenberg-Richter law (GR law) that is a basic scaling relationship in earthquake statistics:

$$\log N = a - bM, \tag{5.1}$$

where N is a number of events having a magnitude $\geq M$, a and b are constants. It expresses the relation between the size of earthquakes and the frequency of their occurrence for a particular earthquake activity. The b-value signifies the ratio of small to large events, the constant a is the logarithm of the number of events with $M_L \geq 0$, which indicates the event productivity of a seismic sequence.

It is generally thought that b-values of common mainshock-aftershock sequences are ≈ 1.0 or lower, while earthquake swarms typically exceed 1.0 and are often as high as 2.5 (e.g., Lay and Wallace, 1995), which implies prevalence of small events against larger ones in individual swarm activities. The b-value is also assumed to be connected with the rock properties. For example, Wyss et al. (1997) and Wiemer et al. (1998) pointed out that low b-values correspond probably to breaking asperities while high b-values correspond to creeping sections of faults or to active magma chambers where seismicity is dominated by the creation of new fractures under stress build-up. According to Urbancic et al. (1992) and Wyss et al. (1997) an increase in applied shear stress or in effective stress decreases the b-value. From these perspectives a comparison of the MFD of earthquake swarms from entirely different tectonic environments, West Bohemia/Vogtland and Southwest Iceland, is very important. For these analyses I used data sets I, III and IV defined in Chapter 2 (Data and velocity models).

Before computing the MFD a few preconditions should be under control to get a reliable b-value: (i) only complete catalogue should be used containing events with magnitudes $M_L \geq M_C$, where M_C is a magnitude of completeness representing a bottom threshold of magnitudes which were detected at full strength; (ii) the M_L range of the analyzed events should be at least over 2.5 magnitudes; (iii) only MFDs derived from the same or similar definition of local magnitude are comparable. Thanks to similarity of formulas (4.2) and (4.3) defining the local magnitude scale by WEBNET and by SIL I was able to compare correctly magnitude-frequency distribution of the West Bohemian and Southwest Icelandic earthquake activities.

For the MFD analysis I derived the completeness magnitude M_C for all seismic activities by the maximum curvature approach (MAXC; Wiemer and Wyss, 2000; Woessner and Wiemer, 2005). This technique defines M_C at the point of maximum curvature corresponding to the maximum value of the second derivative of the magnitude-frequency curve. In practice, the maximum curvature point

matches the magnitude bin with the highest frequency of events in the non-cumulative MFD.

I found that M_C of the 2011, 2014 and 2017 West Bohemian catalogues (produced automatically) is -0.25 for the 2011, -0.50 for the 2014 and -0.25 for the 2017 one, while M_C of the 1997, 2000 and 2008 swarms (obtained by manual picking) are higher, -0.15 for the 1997 swarm and 0.25 for both 2000 and 2008 swarms. Concerning the Icelandic activities, for those in Hengill and Ölfus M_C is 0.25, whereas for the Krísuvík 2003 and 2017 activities the M_C is 0.50 and 0.30, respectively (see Tab. 5.1). In order to get comparable results I set M_C for all the activities to be $M_C = 0.25$, only for the Krísuvík swarms in 2003 and 2017 I left the higher values, $M_C = 0.50$ and 0.30.

activity	West Bohemia						Southwest Iceland			
	1997	2000	2008	2011	2014	2017	Hen 1997	Ölf 1998	Krí 2003	Krí 2017
M_C	-0.15	0.25	0.25	-0.25	-0.50	-0.25	0.25	0.25	0.50	0.30

Table 5.1: Magnitudes of completeness M_C of the studied activities from West Bohemia and Southwest Iceland.

The MFDs for the activities in question are depicted in Fig. 5.1a. Even though the West Bohemia/Vogtland and Southwest Iceland are of an entirely different tectonic character, most of events of each activity obey the GR law with the b-value 1.0 regardless of whether they are an earthquake swarm or a mainshock-aftershock sequence. However, the events at the highest magnitude level are apparently deflected from the linear trend of the GR curve downwards, thus the GR law is cut-off. Furthermore, there are pronounced magnitude gaps between the strongest events and the following weaker events, mainly in MFD of the West Bohemia swarms in 2008, 2011 and 2017, and also in MFD of all the Southwest Icelandic swarms. In these aspects, the MFD features of all these swarms point to the characteristics of the mainshock-aftershock sequences. The mainshock-aftershock character of the MFD is nicely seen in case of the whole 2014 West Bohemian activity where the activity complies quite well with the GR law of $b = 1$ in the magnitude range of $M_L 0.25 - 3.0$, and the three mainshocks are clearly away from the GR curve; less significant irregularity of the GR curve at magnitudes around $M_L 2.5$ is probably due to the absence of the $M_L > 2.3$ aftershocks of the $M_L 3.5$ and 3.6 mainshocks.

So I infer that the swarms may be comprised of overlapping aftershock sequences, each of them dominated by a "mainshock". This idea is supported by the findings of Hainzl and Fischer (2002) who showed that the West Bohemian 2000 swarm can be represented by such aftershock sequences. I am aware of the smaller significance of this observation caused by low sampling numbers for the largest magnitudes, nevertheless, this idea should be taken into consideration as one of possibilities of an earthquake swarm nature.

(a)

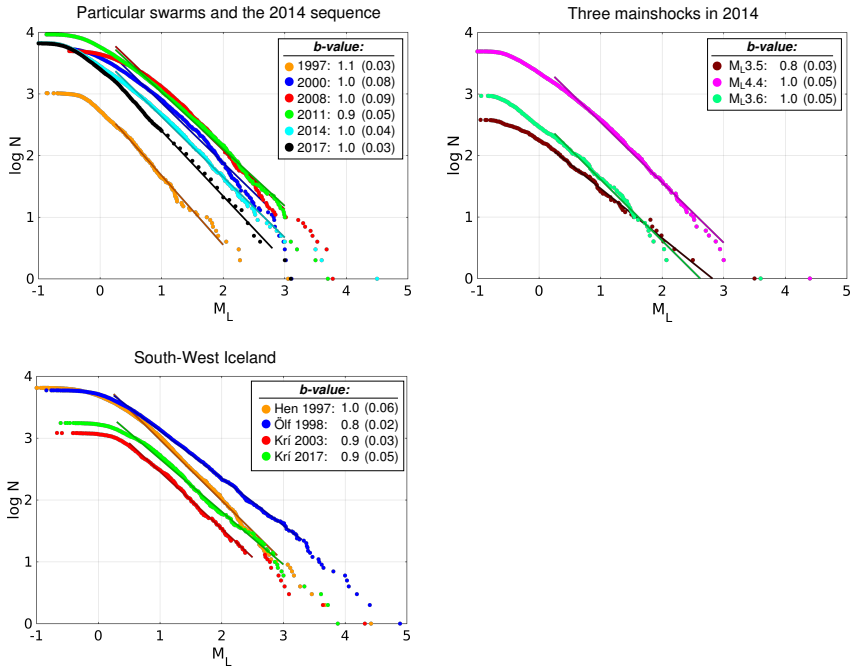

(b)

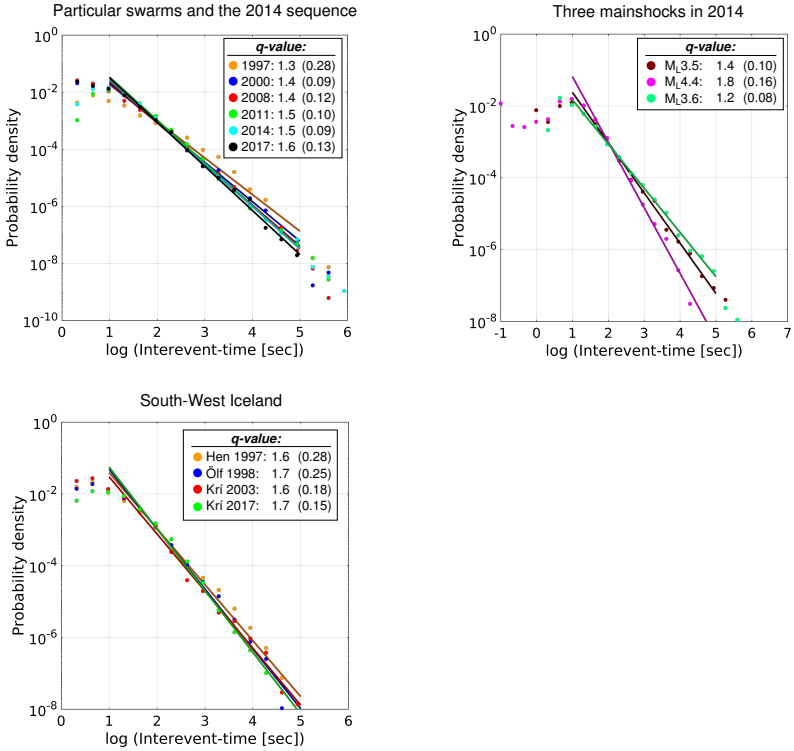

Figure 5.1: (a) Cumulative magnitude-frequency distribution (MFD), (b) probability density function of interevent times. For both (a) and (b): *Top left* - the West Bohemian swarms of 1997 *(orange)*, 2000 *(blue)*, 2008 *(red)*, 2011 *(green)*, 2017 *(black)* and the non-swarm activity 2014 *(light blue)*; *Top right* - the aftershock sequences of the 2014 mainshocks of $M_L3.5$ *(brown)*, $M_L4.4$ *(violet)* and $M_L3.6$ *(light green)*; *Bottom left* - the Southwest Icelandic swarms of Hengill *(orange)*, Ölfus *(blue)*, Krísuvík 2003 *(red)* and Krísuvík 2017 *(green)*. The numbers in brackets represent RMS of the linear regression.

Constant a (event productivity) is usually disregarded but it provides a relevant estimate of the $M_L \geq 0$ events in individual activities, which is useful in case of the completeness magnitude being $M_C > 0$. If b-values are similar ($b \approx 1$ in our case) the event productivity a should increase with increasing M_{Lmax} of an activity in a given area (the higher M_{Lmax} the higher a). Regarding the earthquake activities in West Bohemia, it roughly holds for earthquake swarms: $a =$ 270, 2500, 3800, 4400 and 5700 for the swarms of 2013 (M_L2.3), 2017 (M_L3.1), 2000 (M_L3.3), 2008 (M_L3.8) and 2011 (M_L3.7). But it does not apply in case of the M_L4.4 non-swarm activity in 2014 for which $a = 2800$ only. The reason is that the greater part of the 2014 total seismic moment released in the three mainshocks (M_L3.5, 4.4 and 3.6), and remaining seismic moment in the series of the $M_L \leq 3.0$ events. This issue is discussed in more details in Section 5.2. It suggests that mainshock-aftershock sequences generally comprise much fewer events than earthquake swarms to release similar seismic moment. This implication nicely correlates with the definition of a mainshock-aftershock sequence that the mainshock is significantly larger than the aftershocks.

The MFDs of the Southwest Icelandic activities point to strikingly small event productivity of the two earthquake swarms in the Krísuvík region (on the Reykjanes Peninsula); the constants $a = 1160$ and 1660 for the swarms of 2003 and 2017 (M_L4.3 and 3.9) are several times lower than the constant a of the swarm in the Hengill volcanic complex (M_L4.4), as well as of all the West Bohemian swarms with $M_{Lmax} \geq 3.3$ (i.e. swarms of 2000, 2008 and 2011). It indicates that the swarms in the Krísuvík geothermal area may be of different character than the Hengill and West Bohemian swarms.

The Gutenberg-Richter law is a very useful tool of earthquake statistics but without any physical meaning due to the magnitude scale dependence of the constants a and b. However, if the magnitude-seismic moment relation is known, the GR law can be transformed into the power law size distribution being of physical meaning and, unlike the a and b-value, magnitude-scale independent.

So I was able to derive it for the West Bohemian earthquake activities. Combining formula (4.6) and GR law we get the power law size distribution $N \sim M_0^{-\beta}$, where N is the number of events with seismic moment equal or larger than M_0, and $\beta = b/1.1$. The linear scale for N enables counting the total seismic moments within different moment bins M_{0i} as $N_i * M_{0i}$. This leads to $N_i * M_{0i} \sim M_0^{1-\beta}$ which gives a physical meaning to the exponent β. In other words, $1-\beta$ describes the ratio of seismic moments released by small and large events. The coefficient β is equal for the swarms of 2000 and 2008, the whole 2014 sequence, and for the M_L4.4 and 3.6 episodes separately ($\beta = 0.91$), and differs slightly for 1997 and 2011 swarms ($\beta = 1.0$ and 0.82) and a bit more for the 2014 M_L3.5 episode ($\beta = 0.72$).

5.1.2 Interevent time distribution

A temporal behavior of a mainshock-aftershock seismic sequence is usually analysed using the Omori law:

$$\lambda(t_d) = K(c + t_d)^{-p}, \tag{5.2}$$

where λ is the occurrence rate of the aftershocks, t_d is the time delay after the mainshock, and K, c, p are fault-dependent constants (Utsu et al., 1995). This

relation represents a decay rate of aftershocks within a time interval following a mainshock controlled by parameter p ranging usually between 0.9 and 1.5. Utsu et al. (1995) modified the Omori law by replacing the aftershocks' delay times t_d by interevent times T_w, i.e. delay times between two successive events in a seismic sequence. Such distribution should correspond to the power law:

$$N = k(T_w)^{-q}, \tag{5.3}$$

where N is a number of interevent times T_w, and k, q are constants; according to Utsu et al. (1995) the constants p in (5.2) and q are related as $q = 2 - p^{-1}$.

To compare the T_w distributions of all the analysed swarms I computed their probability density functions (PDF) for the $M_L \geq M_C$ events, the results are presented in the Fig. 5.1b. The PDFs of all the West Bohemian swarms, the complete 2014 non-swarm sequence, and all the Southwest Icelandic swarms comply nicely with power law $\propto T_w^{-q}$. The q-values vary between 1.3 and 1.6 for the West Bohemian activities and 1.6 and 1.7 for the Southwest Icelandic ones, which implies comparable event rate (rapidity) of all these activities, nevertheless the rapidity of the Icelandic swarms is evidently higher.

However, the PDFs of the aftershock sequences of the individual 2014 episodes strikingly differ, indicating the q-value 1.4 for the M_L3.5 (May 24), 1.8 for the M_L4.4 (May 31), and 1.2 for the M_L3.6 (August 3) aftershock sequences. It implies a fairly high rapidity (event rate) of the aftershocks after the M_L4.4 mainshock which is much higher than that after the M_L3.5 and M_L3.6 maishocks, and even higher than the rapidity of all the swarms in West Bohemia and Southwest Iceland. The q-value 1.8 corresponds to constant $p = 5.0$ in the Omori law formula (5.2), which indicates much higher decay of aftershocks with time compared to standard mainshock-aftershock sequences characterised by $p = 0.9$–1.5. The q-value 1.8 for the M_L4.4 mainshock-aftershock sequence agrees very well with the maximum likelihood fit of the Omori-decay function which yields $p = 5.1$ by Hainzl et al. (2016). On the contrary, the lowest event rate among all the activities in question was found for aftershocks of the M_L3.6 mainshock. A respective $q = 1.2$ corresponds to $p = 1.25$ which is a typical value for a mainshock-aftershock sequence.

The deviations for the interevent times being shorter than 10 s are caused by lost events hidden in the waveforms of the former, often stronger ones. More detailed analysis of the interevent time distribution, such as the epidemic-type-aftershock-simulation (Hainzl and Ogata, 2005), is beyond the scope of my thesis, nevertheless, it is an issue worth in-depth investigation.

5.2 Temporal development of the activities and the seismic moment release

I analysed the time course of the activities and seismic moment release, and its rate for the individual activities to get deeper insight into their nature. The time courses of the activities are represented by magnitude-time plots in Fig. 5.2, which show distribution of events that occurred within three months from the beginning of each activity. Besides, I calculated seismic moments applying formula (4.6) to the dataset I for the West Bohemia activities and using local moment magnitude M_{Lw} being included in the dataset III for the Southwest Iceland swarms. The total seismic moments M_{0tot} and local magnitudes M_{Ltot} or M_{Lw} of corresponding hypothetic single events for the individual West Bohemian and Southwest Icelandic activities are given in Tables 5.2 and 5.3, respectively. I analysed the time course of the seismic moment release (by means of the cumulative seismic moment, Fig. 5.3a) and the rate of the seismic moment release. For the latter I calculated the normalised cumulative seismic moment by the following way: The cumulative seismic moment per day is divided by the total seismic moment, these daily values are sorted in descending order, and then their cumulative distribution is computed. As a result, the days with the most intense activity are at the beginning, while the days with weak activity are at the end of the individual diagrams in Fig. 5.3b. As a criterion for estimation of the rate of the seismic moment release I used the period during which 95% of total seismic moment was released.

The patterns of the temporal event distribution and of the seismic moment release in the individual activities are given in Figs. 5.2 and 5.3. The activities evidently differ (e.g., in duration and number of phases, number of dominant events and their magnitudes M_L, or in total seismic moment M_{0tot}), nevertheless, the patterns show some characteristic features of the West Bohemian or Southwest Icelandic activities which may be important for deeper insight into the nature swarm-like activities in the regions concerned.

(i) Normalised cumulative seismic moments of the activities from both regions (Fig. 5.3b) indicate generally higher rate of the seismic moment release in the Southwest Icelandic swarms compared to that in the West Bohemia swarms; in other words, the swarms in the Southwest Iceland, particularly those in the Krísuvík geothermal area, are apparently faster than the swarms in West Bohemia.

(ii) The West Bohemian and Southwest Icelandic earthquake swarms also differ in a number of phases in which most of seismic moment released. The step-by-step seismic moment release is typical for the West Bohemia swarms, i.e. the swarms consist of several intense phases (except weaker swarms in 1997 and 2017). On the contrary, the Southwest Icelandic swarms are characterised by one dominant phase during which the most of seismic moment released (Fig. 5.3a); the phase is dominated by one or only a few strong events having magnitudes of about 0.5 higher than magnitudes of the other events (Fig. 5.2). So these swarms resemble mainshock-aftershock sequences, particularly those in Ölfus (M_L4.9) and in Krísuvík in 2003 (M_L4.3) and 2017 (M_L3.9). These swarms and also the West Bohemia swarm in 2017 (M_L3.1),

in which a major part of event occurred in the early stage of the swarm activity, are similar to the $M_L4.4$ mainshock-aftershock sequence that occurred in West Bohemia in 2014.

(iii) As for the West Bohemian activities, the total seismic moment released, M_{0tot}, accelerated in each subsequent activity starting from the 2000 swarm up to the 2014 sequence and 2017 swarm (Figs. 5.2 and 5.3). In other words, each new sequence was faster than the previous one leaving the 2014 non-swarm activity the most rapid. It is proved by a decrease of the characteristic period during which 95% of total seismic moment was released (Fig. 5.3b). This period lasted for 18 days in 2000, 14 days in 2008, 13 days in 2011 and 5 days in 2014 and 2017. It is noticeable that a time period in which most of the events of each sequence are accumulated is shortening with time. It indicates that the increasing rate of the seismic moment release could be connected with a transition from the swarm-like to the mainshock-aftershock character of the 2014 and possibly of the 2017 seismicity.

(iv) Although the 2008, 2011 and 2014 West Bohemia activities show similar size of M_{0tot}, the time course of the seismic moment release is fairly different which implies different number and magnitudes of strong events, and consequently different maximum ground motions in each activity; for example the maximum observed ground acceleration in the 2014 non-swarm activity was $a_{max} = 2.2\,\mathrm{m/s^2}$ (station KAC), while $a_{max} = 0.65\,\mathrm{m/s^2}$ (station STC) in the 2008 swarm. It is obvious that an earthquake swarm produces number of strong events to release the same seismic moment as a mainshock. For example seismic moments M_0 released in the 2014 $M_L4.4$ mainshock corresponds to sum of all the $M_L3.0-3.8$ events in the 2008 swarm (eight events) except the $M_L3.8$ event in the last swarm phase (for details see Tab. 2 in Fischer et al., 2010).

(a)

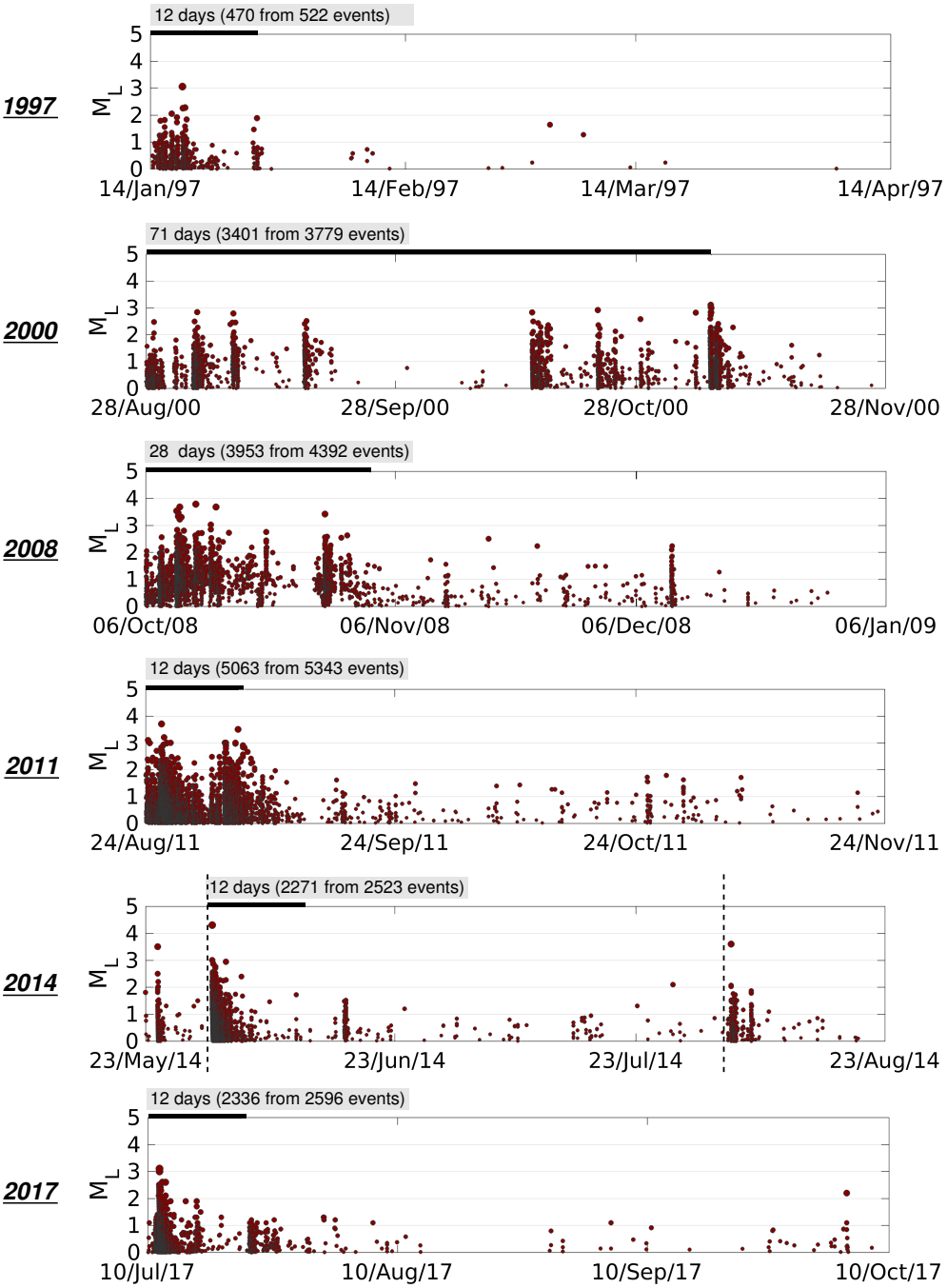
12 days (470 from 522 events)
1997
M_L
14/Jan/97
14/Feb/97
14/Mar/97
14/Apr/97
71 days (3401 from 3779 events)
2000
28/Aug/00
28/Sep/00
28/Oct/00
28/Nov/00
28 days (3953 from 4392 events)
2008
06/Oct/08
06/Nov/08
06/Dec/08
06/Jan/09
12 days (5063 from 5343 events)
2011
24/Aug/11
24/Sep/11
24/Oct/11
24/Nov/11
12 days (2271 from 2523 events)
2014
23/May/14
23/Jun/14
23/Jul/14
23/Aug/14
12 days (2336 from 2596 events)
2017
10/Jul/17
10/Aug/17
10/Sep/17
10/Oct/17

(b)

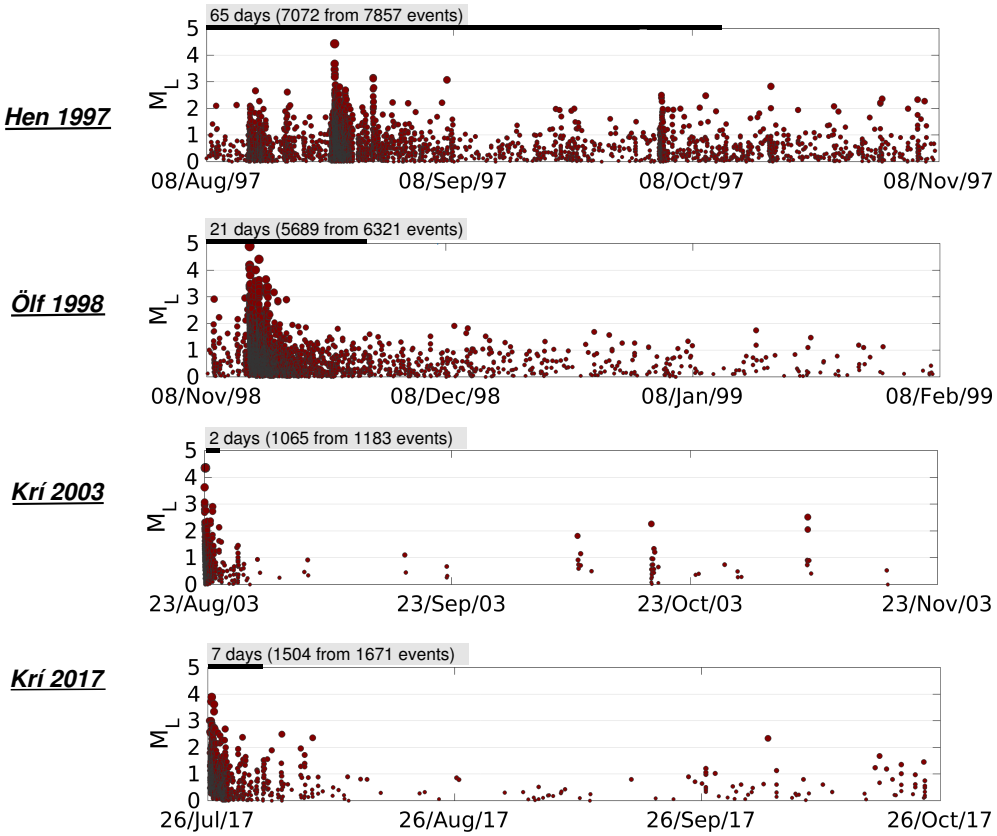

Figure 5.2: Magnitude-time course of the West Bohemian swarms of 1997, 2000, 2008, 2011, 2017 and the 2014 activity (a), and the Southwest Icelandic swarms of Hengill (Hen 1997), Ölfus (Ölf 1998), Krísuvík 2003 (Krí 2003) and Krísuvík 2017 (Krí 2017), within 3 months. The datasets I and III for West Bohemia and Southwest Iceland are used. *Numbers on gray rectangles* - number of days during which 90 % of events, which were recorded within three months, occurred. For the 2014 activity the time interval covers only the M_L4.4 aftershocks (two months indicated by the *dashed black lines*). Note different patterns of the individual swarms and the 2014 activity exhibiting a character of three mainshock-aftershock sequences.

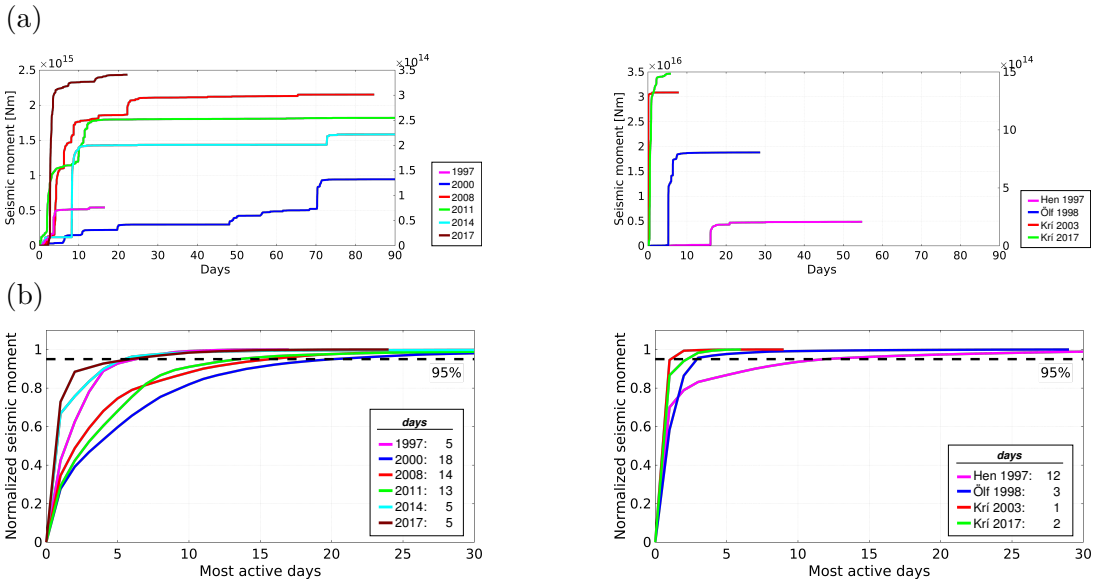

Figure 5.3: (a) Cumulative seismic moment of $M_L \geq 0$ events; (b) normalised cumulative seismic moment by the total seismic moment, sorted based on its daily amount in a descending order. In both (a) and (b): *Left* - West Bohemian swarms of 1997 *(violet)*, 2000 *(blue)*, 2008 *(red)*, 2011 *(green)*, 2017 *(brown)*, and the activity of 2014 *(light blue)*; *Right* - the Southwest Icelandic swarms of Hengill *(violet)*, Ölfus *(blue)*, Krísuvík 2003 *(red)* and Krísuvík 2017 *(green)*. *The dashed black line* in (b) - 95% of total seismic moment. *Number of days* in (b) - time necessary to release 95 % of total seismic moment. For the West Bohemian swarms in (a), two vertical axes of the values of seismic moment are shown: the *left axis* is valid for the swarms of 2000, 2008, 2011, and the 2014 activity, the *right axis* is valid for the swarms of 1997 and 2017.

Activity	M_{0tot} [Nm]	M_{Ltot}
1997	7.60×10^{13}	3.5
2000	9.50×10^{14}	4.4
2008	2.15×10^{15}	4.8
2011	1.86×10^{15}	4.7
2014	1.58×10^{15}	4.6
2017	3.41×10^{14}	4.0

Table 5.2: Total seismic moments of the West Bohemia swarms. M_{Ltot} - local magnitude of a hypothetical earthquake corresponding to the given M_{0tot}.

Activity	M_{0tot} [Nm]	M_{Lwtot}
Hen 1997	4.84×10^{15}	5.0
Ölf 1998	1.88×10^{16}	5.4
Krí 2003	3.09×10^{16}	5.5
Krí 2017	1.48×10^{15}	4.7

Table 5.3: Total seismic moments of the Southwest Icelandic swarms. M_{Lwtot} - local magnitude of a hypothetical earthquake corresponding to the given M_{0tot}.

5.3 Space-time distribution of events in the West Bohemia and Southwest Iceland earthquake activities

Knowledge of the space-time distribution of events and fault geometry of the swarm areas is an essential condition for understanding of underlying processes leading to earthquake swarms. Therefore, the analyses of the space-time distribution of foci in the West Bohemian and Southwest Icelandic earthquake swarms and their interpretations form the important part of my thesis.

5.3.1 West Bohemian swarm and non-swarm activities and the structure of the Nový Kostel focal zone

As regards the West Bohemia/Vogtland region the spatial and temporal distribution of local swarm events, especially in the main focal zone NK, has been one of primary tasks since beginning of the WEBNET observations. The first study of the space-time distribution of events in the NK zone comes from Horálek et al. (1996), further papers by Fischer and Horálek (2000, 2003), Fischer and Michálek (2008), Horálek et al. (2009), Horálek and Fischer (2010), Fischer et al. (2010), Bouchaala et al. (2013), Čermáková and Horálek (2015) and Jakoubková et al. (2017) clearly show a progress in this issue. However, it should be noted that until the 2011 earthquake swarm it was generally thought that the NK zone was of planar character, formed by a single fault. Three new activities, the earthquake swarms of 2011 and 2017 and the non-swarm sequence of 2014, presented a challenge to examine mutual locations of individual swarms and the non-swarm sequence and thus to disclose a more real pattern of the fault geometry in the NK zone. The dataset II was used for refined locating of all the NK zone events from 1997 to 2017 (I would note that considerable part of the P- and S-wave onsets of the 2011 a 2014 activities I picked myself). In the first step, I relocated all the 1991 – 2013 events by the NLLoc code (absolute location), thus I ensured a similar accuracy of the absolute locations in the dataset II (see Section 4.3.2). In the second step, I applied the hypoDD code to the dataset II (all events jointly relocated).

The space distribution of the foci of the earthquakes/microearthquakes in the main focal zone NK in the period 1997 – 2017 is given in Fig. 5.4. The spatial distribution is represented in a conventional projection used in the previous papers consisting of three sections (views): a map of epicenters (ground plan), a depth cross section (across the focal belt) and a section along the focal belt. The origin of coordinates corresponds to the location of the central WEBNET station NKC (latitude $\approx 50.232°$N, longitude $\approx 12.447°$E). Depth is related to an average elevation of the WEBNET stations ~ 655 m. The temporal distribution is depicted by the magnitude-time plot. In addition, the depth-time plot is added to show clearly depths of foci of the individual activities.

All the swarms form a continuous focal belt about 10 km long, striking in the north-south direction. The events are located in depths between 6 and 13 km, however the depth limit for earthquake swarms appears to be 11 km. The deeper foci are associated with microswarms or scattered events. Similar event depths

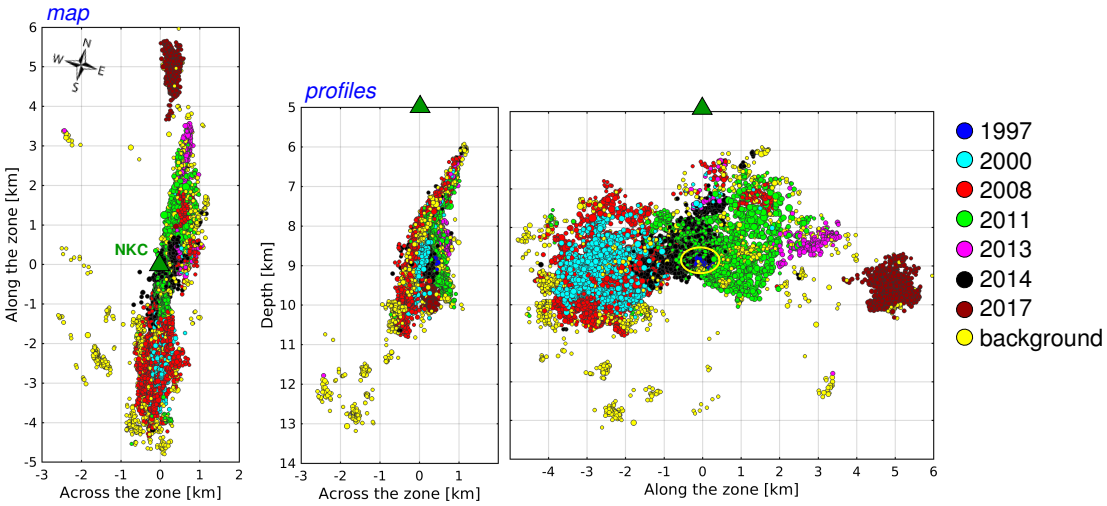

Figure 5.4: Spatial distribution of the earthquake swarms of 1997 (*dark blue dots* highlighted by *yellow ellipse*), 2000 (*light blue*), 2008 (*red*), 2011 (*green*) and 2013 (*violet*), the 2014 sequence (*black*), and the swarm of 2017 (*dark brown*) in the NK zone. *Yellow dots* indicate background activity in the time period of 1994–2017. The projection is represented by the map view *(left)* and two depth sections, across *(middle)* and along the focal belt *(right)*. The horizontal coordinates are rotated 15° clockwise from the north, the origin corresponds to the location of the central WEBNET station NKC *(green triangle)*.

have also been reported in the papers given above in the second paragraph. The focal belt indicates a hidden fault or rather a system of faults. In this context, we use the terms fault and fault plane in a general sense; fault segment and the smaller patch are parts of the fault delimited by hypocenters.

Figure 5.4 indicates that the NK zone comprises a number of fault segments which were separately activated by each West Bohemia activity. In a view of this segmentation we can distinguish northern and southern part of the NK zone having a center approximately below the central NKC station. The southern part was activated mainly in the 2000 and 2008 swarms (M_L3.3 and 3.8), whereas the northern part in the 2011 swarm (M_L3.7), 2013 "mini-swarm" (M_L2.3) and 2017 swarm (M_L3.1). Besides, the moderate 1997 swarm (M_L3.0) was also located in the northern part. The 2014 non-swarm sequence (M_L3.5, 4.4, 3.6) occurred just on the boundary of the northern and southern parts.

As can be seen from Figures 5.4 and 5.5, the 2000 and 2008 swarms took place on the same fault segment, which can be approximated by a single plane striking 166° and dipping 75° roughly of a circular shape with diameter of about 4 km (fault segment A in our notation). Similar results have been published by Fischer et al. (2010) who showed that the 2000 and 2008 hypocenters fall precisely on the same fault portion of the NK focal zone. It is worth noticing that in the very end of both swarms a small fault patch close to the northern tip of the fault segment A was activated. Although the 2000 and 2008 are very similar in terms of their locations, they fairly differ in their time course (Fig. 5.2). The 2008 swarm also showed much higher seismic-moment rate (Fig. 5.3) and the total seismic-moment released ($M_{0tot} \approx 2.15 \times 10^{15}$ Nm vs. 9.50×10^{14} Nm in the 2000 swarm).

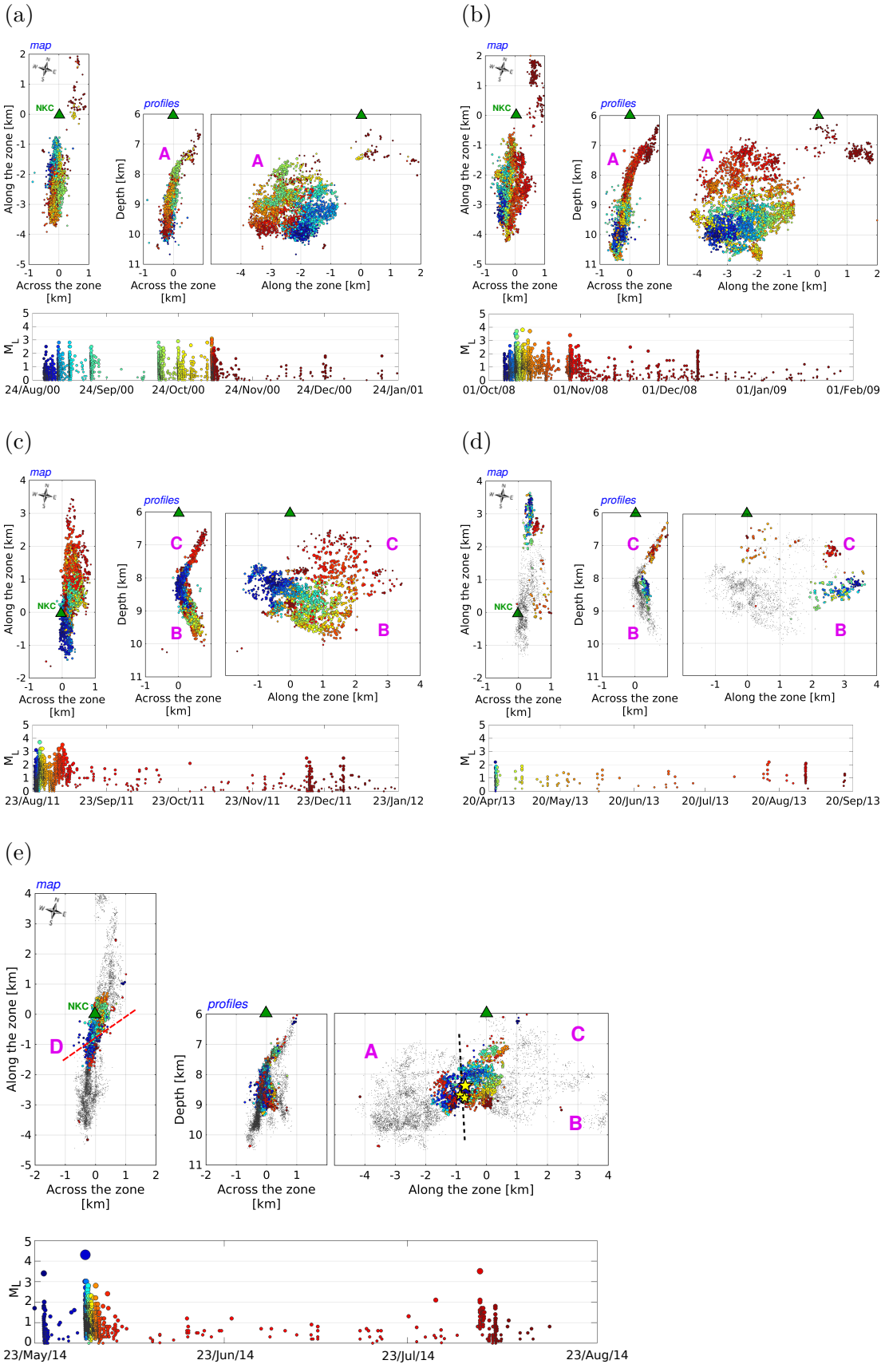
(a)
map
profiles
NKC
A
Along the zone [km]
Across the zone [km]
Depth [km]
M_L
24/Aug/00
24/Sep/00
24/Oct/00
24/Nov/00
24/Dec/00
24/Jan/01
(b)
01/Oct/08
01/Nov/08
01/Dec/08
01/Jan/09
01/Feb/09
(c)
B
C
23/Aug/11
23/Sep/11
23/Oct/11
23/Nov/11
23/Dec/11
23/Jan/12
(d)
20/Apr/13
20/May/13
20/Jun/13
20/Jul/13
20/Aug/13
20/Sep/13
(e)
D
23/May/14
23/Jun/14
23/Jul/14
23/Aug/14

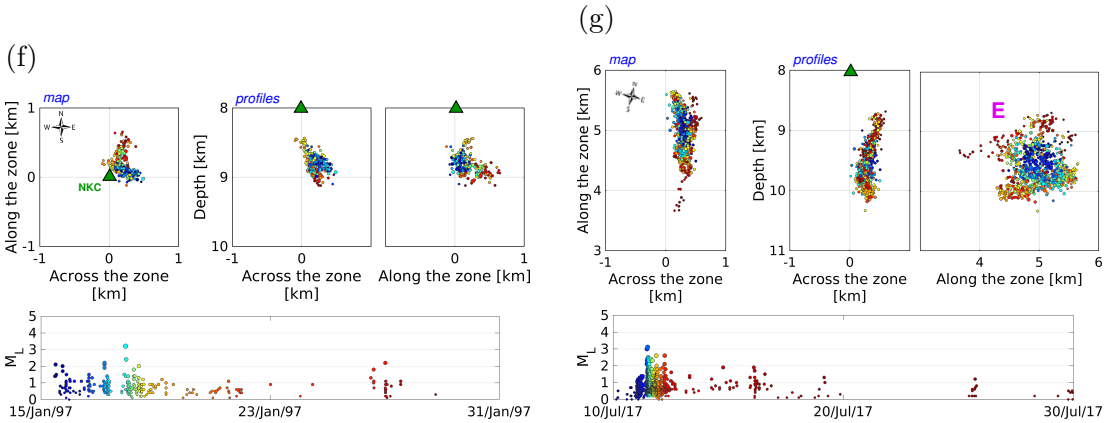

Figure 5.5: Spatio-temporal distribution of events in the West Bohemian swarms of 2000 (a), 2008 (b), 2011 (c), 2013 (d), the 2014 sequence (e), and the swarms of 1997 (f) and 2017 (g). Colour coding is proportional to the origin time. In (a) – (g): *Top* - Distribution of hypocenters (coloured dots) represented by the map view (*left*) and two depth sections, across (*middle*) and along the focal belt (*right*). A, B, C, D and E denote fault segments which are bounded by hypocenter clusters. In (e), the *yellow stars* show locations of the three 2014 mainshocks, the *black dashed line* denotes the boundary between the southern and northern part of the NK zone. The horizontal coordinates in (a), (b), (e) and (g) are rotated by 15° clockwise, in (b) and (c) by 9° clockwise (i.e. by an angle that equals the strike of the focal belt). The axes are scaled in km, the origin of the horizontal axes corresponds to the location of the central WEBNET station NKC which is marked by a *green triangle* (latitude ≈ 50.23°N, longitude ≈ 12.45°E). *Pale-gray dots* in (d) mark the 2011 hypocenters, in (e) the 2000, 2008 and 2011 hypocenters. *Bottom* - Time course of the swarm activity in the magnitude-time plot.

The pattern of geometry of the NK zone was markedly changed after the 2011 swarm. Event locations of this swarm disclosed two separately dipping clusters of a corner-like shape in the northern part of the NK. Their narrow width points to their planar character (fault segments B and C; see Fig. 5.5). The plane striking approximately 351° and dipping to about 72° eastwards fits segment B best, whereas the plane striking 171° and dipping 63° westwards fits segment C best. The size of both segments is similar, roughly 4×2 km. Segments B and C were partly activated during the 1997 swarm, and then during the 2013 mini-swarm which occurred on patches of both segments (B and C, Fig. 5.5). Therefore, the 2013 mini-swarm can be considered as a complement of the swarm of 2011. The 2011 swarm was comprised of two distinct phases (Fig. 5.2) corresponding to the activity on segments B and C. The seismic moment rate is similar to that in the 2008 swarm (Fig. 5.3), the total seismic moment released is $M_{0tot} \approx 1.86 \times 10^{15}$[Nm], which is a bit lower when compared to M_{0tot} of the 2008 swarm. More details about the 2011 swarm and geometry of segments B and C are given in Čermáková and Horálek (2015).

(a)

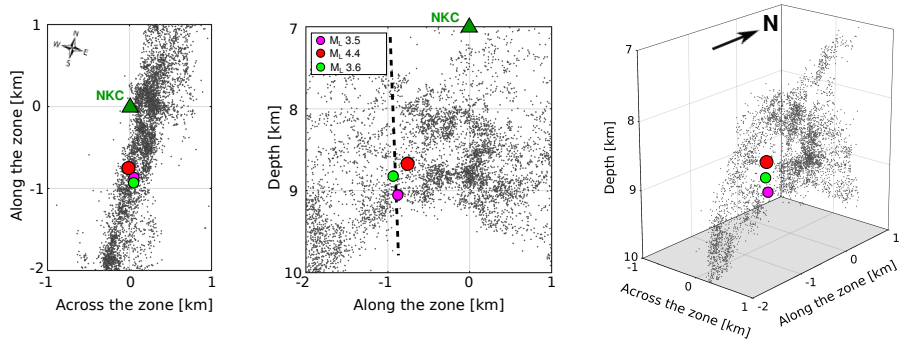
NKC
Along the zone [km]
Across the zone [km]
Depth [km]
Along the zone [km]
M_L 3.5
M_L 4.4
M_L 3.6
N
Depth [km]
Across the zone [km]
Along the zone [km]

(b)

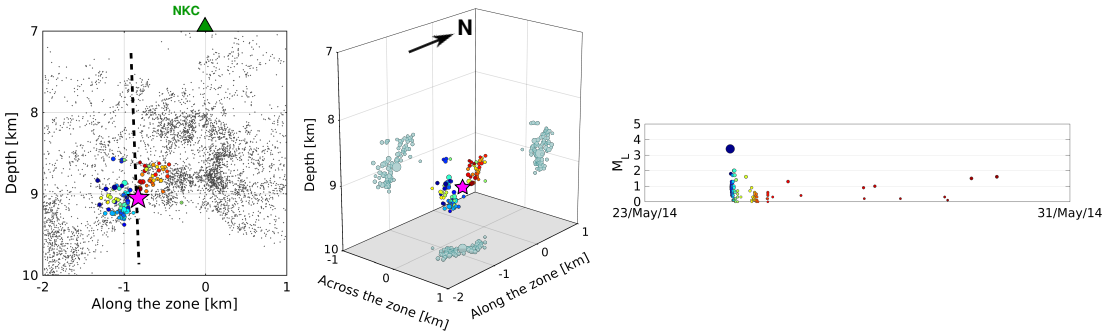
NKC
Depth [km]
Along the zone [km]
N
Depth [km]
Across the zone [km]
Along the zone [km]
M_L
23/May/14
31/May/14

(c)

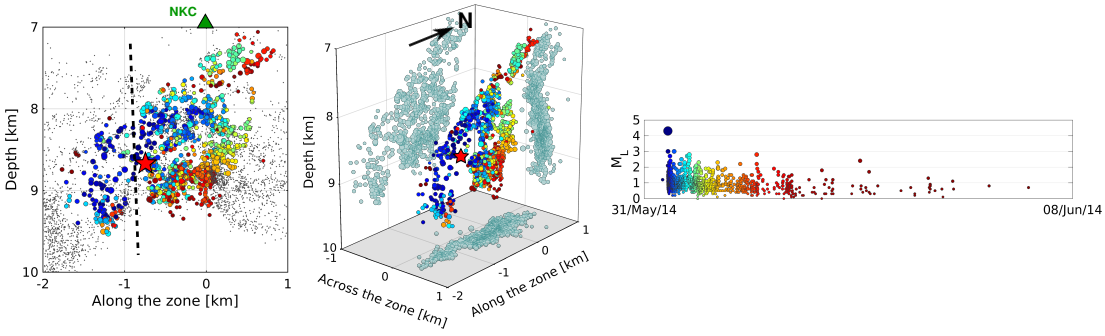
NKC
Depth [km]
Along the zone [km]
N
Depth [km]
Across the zone [km]
Along the zone [km]
M_L
31/May/14
08/Jun/14

(d)

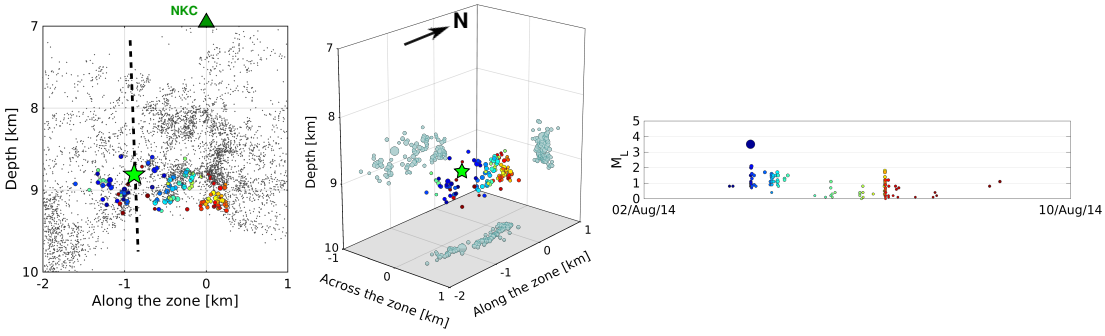
NKC
Depth [km]
Along the zone [km]
N
Depth [km]
Across the zone [km]
Along the zone [km]
M_L
02/Aug/14
10/Aug/14

Figure 5.6: (a) Locations of the 2014 mainshocks of M_L3.5 (*violet*), M_L4.4 (*red*) and M_L3.6 (*green*) depicted by the map view (*left*), depth section along the focal zone (*middle*) and 3D view (*right*). (b) to (d) Space-time event distribution (*colour-coded dots*) for the individual M_L3.5 (b), M_L4.4 (c) and M_L3.6 (d) episodes. The spatial distribution of the foci for each episode is delineated by the depth section along the focal zone (*left*), and 3D view (*middle*) supplemented by projection onto three perpendicular planes (*light blue dots*). *Grey dots* - foci of the 2000, 2008 and 2011 swarms; *black dashed line* - the boundary between the southern and northern part of the NK zone. The temporal distribution of the foci is depicted by the magnitude-time plot (*right*).

The 2014 mainshock-aftershock activity revealed a small (in terms of size) but significant fault segment or rather a fault barrier, termed D, which is situated in the transition zone between the southern and northern parts of the NK focal zone, i.e. among fault segments A, B and C (Figs. 5.4 and 5.5). The transition zone was active only rarely, e.g., at the microearthquake level, before the 2014 activity (at least in the previous 27 years of West Bohemian seismic observations).

Segment D is mainly defined by the three M_L3.5, 4.4 and 3.6 mainshocks (Tab. 5.4 and Fig. 5.6) because the majority of aftershocks of all the three mainshocks are scattered in fault segments A, B, and C (see Fig. 5.6). Therefore, the geometry of segment D was estimated from the focal mechanisms of the mainshocks and proved by calculating an equation of the plane defined by the mainshocks hypocenters. This way I found that the plane striking ∼40°E and dipping ∼60° to SE may be an approximation of segment D.

Mainshock	Date	Origin time (UTC)	M_L	LT [°N]	LN [°E]	D [km]
M_L3.5	2014-05-24	14:35:35.49	3.5	50.225	12.451	9.04
M_L4.4	2014-05-31	10:37:20.99	4.4	50.226	12.450	8.66
M_L3.6	2014-08-03	23:58:40.38	3.6	50.224	12.451	8.81

Table 5.4: Origin times, locations and local magnitudes of the three mainshocks. Note that the location is relative, therefore it can differ from the absolute location in the order of first hundreds of meters.

Mutual distances among the mainshocks are $|M_L4.4\ M_L3.5| = 410\,\mathrm{m}$, $|M_L4.4\ M_L3.6| = 240\,\mathrm{m}$, and $|M_L3.5\ M_L3.6| = 240\,\mathrm{m}$. Figure 5.6 shows that each mainshock is surrounded by a seismic gap without aftershocks, which may indicate the rupture area. To verify this idea I performed a rough estimate of the rupture area by two fully independent formulas: (i) the formula by Madariaga (1976) for a circular source:

$$r = kv_rT_d, \tag{5.4}$$

where r is radius of the source, k is a model dependent constant, v_r is the rupture velocity, and T_d is duration of the pulse of the direct P wave, and (ii) the formula by Michálek and Fischer (2013) based on the source spectra of the West Bohemian events which relates the rupture radius r to seismic moment M_0:

$$r = 0.155M_0^{0.206}. \tag{5.5}$$

In (i), the constant k for a circular source and P waves is $k = 0.32$ (Madariaga, 1976), the rupture velocity was assumed to be $v_r = 3000\,\mathrm{m/s}$, and T_d was measured on the vertical component in the displacement seismograms and taken as an average value from all the stations used. In (ii), the seismic moments $M_0 \approx 8.0 \times 10^{14}\,\mathrm{Nm}$, $1.1 \times 10^{14}\,\mathrm{Nm}$ and $9.0 \times 10^{13}\,\mathrm{Nm}$ for the M_L4.4, 3.6 and 3.5 mainshocks were estimated using the relation M_0 vs. M_L (4.6). The estimated radii for the M_L4.4, 3.6 and 3.5 mainshocks based on formula (i) and (ii) are shown in Table 5.5.

Formula	M_L4.4	M_L3.6	M_L3.5
Madariaga (1976)	150	120	130
Michálek and Fischer (2013)	180	120	115

Table 5.5: Estimated radii in meters for the M_L4.4, 3.6 and 3.5 mainshocks based on formula by Madariaga (1976) and by Michálek and Fischer (2013).

I am aware of a simplified estimation of the size of the seismic source using the formulas (i) and (ii). However, the radii of the rupture areas estimated by the two formulas agree quite well, so they are enough for getting an idea about size of the rupture area. Besides, the estimated radii of the ruptures of the three mainshocks are comparable to the distances between the events' hypocenters, being of the order of a few hundreds of meters. It implies that the mainshocks served in fact as three-step rupturing of a barrier (segment D) which was a bridge among fault segments A, B and C (dashed line in Fig. 5.5e).

The locations of the 2014 aftershocks are the issue. Unlike standard aftershocks that occur randomly along the edges of the mainshock rupture, the 2014 aftershocks occurred not on the mainshock fault D but beyond it along the preexisting oblique fault segments A, B and C. This indicates that the 2014 mainshock-aftershock sequence is rather untypical in relation to common mainshock-aftershock seismicity observed at plate boundary faults.

The total seismic moment released during the entire 2014 activity is $M_{0tot} \approx 1.58 \times 10^{15}\,\mathrm{Nm}$ which corresponds to a M_L4.6+ single event. The three 2014 mainshocks (M_L3.5, 4.4 and 3.6) and the M_L4.4 mainshock itself represent 66% and 54% of the total seismic moment released, respectively. More details about the 2014 non-swarm activity and its comparison with the previous swarms are given in Jakoubková et al. (2017).

The 1997 swarm was the first larger West Bohemia/Vogtland earthquake activity after the intense M_L4.6 swarm of 1985/86 and the first one recorded by the WEBNET network. It was investigated from several perspectives, e.g., space-time distribution of events by Fischer and Horálek (2000), source mechanisms by Horálek et al. (2002) and its scenario by Horálek et al. (2000b), but without any relations to other activities in the NK zone. The swarm took place on a corner-like patch (Fig. 5.5) in the NK transition area. As can be seen from Fig. 5.4, the patch is located inside and on the edge of segment B (yellow ellipse in Fig. 5.4).

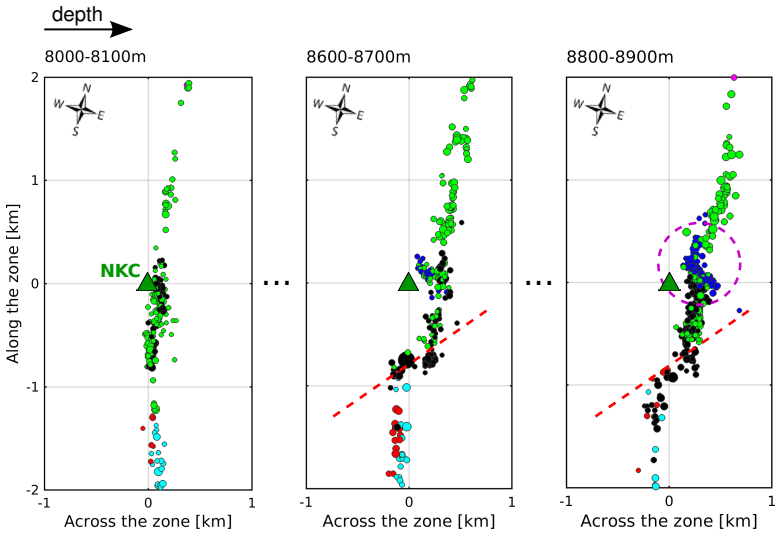

Figure 5.7: Distribution of the foci in the transition area between fault segments A, B and C represented by three horizontal sections at depths of 8000-8100 m (above the 2014 mainshocks), 8600-8700 m and 8800-8900 m (corresponding to depth of the M_L 4.4 and 3.6 mainshocks). The colour-coding matches that in Fig. 5.4. Note a fault jog (middle and right sections) separating the northern segments B and C from the southern segment A being bridged by a fault barrier D (*black dots*). *Red line* - the strike of the barrier indicated by focal mechanisms of the 2014 mainshocks. *Violet dashed circle* highlights a short segment which hosted the 1997 and 2011 swarms, and the 2014 activity.

Figure 5.7 depicts the transition area in detail by means of three horizontal sections in depths between 8000 and 8900 m. It is clear that the transition area is partitioned into several segments; interestingly, some of them were repeatedly activated, namely during the swarms of 1997 and 2011 and the 2014 activity (aftershocks). The sections at depths of 8600 – 8700 m and 8800 – 8900 m nicely show that the corner-like patch of the 1997 swarm represents a distinct offset between southern and northern parts of the NK focal zone. The 1997 swarm was rather anomalous. It contained one dominant M_L3.0 earthquake and notably small number of weaker events, only 500 events with $M_L \geq 0$. Accordingly, a cumulative seismic moment $M_{0tot} \approx 7.60 \times 10^{13}$ Nm is also rather small.

The recent M_L3.1 swarm in July 2017 was specific because of its location and a high rate of the seismic moment release. The swarm events were located in the very north of the NK zone, off the focal belt. The focal cluster indicates a separate, about 2 km long fault segment at depths between ∼8.5 and 10.3 km (Fig. 5.4). This new segment, termed E, can be approximated by a single plane striking 165° and dipping 75°, i.e. having practically the same orientation as segment A (see Fig. 5.5). The 2017 swarm showed a fairly high rate of the seismic moment release, even higher than that in the 2014 mainshock-aftershock sequence. The total seismic moment released is $M_{0tot} \approx 3.41 \times 10^{14}$ Nm (more than one third of M_{0tot} in the 2000 swarm), about 80% of them released in short-time episode (lasting less than one day), mostly in a few largest events.

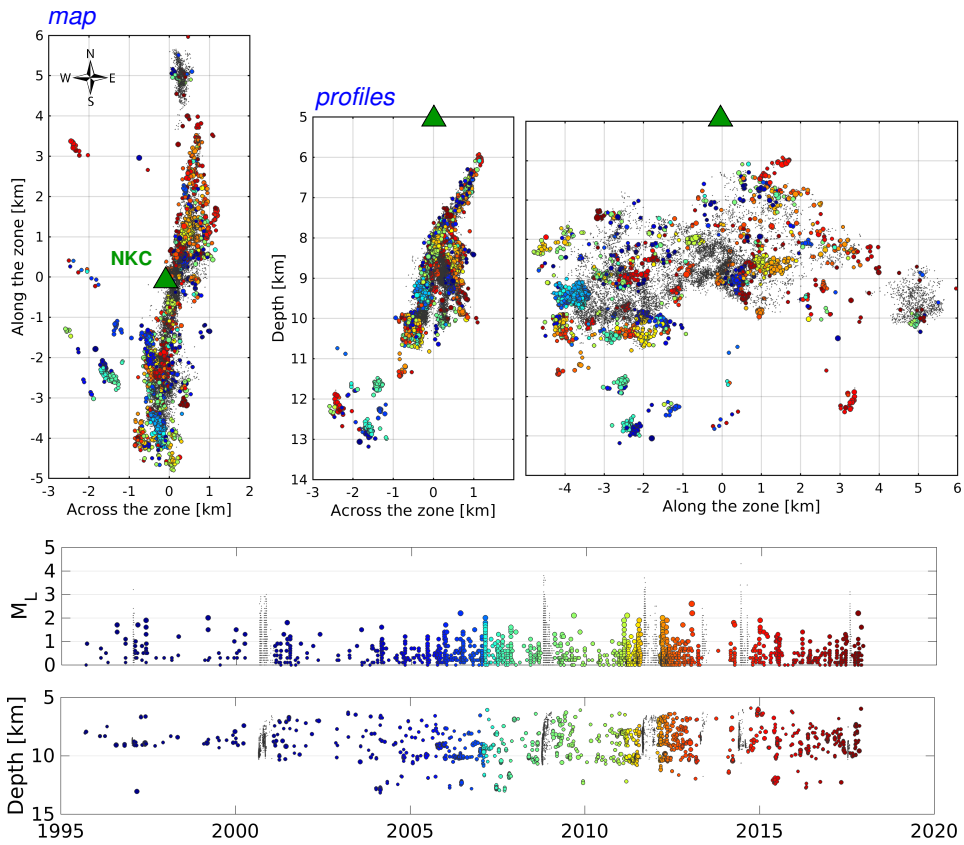

Figure 5.8: Spatio-temporal distribution of events of background seismicity in the NK zone in period 1995 – 2017. *Top* - Distribution of hypocenters (coloured dots) represented by the map view (*left*) and two depth sections, across (*middle*) and along the focal belt (*right*). The axes are scaled in km, the origin of the horizontal axes corresponds to the location of the central WEBNET station NKC which is marked by a *green triangle* (latitude ≈ 50.23°N, longitude ≈ 12.45°E). *Pale-gray dots* mark hypocenters of the West Bohemian swarms of 1997, 2000, 2008, 2011, 2017, and the 2014 activity. *Middle* - Time course of the swarm activity in the magnitude-time plot. *Bottom* - Time course of the swarm activity in the depth-time plot.

Furthermore I analysed space-time distribution of the swarm-like activity and single events on the microearthquake level (called background seismicity) in the NK zone in the time period September 1995 to November 2017. The previous studies on the background seismicity in the NK zone comes from Fischer and Horálek (2003) and Fischer and Michálek (2008). Figure 5.8 shows that background seismicity in the NK zone is persistent comprising a large number of swarm-like episodes (see magnitude-time plot in Fig. 5.8). The background seismicity is mainly scattered inside the whole focal belt of the earthquake swarms and occurred in small patches of each fault segment (A to E), some of them were reactivated in the period concerned. A minor part of the background seismicity (mostly of the swarm-like episodes) is extended into greater depths when compared to the earthquake swarms, the locations of these episodes indicate a prolongation of the fault segment A down to depths of 13 km (see the cross-section in the middle panel in Figure 5.8).

These analyses allowed me to construct a scheme of the fault structure in the

main focal zone NK. The first version of it is given in Jakoubková et al. (2017), an updated one (complemented by the fault segment E) is presented in Fig. 5.9. The scheme shows only the major fault segments where the majority of seismic moment has been released, eliminating the patches activated in the 1997 swarm and the background seismicity. I believe this scheme will be beneficial for continued broader research into the West Bohemia/Vogtland swarms. The analyses of the West Bohemian earthquake swarms also point to a gradual northward trend in migration of the swarm activity in the NK zone. As for migration of events, it differs substantially in the individual swarms, so I did not succeed in finding any trends in migration of the swarm activity.

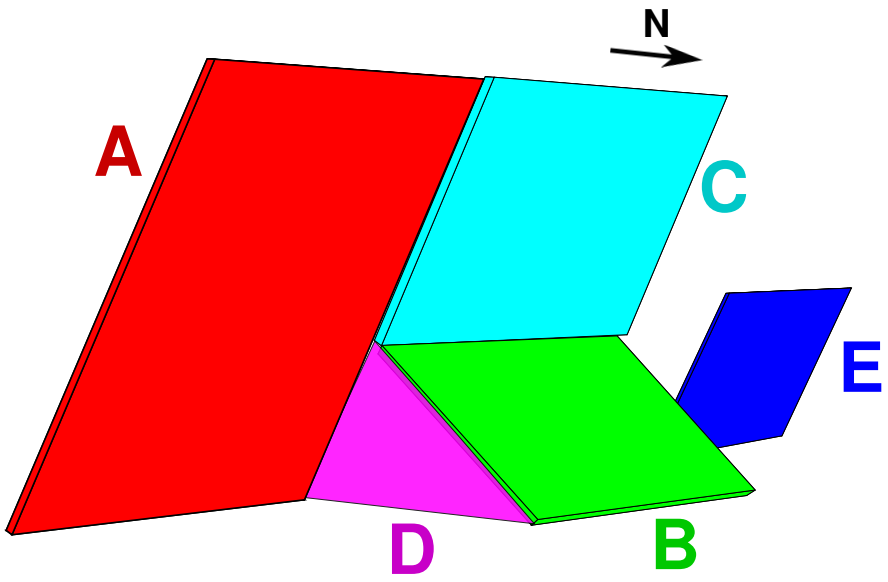

Figure 5.9: Basic scheme of the NK focal zone. Segment A (*red*) was triggered in the 2000 and 2008 swarm, segments B and C (*green and light blue*) in the 2011 swarm, segment/barrier D (*violet*) in the 2014 sequence, and segment E (*blue*) in the 2017 swarm.

5.4 Earthquake swarms in Southwest Iceland from the space-time event distribution point of view

The earthquake swarms in Southwest Iceland, unlike those in West Bohemia/Vogtland, have not been investigated systematically or in more details yet. The reason is that they do not pose a higher seismic risk for local inhabitants in contrast to strike-slip earthquakes from the South Iceland Seismic Zone (SISZ) (Sólnes et al., 2004); logically the SISZ earthquakes are the main topic of interest of seismologists. In depth studies of the Southwest Icelandic earthquake swarms are sporadic in international scientific journals (e.g., Tryggvason, 1973; Keiding et al., 2009), so it is not easy to compare my results with any previous ones. Besides, I had the use of limited catalogue data containing only four Southwest Iceland swarms, and the 2017 Krísuvík swarm which was the first larger activity on the Reykjanes Peninsula (RP) since the starting of the REYKJANET observations. So I was

able to examine the space-time event distribution of the individual swarms without possible interrelations between some of them. Hence, the following analyses are less detailed than those of the West Bohemian earthquake activities; they basically represent an initial step to a deeper understanding of the structure of the Southwest Icelandic earthquake swarms.

For analysing the 1997 Hengill, 1998 Ölfus and 2003 Krísuvík swarms I used the SIL catalog (dataset III). The errors of the absolute locations (in the SIL velocity model) are less than 350 m in the horizontal coordinates and 1000 m in depths, relative location errors are less than 100 m in the horizontal coordinates and 200 m in depths (Dr. Gunnar B. Guðmundsson, IMO, personal communication). The 2017 Krísuvík swarm events are located in the same way as the West Bohemian ones: the absolute locations applying the NLLoc code to the REYKJANET data (dataset IV) and their refinement by the hypoDD code. In order to preserve compatibility I used the SIL velocity model.

The maximum errors of the absolute locations are $\sim$250 m in the horizontal coordinates and 500 m in depths, relative location errors are about 50 m in hor-

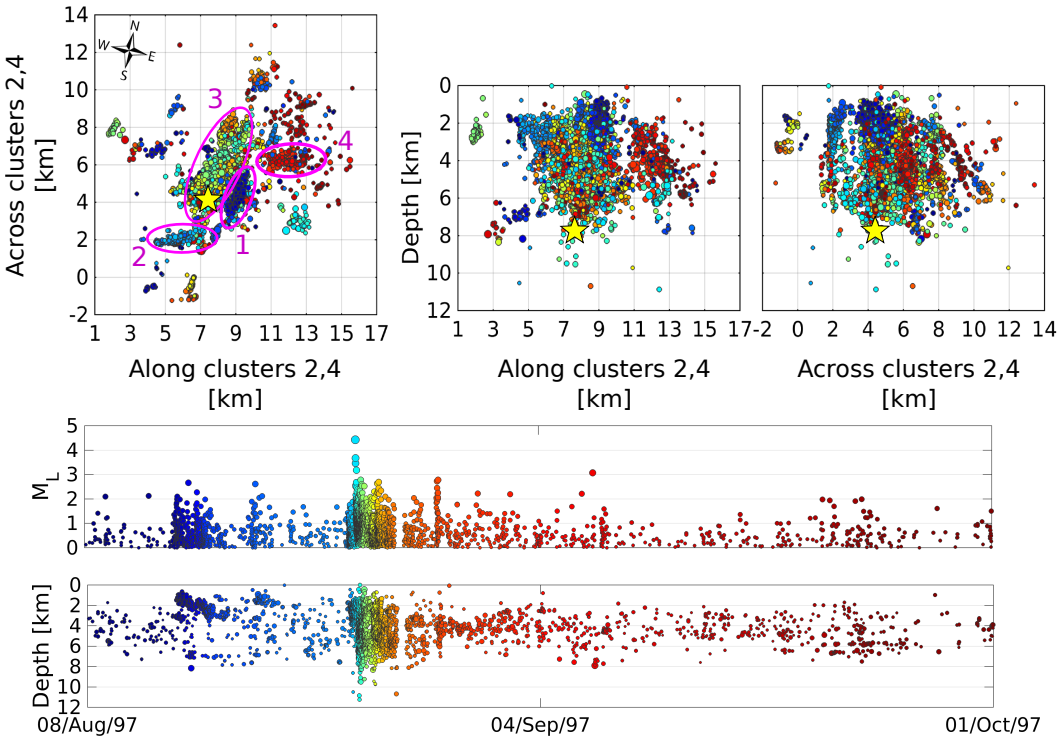

Figure 5.10: Spatio-temporal distribution of events of the Hengill swarm in 1997. Colour coding is proportional to the origin time. *Top* - Distribution of hypocenters (coloured dots) represented by the map view (*left*) and two depth sections, from the south (*middle*) and east (*right*). *Violet numbers* 1 – 4 denote event clusters delineated by *violet ellipses*, which were activated successively during the swarm. The *yellow star* shows location of the strongest event (M_L4.4). The horizontal coordinates are rotated by 13° clockwise (i.e. by an angle that enables distinguishing the event clusters). The axes are scaled in km, the origin of the horizontal axes corresponds to the minimum latitude and longitude of the depicted dataset. *Middle* - Time course of the swarm activity in the magnitude-time plot. *Bottom* - Time course of the swarm activity in the depth-time plot.

izontal and 100 m in vertical coordinates. The results are given in Figures 5.10 (Hengill of 1997), 5.11 (Ölfus of 1998), 5.12 (Krísuvík 2003) and 5.13 (Krísuvík 2017). It is obvious that all these swarms are significantly shallower when compared with the West Bohemia ones. The foci of the 1997 Hengill, 1998 Ölfus and 2003 Krísuvík swarm events are located already at depth less than 1 km, however, the shallowest foci might be outliers remaining in the SIL catalogs. The locations of the 2017 Krísuvík events, which I checked for potential outliers, show the shallowest events at depth of 1.5 km. My first results indicate the depth limit for the swarm earthquakes is $\sim 6-7$ km on Reykjanes Peninsula (along the MAR), 8 km in the Hengill volcanic complex, and 10 km in Ölfus area (transition zone between Hengill and SISZ) which is situated apart from the MAR. The patterns of the space-time distribution of the individual earthquake swarms significantly differ but one feature is common: the most of the total seismic moment M_{0tot} in each swarm was released in one short-term phase including a few dominant events (see Figs. 5.3a right, and 5.10 – 5.13). I would like to note that similar specificity was also observed for the 2017 West Bohemia swarm (Fig. 5.3a left and 5.5g).

The swarm in Hengill (M_L4.4) and a subsequent swarm in Ölfus (M_L4.9) are located in close proximity to one another (Fig. 5.14), the Ölfus swarm was a continuation of the 1997 Hengill activity. I would note that a similar scenario had occurred in 1994 – 1995. The space-time distribution of the swarm in Hengill (Fig. 5.10) reflects a big complexity of this volcanic complex which represents a triple junction of two rift zones (Reykjanes Peninsula and Western Volcanic Zone) and the transform shear zone of the South Iceland Seismic Zone (SISZ). The magnitude-time plot indicates several swarm phases, some of them ran simultaneously, which took place on several different fault segments; at least four main phases can be distinguished. The dominant phase, in which most of seismic moment released, corresponds to the N-S striking fault segment 3.

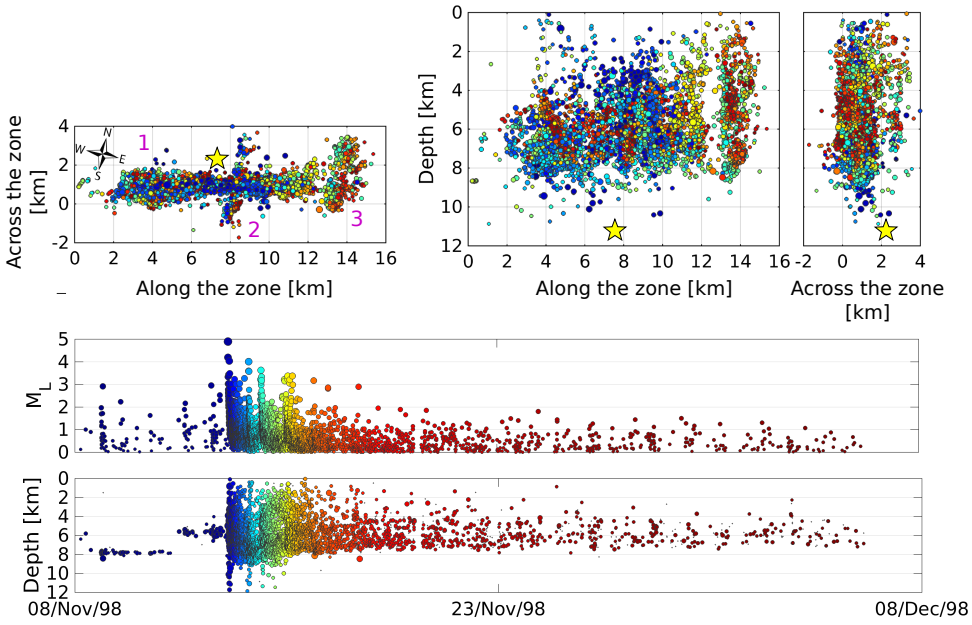

Figure 5.11: Spatio-temporal distribution of events of the Ölfus swarm in 1998. For the figure arrangement, projection and colour coding see Fig. 5.10. Location of the strongest event of M_L4.9 is shown by *yellow star*.

The M_L4.9 Ölfus swarm was located in the transition area among the eastern Reykjanes Peninsula, Hengill complex and SISZ. It was fairly intensive and lasted about one month; the total seismic moment released, $M_{0tot} \approx 1.88 \times 10^{16}$ Nm, is roughly by one order higher than M_{0tot} of the West Bohemia swarms in 2008 and 2011. The size of the focal belt, about 13 km in the EW direction (Fig. 5.11), is larger than the size of the whole focal zone NK in West Bohemia. The focal cluster is quite simple and indicates three differently oriented faults/fault segments (marked 1, 2, 3 in Fig. 5.11) which were activated during the swarm. The cross-section in Figure 5.11 (the upper right box) indicates nearly vertical dip of all the tree faults. The map of epicenters (the upper left box in Figure 5.11) shows an intersection of the ENE-WSW and N-S striking faults (conjugate faults 1 and 2 in Fig. 5.11), which is quite important result.

According to Einarsson (2010), the N-S striking faults in the SISZ/Ölfus region are liable for larger strike-slip earthquakes; it is worthy of notice that one of the mainshocks (M_{Lw}6.3) of the 2008 activity was located on the eastern edge of the fault segment 3. Moreover, the spatial distribution of the 1998 swarm events corresponds well to the distribution of the 2008 aftershocks (e.g., Brandsdóttir et al., 2010; Khodayar and Björnsson, 2014; Li, 2017). It may signify that the N-S striking faults in the area concerned are liable to stronger mainshock-aftershock activities, while the ENE-WSW faults are predisposed to earthquake swarms. Nevertheless, the location of a dominant M_L4.9 earthquake under the main focal cluster is an enigma. It might be due to the erroneous location, but unfortunately, I am not able to check it because I do not have the original seismograms. Other explanation is that the M_L4.9 earthquake was a mainshock located on a hidden N-S fault off the main focal cloud which triggered swarm-like seismicity on the ENE-WSW fault (marked 1-2) and at last the N-S fault segment 3. This idea is supported by the scenario of the 2008 Ölfus activity.

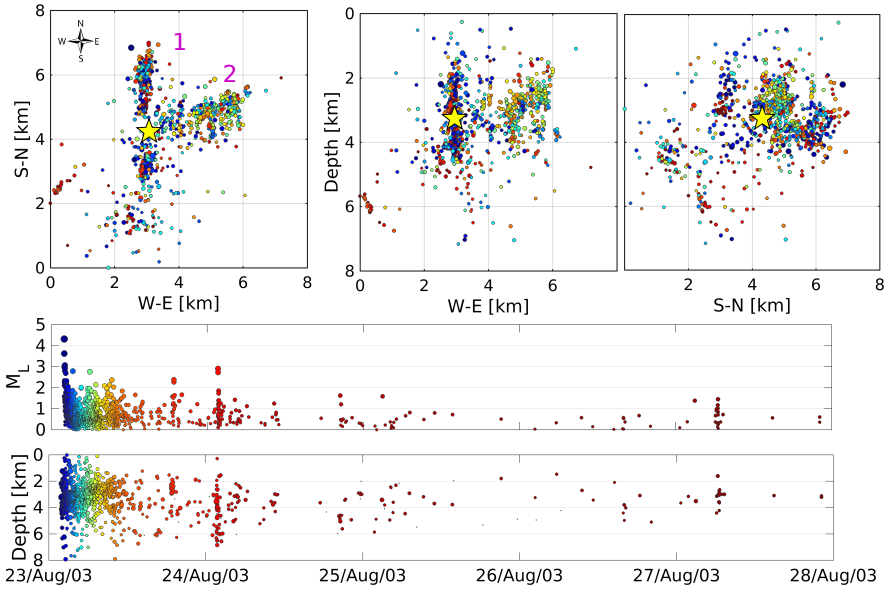

Figure 5.12: Spatio-temporal distribution of events of the Krísuvík swarm in 2003. For the figure arrangement, projection and colour coding see Fig. 5.10; the only difference is that the horizontal coordinates are not rotated. Location of the strongest event of M_L4.3 is shown by *yellow star*.

The 2003 a 2017 Krísuvík swarms were located near each other, at a distance of about 5 km (see Fig. 5.15), but the sites may tectonically differ. The 2003 swarm was located in the Krísuvík geothermal field, whereas 2017 swarm beneath the Fagradalsfjall volcano. The 2003 swarm (M_L4.3) is the most intense activity in terms of the total seismic moment released which I have investigated in my thesis. Its $M_{0tot} \approx 3.09 \times 10^{16}$ Nm corresponds to the moment magnitude (by Kanamori, 1977) of an equivalent single earthquake with $M_w = 4.9$. M_{0tot} of the 2017 swarm (M_L3.9) is by more than one order lower; its value of $\approx 1.48 \times 10^{15}$ Nm corresponds to $M_w = 4.0$ single event, and so it is comparable to M_{0tot} of the West Bohemian non-swarm activity in 2014.

However, both these swarms show a markedly small number of the $M_L \geq 0$ events (event productivity a), particularly that of 2003; for comparison with other Southwest Icelandic and West Bohemian swarms see Tables 1.1 and 1.2. A notably small event productivity of the Krísuvík swarms relative to the other ones is nicely manifested in the MFD plots in Figure 5.1a. Besides, both swarms exhibit very high rate of the seismic moment release, most of it released at the very beginning of each swarm (see Fig. 5.3b). In this respect both Krísuvík swarms point to the mainshock-aftershock activity.

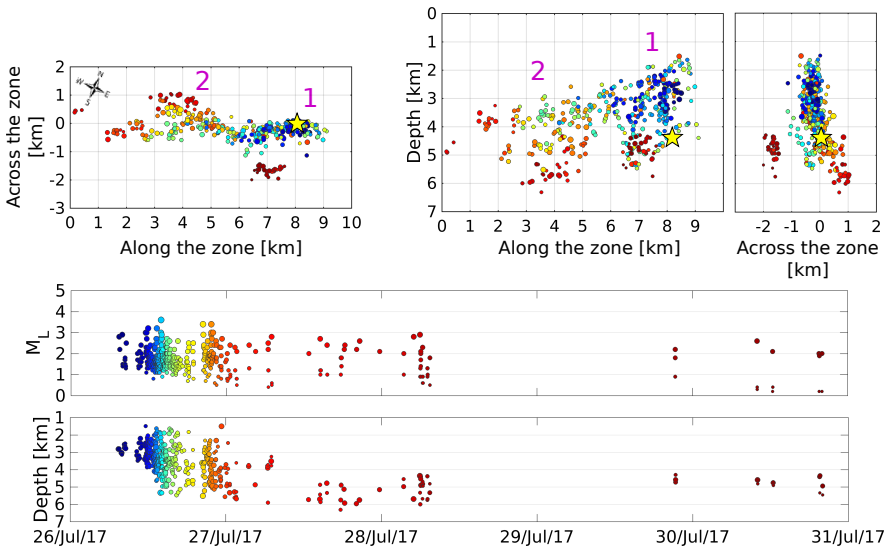

Figure 5.13: Spatio-temporal distribution of events of the Krísuvík swarm in 2017. For the figure arrangement, projection and colour coding see Fig. 5.10; the only difference is that the horizontal coordinates are rotated by 23° clockwise. Location of the strongest event of M_L3.9 is shown by *yellow star*.

Prevailing depths of the foci of both 2003 and 2017 swarms are between 2 and 5 km; the dominant events are located at depth of about 4 km (i.e. much smaller depth than those in the Hengill and Ölfus swarms). The focal clusters in Figures 5.12 and 5.13 indicate two active faults/fault segments in each swarm. The 2003 swarm took place on two differently oriented faults: the primary one (marked 1) striking N-S and the secondary one striking EN-WS (marked 2 in Fig. 5.12), the dominant earthquake occurred at their crossing. The major swarm phase (in terms of the seismic moment released) occurred on the fault 1 which triggered subsequently the activity on the fault 2. The two disclosed faults correspond very well with the tectonic pattern of the Reykjanes Peninsula that show a series

of N-S oriented faults with typical spacing of 1 km or less and large number of NE-SW trending volcanic fissures (Clifton and Kattenhorn, 2006; Einarsson, 2008). According to Árnadóttir et al. (2004) the system of N-S striking faults appears to be responsible for most of recent larger earthquakes on the peninsula. Correspondence between the fault segment 2 and the topography of the Krísuvík area is nicely demonstrated in Figure 5.15.

However, the space-time distribution of the 2017 swarm fairly differs from that of the 2003 one. The 2017 activity started at the eastern margin of the ENE-WSW trending and steeply dipping fault (1 in Fig. 5.13) and migrated gradually westwards. Subsequently a contiguous E-W striking fault was activated (2 in Fig. 5.13). The faults 1 and 2 are parallel or nearly parallel with the ENE-WSW trending MAR plate boundary on the central Reykjanes Peninsula (RP). This is quite important finding because the previous M_L3.0 swarm in 2009 in the Fagradalsfjall area occurred on the N-S faul(s) (Li, 2017). Besides, the E-W and ENE-WSW oriented seismogenic structures on the RP have not been reported in a commonly available literature, yet. But I would note that Keiding et al. (2009) examined fault orientations predisposed to a rupture in a modelled tectonic stresses on the RP at depth of 4 km, which was estimated based of GPS velocities, and inferred that also ENE-WSW oriented faults might be in some cases seismogenic ones. It suggests that the Reykjanes Peninsula is a challenging area for investigating relations between local tectonics and earthquake swarms.

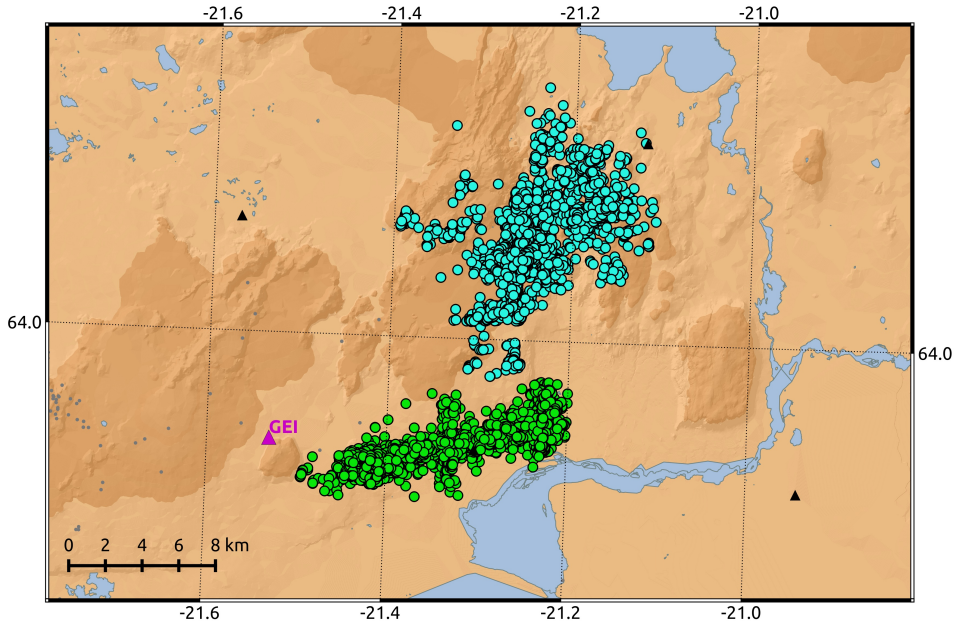

Figure 5.14: Space distribution of swarm events in Hengill in 1997 (*light blue circles*) and in Ölfus in 1998 (*green circles*). *Violet triangles* denote seismic stations of the local REYKJANET network, the smaller *black triangles* represent stations of the regional SIL network.

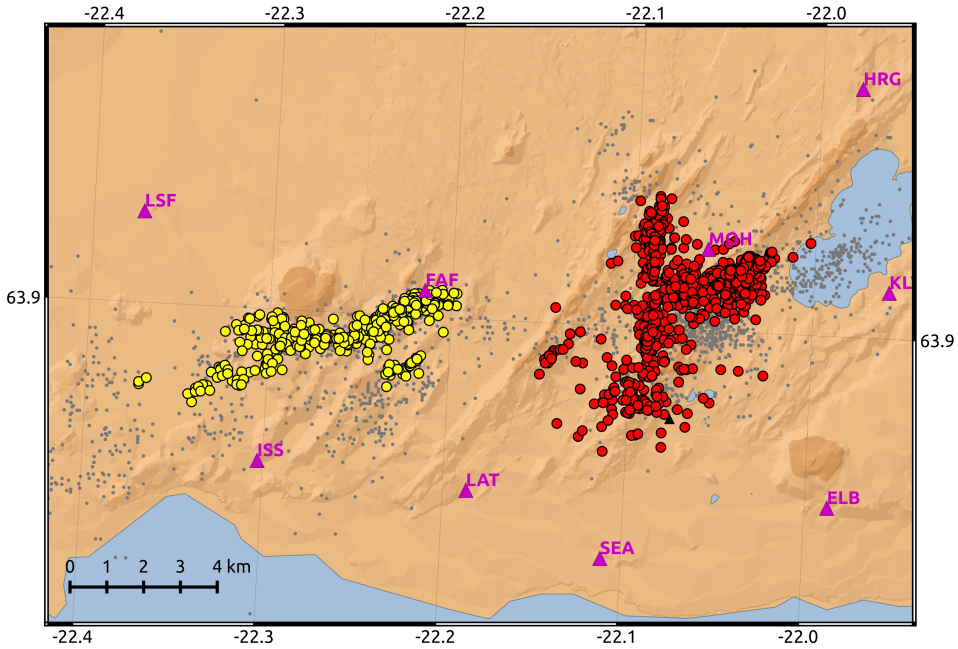

Figure 5.15: Space distribution of swarm events Krísuvík in 2003 (*red circles*) and in 2017 (*yellow circles*). *Violet triangles* denote seismic stations of the local REYKJANET network, the smaller *black triangles* represent stations of the regional SIL network.

5.5 Focal mechanisms in West Bohemia

The results given in the previous Section raise the question of whether geometry of the individual faults (fault segments) in the NK zone agrees with prevailing focal mechanisms in the respective activities. As for the mechanisms in the 1997 and 2000 swarms I utilized the moment tensors (MTs) studies by Horálek et al. (2002) and Horálek and Šílený (2013) and used double-couple (DC) components of resultant MTs retrieved in the two studies.

To estimate the prevailing focal mechanisms in the swarms of 2008, 2011 and 2017 and mechanisms of the 2014 mainshocks, I used the AMT code by Vavryčuk (2011). It inverts P-waves ground displacement amplitudes on the vertical component and provides the full moment tensor. The code also includes the computation of the Green's function for each event. The same velocity model as for locations is used (modified model of Málek et al., 2005). I selected 55 $M_L \geq 2.0$ events of the 2008 swarm, 129 $M_L \geq 2.0$ events of the 2011 swarm, three mainshocks (M_L 3.5, 4.4, 3.6) of the 2014 non-swarm sequence and two dominant events of the 2017 swarm (M_L 3.1 and 3.0). I used data from 12 to 22 stations for each event. The ground-displacement peak amplitudes of the P-waves of the 2008 events had been extracted previously by J. Horálek for his analyses, and those of 2011 and 2014 were picked automatically by the software package SeisMon (Doubravová and Horálek, 2013), supervised by an interpreter. Though the full moment tensors are calculated in the AMT code, I used only their DC components.

Detailed tests of stability of the 1997 and 2000 source mechanisms are given in

Horálek et al. (2002) and Horálek and Šílený (2013). Regarding the 2008, 2011, 2014 and 2017 mechanisms, the stability of the DC components was verified by applying the jack-knife technique to the MT solutions. I computed moment tensors from the subset of the data with one or few stations removed and observed the effect on the strike, dip, and rake angles. Only stable solutions have been taken into account. So I determined 65 focal mechanisms for the 2008 swarm (segment A), 129 for the 2011 swarm, 85 of them for segment B and 44 for segment C, mechanisms of the three 2014 mainshocks which determine segment D, and of the two largest events in the 2017 swarm (segment E).

Characteristic source mechanisms of the West Bohemian activities are given in Figure 5.16. Two groups of focal mechanisms, the strike-slips with a weak normal (oblique-normal) or thrust (oblique-thrust) component, can be clearly distinguished in each swarm (except the 2017). The mechanisms of the oblique-normal type predominates in 2000 and 2008 swarms and their predominant strikes of $160° - 170°$ and dips of $72° - 80°$ fit well geometry of the fault segment A. As regards the 2011 swarm, the oblique-thrust mechanisms are typical for the deeper segment B, while the oblique-normal mechanisms for the shallower segment C. The nodal planes striking roughly in the N-S direction, and dipping to the east for B and to the west for C segments, signify true fault planes as they readily

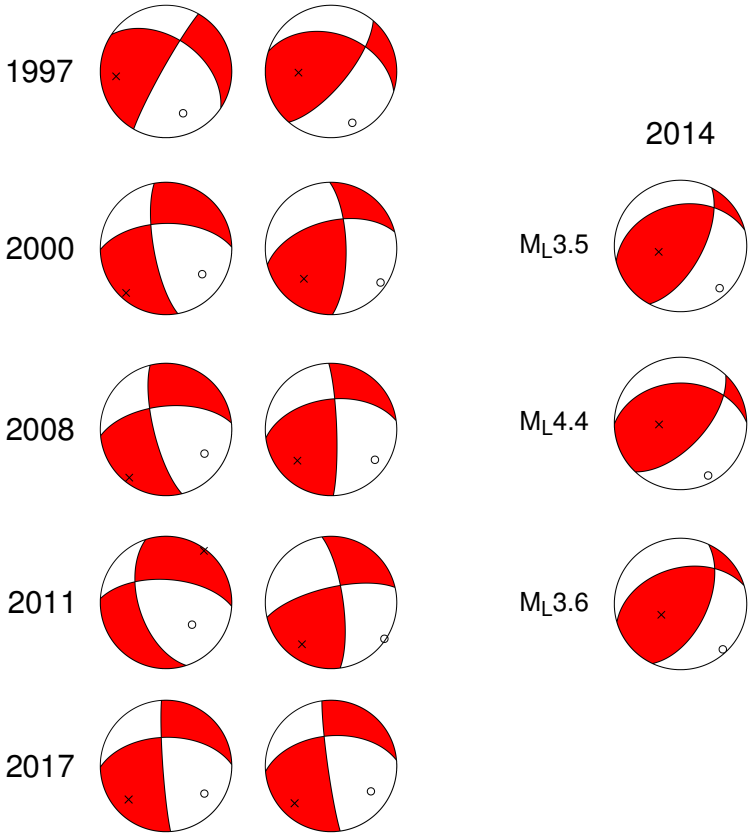

Figure 5.16: Characteristic source mechanisms of the West Bohemian swarms of 1997, 2000, 2008, 2011 and 2017 (*left*), and the three mainshocks of the 2014 activity (*right*). All the fault plane solutions are represented in the equal-area, lower-hemisphere projection. The principal axes P are marked by *circles*, axes T by *crosses*.

match the geometry of corresponding fault segments. In segment C, the strikes vary between 160° and 180°, and dips between 50° and 80°. In segment B, the strikes vary more broadly, ranging between 340° and 10°, and the dips are similar or steeper compared to those in C. Figure 5.16 shows a representative focal mechanism of segment B (strike 352°, dip 75°), which fits the segment orientation of strike 351° and eastward dip 72°, and of segment C (strike 162°, dip 56°) which nicely corresponds to the segment orientation of strike 171° and westward dip 63° (for more details refer to Čermáková and Horálek, 2015). Focal mechanisms of the two strongest events in the 2017 swarm are practically identical, of the oblique-normal type showing strike 175° and dip 85°, which fit well geometry of the segment E. Note that these mechanisms are nearly the same as the oblique-normal ones in segment A.

The source mechanisms of the three 2014 mainshocks are quite similar indicating an oblique-thrust faulting with a significant dip-slip component. Thus they differ significantly from predominant mechanisms in swarms of 2000, 2008, 2011 and 217, which are strike-slips with weak either normal or thrust component. However, source mechanisms of the oblique-thrust type with significant dip-slip components were already observed in the second phase of 1997 swarm showing quite similar DC angles to those of 2014 (Horálek et al., 2002). The strike, dip, and rake angles of both fault-plane solutions for each mainshock are given in Table 3 in Jakoubková et al. (2017). True fault planes in the 2014 mechanisms were distinguished by calculating an equation of the plane defined by the mainshocks hypocenters. This way we estimated the fault planes striking NE-SW and dipping $\approx 60°$ to SE to be the true fault planes, which suggest geometry of segment D (ruptured barrier). The 1997 swarm has been studied from many aspects but it still remains an outstanding issue, particularly a relation between its geometry and focal mechanisms. Since it took place on rather small patch (Fig. 5.5f) it is difficult to match its geometry with the 1997 fault plane solutions. Nevertheless, the location of this swarm in the transition area between fault segments A, B and C, close the barrier D (Fig. 5.7) implies that the NE-SW striking fault planes are the true ones.

6. Summary of the results and conclusions

In my doctoral thesis I have investigated five intraplate earthquake swarms and one non-swarm sequence from West Bohemia/Vogtland and four interplate swarms from two different tectonic areas in Southwest Iceland: the Hengill volcanic complex - Ölfus transition zone, and the Reykjanes Peninsula. I analysed these activities from the perspective of the magnitude-frequency distribution and distribution of the interevent times, their temporal development and the seismic moment release, and the space and time distribution of the foci. The aim was to determine the swarm characteristics that are dependent or vice-versa independent on the tectonic environment, and also the characteristics which should help us to distinguish more precisely earthquake swarms from mainshock-aftershock sequences. Furthermore, I analysed a fault structure of the main focal zone of West Bohemia, Nový Kostel (NK), and a relation between geometry of the individual faults/fault segments and corresponding focal mechanisms.

Prior to these analyses I calibrated local magnitudes M_L provided by the WEBNET and REYKJANET networks and improved formulas for their estimation, and I derived scaling relation between the WEBNET local magnitude M_L and seismic moment M_0. In order to have as much consistent West Bohemia/Vogtland data as possible, I located again all events recorded by WEBNET since 1991 by the NLLoc code and re-estimated local magnitude M_L of all the events. Homogeneous magnitudes M_L and a correct $M_0 - M_L$ relation enabled me to evaluate seismic moment released in the investigated earthquake activities. For evaluation of the seismic moment released in the Southwest Icelandic earthquake swarms I used local moment magnitude M_{Lw} provided by Icelandic Meteorological Office. For refined relative locations I used the hypoDD code. To ensure a proper performance of the hypoDD code, I optimised its input parameters and using synthetics I examined location errors of West Bohemian/Vogtland hypocenters relocated by hypoDD.

For analyses of the West Bohemian earthquake activities I used solely data from WEBNET (with many events in 2008, 2011 and 2014 picked manually by myself); as for the Southwest Icelandic activities I used catalogue data of the SIL network for the earthquake swarms from Hengill (1997), Ölfus (1998) and Krísuvík (Reykjanes Peninsula) in 2003, and our data from REYKJANET for the Krísuvík-Fagradalsfjall swarm in 2017.

Most of the results in my thesis regarding the West Bohemian earthquake activities have been published in two papers by Čermáková and Horálek (2015) and Jakoubková et al. (2017). The results concerning Southwest Icelandic swarms have been quite fresh, so far unpublished. The results of common analyses can be summarised as follows:

(i) Generally, the investigated Southwest Icelandic activities are much larger in terms of magnitudes of the strongest events, total seismic moment released, and in size of the activated focal areas when compared to the West Bohemia ones.

(ii) The West Bohemian and Southwest Icelandic activities show similar magnitude-

frequency distribution complying with the GR law having the b-value ≤ 1.0, and also the interevent time distributions (probability density functions) are nearly the same for all the activities. It implies similar ratio of small to large events and similar event rate in all the West Bohemian and Southwest Icelandic activities. A cut-off of the GR law at the highest magnitude level, the apparent deflection of the strongest events from the linear trend of the GR curve, and the pronounced magnitude gaps between the strongest and the following weaker events is an issue. It may suggest that the swarms comprise overlapping aftershock sequences, each of them dominated by a "mainshock" (strongest events deflected from the GR law similar to the mainshocks in the 2014 mainshock-aftershock sequence).

(iii) Although the total seismic moment M_{0tot} released in the 2008, 2011 and 2014 West Bohemian earthquake activities is comparable, the parameter a of the GR law (event productivity indicating number of the $M_L \geq 0$ events) of the 2014 mainshock-aftershock sequence is significantly lower than that of the 2008 and 2011 swarms. It is probably more general feature due to a bigger magnitude difference ΔM_L between the strongest event and the lower ones which is much bigger for mainshock-aftershock sequences than for swarms. Notably small a value I found for both 2003 and 2017 swarms on the Reykjanes Peninsula (in Krísuvík and Fagradalsfjall areas), and also for the 1997 swarm in West Bohemia.

(iv) The Southwest Icelandic swarms exhibit much higher rate of the seismic moment release than the West Bohemian ones (even though the event rate of both is similar). The West Bohemia swarms are characterised by step by step seismic moment release (which is reflected by several swarm phases), whereas one dominant short-term phase, including one or a few dominant events in which most of M_{0tot} release, is typical of the Southwest Icelandic swarms. For example, 95% of the total seismic moment $M_{0tot} \approx 2 \times 10^{15}$ Nm of the 2008 and 2011 West Bohemia swarms released during 15 and 5 days, while 95% of $M_{0tot} \approx 1.8 \times 10^{16}$ Nm in Ölfus released during 2.5 days, and 95% of $M_{0tot} \approx 3 \times 10^{16}$ Nm of the 2003 Krísuvík swarm released during 1.5 days.

(v) All the West Bohemia swarms occurred in the Nový Kostel (NK) focal zone and form a continuous focal belt about 10 km long, striking in the north-south direction. The events are located in depths between 6 and 13 km, however the depth limit for earthquake swarms appears to be 11 km. The deeper foci are associated with microswarms or scattered events. The Southwest Icelandic swarms are significantly shallower, the shallowest events are located at depths of about 1 – 2 km. My first results indicate the depth limit for swarm earthquakes $\approx 6 - 7$ km on Reykjanes Peninsula (along the MAR), 8 km in the Hengill volcanic complex, and 10 km in Ölfus area which is situated apart from the MAR.

(vi) The NK zone comprises a number of fault segments which were separately activated by each West Bohemia activity. The 2000 and 2008 swarms took place on the same fault segment striking 166° and dipping 75° to the west

(fault segment A in our notation). The 2011 swarm disclosed two corner-like oriented fault segments B (striking 350° and dipping 72° eastwards) a C (striking 171° and dipping 63° westwards). The M_L3.5, 4.4 and 3.6 mainshocks in 2014 represent three-step rupturing of the barrier (striking 40° and dipping 60° to the north-east, segment E) in the transition area among segments A, B and C. I found that the transition area is partitioned into several segments, some of them were repeatedly activated. The 1997 swarm took place on two corner-like patches just embodied in these segments. A moderate 2017 swarm was located in the very north of the NK zone, off the focal belt, on a separate fault segment having practically the same orientation as segment A. The locations of the West Bohemian earthquake swarms since 2000 signify a gradual northward trend in migration of the swarm activity in the NK zone.

I also calculated focal mechanisms in the double-couple representation and found that prevailing mechanisms in each activity correspond well to geometry of the respective fault segments. Based on that I constructed a scheme of the fault structure in the main focal zone NK that ought to be gradually improved.

(vii) The M_L4.9 Ölfus swarm in 1998 represents a continuation of the M_L4.4 Hengill activity in 1997, but patterns of their spatial distribution fairly differ. The Hengill pattern reveals a big complexity of the triple-junction volcanic complex comprising number of differently oriented fault segments which were activated during the swarm; the pattern is obviously of a 3D character. In contrast, the 1998 Ölfus foci form a single ENE-WSW striking belt ($\sim$13 km long) which includes one major fault and two differently oriented fault segments. Interestingly, the spatial distribution of aftershocks of the M_{Lw}6.3 mainshock in June 2008 (e.g., Brandsdóttir et al., 2010), which occurred on the eastern edge of the Ölfus area at a boundary with the SISZ, corresponds well to the spatial distribution of the 1998 swarm events. It leads to an idea that the ENE-WSW striking faults in the Ölfus area are predisposed to earthquake swarms while the N-S transform faults produce single strike-slip earthquakes (Einarsson, 2010). Hence, it suggests that the dominant M_L4.9 earthquake of the Ölfus swarm, which was located under the main focal cluster, was a mainshock on a hidden N-S directed transform fault which triggered swarm-like seismicity on the ENE-WSW striking faults.

(viii) The 2003 (M_L4.3) and 2017 (M_L3.9) swarms on the Reykjanes Peninsula exhibit a strikingly small number of the $M_L \geq 0$ events relative to the other investigated swarms in both West Bohemia and Southwest Iceland, which is nicely seen in the magnitude-frequency distribution plots (small value of parameter a). For example, the 2003 swarm with M_L4.3 (the most intense activity in terms of the total seismic moment released investigated in my thesis) contained only 1160 $M_L \geq 0$ events, while the Hengill swarm (M_L4.4) contained 4850 events and the 2011 West Bohemiam swarm (M_L3.7) 5740 events. In this respect both swarms on the Reykjanes Peninsula appear to be the mainshock-aftershock activity. The swarms were located in the rift zone of MAR, beneath the Krísuvík geothermal field (2003 swarm) and

the Fagradalsfjall volcano (2017 swarm), which are ~ 5 km away from each other. The pattern of the spatial distribution of the 2003 foci indicates two intersecting faults trending N-S and NE-SW which agrees with the tectonic pattern of the Reykjanes Peninsula and presumption of seismogenic faults there (e.g., Einarsson, 2010). However, the pattern of the 2017 swarm shows seismogenic faults parallel or nearly parallel with the MAR plate boundary on the central Reykjanes Peninsula. In my opinion it is quite important finding because seismogenic structures parallel with the MAR on the Reykjanes Peninsula have not been ordinary reported in geophysical papers dealing with the problems concerned.

(ix) Based on the results of the analyses performed I came to conclusion that most of the West Bohemia earthquake swarms and also the Hengill swarm were series of subswarms with one or more embedded mainshock-aftershock sequences, while both earthquake activities on the Reykjanes Peninsula represent a transition between earthquake swarm and mainshock-aftershock sequence.

I believe that results of my doctoral thesis may contribute substantially to better understanding of the nature of earthquake swarms, and also to answering the question why strain energy releases in form of earthquake swarm instead of common mainshock-aftershock sequences at some entirely tectonically different seismogenic areas as West Bohemia/Vogtland and Southwest Iceland.

Included papers

P1: H. Čermáková and J. Horálek. The 2011 West Bohemia (Central Europe) earthquake swarm compared with the previous swarms of 2000 and 2008. *J. Seismol.*, 19/4:899–913, 2015. doi: 10.1007/s10950-015-9502-3.

P2: H. Jakoubková, J. Horálek, and T. Fischer. 2014 mainshock-aftershock activity versus earthquake swarms in West Bohemia, Czech Republic. *Pure and Applied Geophysics*, 175/1:109–131, 2017. doi: 10.1007/s00024-017-1679-7.

Bibliography

R. M. Allen, G. Nolet, W. J. Morgan, K. Vogfjörd, B.H. Bergsson, P. Erlendsson, G.R. Foulger, S. S. Jakobsdóttir, B.R. Julian, M. Pritchard, S. Ragnarsson, and R. Stefánsson. The thin hot plume beneath Iceland. *Geophys. J. Int.*, 137: 51–63, 1999. doi: 10.1046/j.1365-246x.1999.00753.x.

R. M. Allen, G. Nolet, W. J. Morgan, K. Vogfjörd, B. H Bergsson, P. Erlendsson, G.R. Foulger, S. S. Jakobsdóttir, B. R. Julian, M. Pritchard, S. Ragnarsson, and R. Stefánsson. Imaging the mantle beneath Iceland using integrated seismological techniques. *J. Geophys. Res.*, 107/B12:2325, 2002a. doi: 10.1029/2001JB000595.

R. M. Allen, G. Nolet, W. J. Morgan, K. Vogfjörd, M. Nettles, G. Ekström, B.H. Bergsson, P. Erlendsson, G.R. Foulger, S. S. Jakobsdóttir, B.R. Julian, M. Pritchard, S. Ragnarsson, and R. Stefánsson. Plume-driven plumbing and crustal formation in Iceland. *J. Geophys. Res.*, 107/B8:2163, 2002b. doi: 10.1029/2001JB000584.

T. Árnadóttir, H. Geirsson, and P Einarsson. Coseismic stress changes and crustal deformation on the Reykjanes Peninsula due to triggered earthquakes on June 17, 2000. *J. Geophys. Res.*, 109/B09307, 2004. doi: 10.1029/2004JB003130.

S. Arnórsson. Geothermal systems in Iceland: Structure and conceptual models-I. High-temperature areas. *Geothermics*, 24:561–602, 1995a. doi: 10.1016/0375-6505(95)00025-9.

S. Arnórsson. Geothermal systems in Iceland: Structure and conceptual models-II. Low-temperature areas. *Geothermics*, 24:603–629, 1995b. doi: 10.1016/0375-6505(95)00026-7.

V. Babuška, J. Plomerová, and T. Fischer. Intraplate seismicity in the western Bohemian Massif (central Europe): A possible correlation with a paleoplate junction. *J. Geodyn.*, 44/3-5:149–159, 2007. doi: 10.1016/j.jog.2007.02.004.

P. Bankwitz, G. Schneider, H. Kämpf, and E. Bankwitz. Structural characteristics of epicentral areas in Central Europe: study case Cheb Basin (Czech Republic). *J. Geodyn.*, 35/1-2:5–32, 2003. doi: 10.1016/S0264-3707(02)00051-0.

S. Björnsson and P. Einarsson. Seismicity of Iceland. *In: Kristjansson L. (eds) Geodynamics of Iceland and the North Atlantic Area. NATO Advanced Study Institutes Series (Series C - Mathematical and Physical Sciences), Springer, Dordrecht*, 11, 1974. doi: 10.1007/978-94-010-2271-2_16.

F. Bouchaala, V. Vavryčuk, and T. Fischer. Accuracy of the master-event and double-difference locations: synthetic tests and application to seismicity in West Bohemia, Czech Republic. *J. Seismol.*, 17/3:841–859, 2013. doi: 10.1007/s10950-013-9357-4.

B. Brandsdóttir, M. Parsons, R. S. White, O. Guðmundsson, J. Drew, and B. S. Thorbjarnardóttir. The May 29th 2008 earthquake aftershock sequence within

the South Iceland Seismic Zone: Fault locations and source parameters of aftershocks. *Jökull*, 60:23–46, 2010.

H. Čermáková and J. Horálek. The 2011 West Bohemia (Central Europe) earthquake swarm compared with the previous swarms of 2000 and 2008. *J. Seismol.*, 19/4:899–913, 2015. doi: 10.1007/s10950-015-9502-3.

A. E. Clifton and S. A. Kattenhorn. Structural architecture of a highly oblique divergent plate boundary segment. *Tectonophysics*, 419:27–40, 2006. doi: 10.1016/j.tecto.2006.03.016.

H. Credner. Das vogtländisch-erzgebirgische Erdbeben vom 23. November 1875. *Z. Ges. Naturwiss.*, 48:246–269, 1876.

G. Daniel, E. Prono, F. Renard, F. Thouvenot, S. Hainzl, A. Marsan, D. Helmstetter, P. Traversa, J. L. Got, L. Jenatton, and R. Guiguet. Changes in effective stress during the 2003-2004 Ubaye seismic swarm, France. *J. Geophys. Res.*, 116/B1, 2011. doi: 10.1029/2010JB007551.

J. Decriem, T. Árnadóttir, A. Hooper, H. Geirsson, F. Sigmundsson, M. Keiding, B. G. Ófeigsson, S. Hreinsdóttir, Einarsson P., P. LaFemina, and R. A. Bennett. The 2008 May 29 earthquake doublet in SW Iceland. *Geophys. J. Int.*, 181/2: 1128–1146, 2010. doi: 10.1111/j.1365-246X.2010.04565.x.

J. Doubravová and J. Horálek. New interactive software for seismic data processing. *Technical Computing Prague 2013. 21th Annual Conference Proceedings*, 2013.

P. Einarsson. Earthquakes and present-day tectonism in Iceland. *Tectonophysics*, 189:261–279, 1991. doi: 10.1016/0040-1951(91)90501-I.

P. Einarsson. Plate boundaries, rifts and transforms in Iceland. *Jökull*, 58:35–58, 2008.

P. Einarsson. Mapping of Holocene surface ruptures in the South Iceland Seismic Zone. *Jökull*, 60:117–134, 2010.

P. Einarsson. Mechanisms of Earthquakes in Iceland. *In: Beer M., Kougioumtzoglou I.A., Patelli E., Au SK. (eds) Encyclopedia of Earthquake Engineering. Springer, Berlin, Heidelberg*, 2014. doi: 10.1007/978-3-642-36197-5_298-1.

J. Farrell, S. Husen, and R. B. Smith. Earthquake swarm and b-value characterization of the Yellowstone volcano-tectonic system. *J. Volcanol. Geotherm. Res.*, 188:260–276, 2009. doi: 10.1016/j.jvolgeores.2009.08.008.

T. Fischer. Automatic location of swarm earthquakes from local network data. *Stud. Geophys. Geod.*, 47/1:83–98, 2003. doi: 10.1023/A:1022251605990.

T. Fischer and M. Bachura. Detection capability of seismic network based on noise analysis and magnitude of completeness. *J. Seismol.*, 18/1:137–150, 2014. doi: 10.1007/s10950-013-9407-y.

T. Fischer and J. Horálek. Refined locations of the swarm earthquakes in the Nový Kostel focal zone and spatial distribution of the January 1997 swarm in Western Bohemia, Czech Republic. *Stud. Geophys. Geod.*, 44/2:210–226, 2000. doi: 10.1023/A:1022162826079.

T. Fischer and J. Horálek. Space-time distribution of earthquake swarms in the principal focal zone of the NW Bohemia/Vogtland seismoactive region: period 1985-2001. *J. Geodyn.*, 35/1-2:125–144, 2003. doi: 10.1016/S0264-3707(02)00058-3.

T. Fischer and J. Horálek. Slip-generated patterns of swarm microearthquakes from West Bohemia/Vogtland (central Europe): Evidence of their triggering mechanism? *J. Geophys. Res.*, 110/B05S21, 2005. doi: 10.1029/2004JB003363.

T. Fischer and J. Michálek. Post 2000-swarm microearthquake activity in the principal focal zone of West Bohemia/Vogtland: Space-time distribution and waveform similarity analysis. *Stud. Geophys. Geod.*, 52: 493, 2008. doi: 10.1007/s11200-008-0034-y.

T. Fischer, J. Horálek, J. Michálek, and A. Boušková. The 2008 West Bohemia earthquake swarm in the light of the WEBNET network. *J. Seismol.*, 14: 665–682, 2010. ISSN 1383-4649. doi: 10.1007/s10950-010-9189-4.

T. Fischer, J. Horálek, P. Hrubcová, V. Vavryčuk, K. Bräuer, and H. Kämpf. Intra-continental earthquake swarms in West-Bohemia and Vogtland: A review. *Tectonophysics*, 611:1–27, 2014. doi: 10.1016/j.tecto.2013.11.001.

T. Fischer, C. Matyska, and J. Heinicke. Earthquake-enhanced permeability - evidence from carbon dioxide release following the ML 3.5 earthquake in West Bohemia. *Earth Planet. Sci. Lett.*, 460:60–67, 2017. doi: 10.1016/j.epsl.2016.12.001.

H. Geirsson, T. Árnadóttir, S. Hreinsdóttir, J. Decriem, P.C. LaFemina, S. Jónsson, R.A. Bennett, S. Metzger, A. Holland, E. Sturkell, T. Villemin, C. Völksen, F. Sigmundsson, P. Einarsson, M.J. Roberts, and H. Sveinbjörnsson. Overview of results from continuous GPS observations in Iceland from 1995 to 2010. *Jökull*, 60:3–22, 2010.

M. T. Guðmundsson, K. Jónsdóttir, A. Hooper, E. P. Holohan, S. A. Halldórsson, B. G. Ófeigsson, S. Cesca, K. S. Vogfjörd, F. Sigmundsson, T. Högnadóttir, and Einarsson P. et al. Gradual caldera collapse at Bárðarbunga volcano, Iceland, regulated by lateral magma outflow. *Science*, 353, 2016. doi: 10.1126/science.aaf8988.

S. Hainzl. Seismicity patterns of earthquake swarms due to fluid intrusion and stress triggering. *Geophys. J. Int.*, 159/3:1090–1096, 2004. doi: 10.1111/j.1365-246X.2004.02463.x.

S. Hainzl and T. Fischer. Indications for a successively triggered rupture growth underlying the 2000 earthquake swarm in Vogtland/NW Bohemia. *J. Geophys. Res.*, 107/B12,2338:1–9, 2002. ISSN 0148-0227. doi: 10.1029/2002JB001865.

S. Hainzl and Y. Ogata. Detecting fluid signals in seismicity data through statistical earthquake modelling. *J. Geophys. Res.*, 110/B05S07, 2005. doi: 10.1029/2004JB003247.

S. Hainzl, T. Fischer, and T. Dahm. Seismicity-based estimation of the driving fluid pressure in the case of swarm activity in Western Bohemia. *Geophys. J. Int.*, 191/1:271–281, 2012. doi: 10.1111/j.1365-246X.2012.05610.x.

S. Hainzl, T. Fischer, H. Čermáková, M. Bachura, and J. Vlček. Aftershocks triggered by fluid intrusion: Evidence for the aftershock sequence occurred 2014 in West Bohemia/Vogtland. *J. Geophys. Res.*, 121/4:2575–2590, 2016. doi: 10.1002/2015JB012582.

B. S. Hardarson, G. M. Einarsson, H. Franzson, and E. Gunnlaugsson. Volcano-tectonic-geothermal interaction at the Hengill Triple Junction, SW Iceland. *Geothermal Resources Council Transactions*, 33:49–54, 2009.

M. Hensch, C. Riedel, J. Reinhardt, and T. Dahm. Hypocenter migration of fluid-induced earthquake swarms in the Tjörnes Fracture Zone (North Iceland). *Tectonophysics*, 447/1-4:80–94, 2008. doi: 10.1016/j.tecto.2006.07.015.

R. B. Herrmann. Fasthypo - A Hypocenter Location Program. *Earthquake Notes*, 50(2):25–38, 1979.

P. D. Hill. A model for earthquake swarms. *J. Geophys. Res.*, 82(8):1347–1352, 1977. doi: 10.1029/JB082i008p01347.

J. Horálek and T. Fischer. Intraplate earthquake swarms in West Bohemia/Vogtland (Central Europe). *Jökull*, 60:67–87, 2010.

J. Horálek and J. Šílený. Source mechanisms of the 2000-earthquake swarm in the West Bohemia/Vogtland region (Central Europe). *Geophys. J. Int.*, 194/2: 979–999, 2013. doi: 10.1093/gji/ggt138.

J. Horálek, F. Hampl, A. Boušková, and T. Fischer. Seismic regime of the West Bohemian earthquake swarm region: Preliminary results. *Stud. Geophys. Geod.*, 40/4:398–412, 1996. doi: 10.1007/BF02300767.

J. Horálek, T. Fischer, A. Boušková, and P. Jedlička. The Western Bohemia/Vogtland region in the light of the WEBNET network. *Stud. Geophys. Geod.*, 44/2:107–125, 2000a. doi: 10.1023/A:1022198406514.

J. Horálek, J. Šílený, T. Fischer, A. Slancová, and A. Boušková. Scenario of the January 1997 West Bohemia Earthquake Swarm. *Stud. Geophys. Geod.*, 44: 491–521, 2000b.

J. Horálek, J. Šílený, and T. Fischer. Moment tensors of the January 1997 earthquake swarm in NW Bohemia (Czech Republic): double-couple vs. non-double-couple events. *Tectonophysics*, 356:65–85, 2002.

J. Horálek, T. Fischer, A. Boušková, J. Michálek, and P. Hrubcová. The West Bohemian 2008-earthquake swarm: when, where, what size and data. *Stud. Geophys. Geod.*, 53:351–358, 2009. doi: 10.1007/s11200-009-0024-8.

J. Horálek, T. Fischer, P. Einarsson, and S. S. Jakobsdóttir. Earthquake swarms. *Encyclopedia of Earthquake Engineering*, pages 1–16, 2015. doi: 10.1007/978-3-642-36197-5_294-1.

S. Hreinsdóttir, P. Einarsson, and F. Sigmundsson. Crustal deformation at the oblique spreading Reykjanes Peninsula, SW Iceland: GPS measurements from 1993 to 1998. *J. Geophys. Res.*, 106(B7):13803–13816, 2001. doi: 10.1029/2001JB000428.

S. S. Jakobsdóttir. Seismicity in Iceland: 1994-2007. *Jökull*, 58:75–100, 2008.

S. S. Jakobsdóttir, G. B. Guðmundsson, and R. Stefánsson. Seismicity in Iceland 1991-2000 monitored by the SIL seismic system. *Jökull*, 51:87–94, 2002.

H. Jakoubková, J. Horálek, and T. Fischer. 2014 mainshock-aftershock activity versus earthquake swarms in West Bohemia, Czech Republic. *Pure and Applied Geophysics*, 175/1:109–131, 2017. doi: 10.1007/s00024-017-1679-7.

H. Kanamori. The energy release in great earthquakes. *J. Geophys. Res.*, 82: 2981–2987, 1977. doi: 10.1029/JB082i020p02981.

A. Kato, S. Sakai, T. Iidaka, T. Iwasaki, and N. Hirata. Non-volcanic seismic swarms triggered by circulating fluids and pressure fluctuations above a solidified diorite intrusion. *Geophys. Res. Lett.*, 37/15, 2010. doi: 10.1029/2010GL043887.

M. Keiding, B. Lund, and T. Árnadóttir. Earthquakes, stress, and strain along an obliquely divergent plate boundary: Reykjanes Peninsula, southwest Iceland. *J. Geophys. Res.*, 114/B9, 2009. doi: 10.1029/2008JB006253.

M. Khodayar and S. Björnsson. Fault ruptures and geothermal effects of the second earthquake, 29 May 2008, South Iceland Seismic Zone. *Geothermics*, 50:44–65, 2014. doi: 10.1016/j.geothermics.2013.07.002.

J. Knett. Das Erzgebirgische Swarmbeben zu Hartenberg vom 1 Jänner bis Feber 1824. *Sitzungsber. Deutsch. Naturwiss. - med. Ver. Böhmen. Lotos Prag N.F.*, 19:167–191, 1899.

M. Korn, S. Funke, and S. Wendt. Seismicity and seismotectonics of West Saxony, Germany - new insights from recent seismicity observed with the Saxonian seismic network. *Stud. Geophys. Geod.*, 52:479–492, 2008. doi: 10.1007/s11200-008-0033-z.

T. Lay and T.C. Wallace. *Modern global seismology.* Academic Press, III. series, 1995.

J. M. Lees. Multiplet analysis at Coso geothermal. *Bull. Seismol. Soc. Am.*, 88/5: 1127–1143, 1998.

G. Leydecker. Erdbebenkatalog für Deutschland mit Randgebieten für die Jahre 800 bis 2008. *Geol. Jahrb.*, pages 1–198, 2011.

K. L. Li. Location and Relocation of Seismic Sources. Master's thesis, Digital Comprehensive Summaries of Uppsala Dissertations from the Faculty of Science and Technology 1532. 73 pp. Uppsala: Acta Universitatis Upsaliensis. ISBN 978-91-513-0013-9, 2017.

A. Lomax, J. Virieux, P. Volant, and C. Berge. Probabilistic earthquake location in 3D and layered models: Introduction of a Metropolis-Gibbs method and comparison with linear locations. *Advances in Seismic Event Location, Thurber, CH and Rabinowitz, N (eds.), Kluwer, Amsterdam*, pages 101–134, 2000.

A. Lomax, A. Michelini, and A. Curtis. Earthquake location, direct, global-search methods. *Encycl. Complex. Syst. Sci., Part 5, Meyers, RA (ed.), Springer, New York*, pages 2449–2473, 2009. doi: 10.1007/978-0-387-30440-3.

R. Madariaga. Dynamics of an expanding circular fault. *Bull. Seismol. Soc. Am.*, 66/3:639–666, 1976.

J. Málek, J. Horálek, and J. Janský. One-dimensional qP-Wave Velocity Model of the Upper Crust for the West Bohemia/Vogtland Earthquake Swarm Region. *Stud. Geophys. Geod.*, 49/4:501–524, 2005. doi: 10.1007/s11200-005-0024-2.

J. Michálek and T. Fischer. Source parameters of the swarm earthquakes in West Bohemia/Vogtland. *Geophysical Journal International*, 195(2):1196–1210, August 2013. ISSN 0956-540X. doi: 10.1093/gji/ggt286. URL `http://gji.oxfordjournals.org/cgi/doi/10.1093/gji/ggt286`.

S. E. Minson, D. S. Dreger, R. Bürgmann, H. Kanamori, and K. M. Larson. Seismically and geodetically determined nondouble-couple source mechanisms from the 2000 Miyakejima volcanic earthquake swarm. *J. Geophys. Res.*, 112/B10308, 2007. doi: 10.1029/2006JB004847.

K. Mogi. Some discussions on aftershocks, foreshocks and earthquake swarms: the fracture of a semi-infinite body caused by an inner stress origin and its relation to the earthquake phenomena (third paper). *Bull. Earthq. Res. Inst. Univ. Tokyo*, 41:615–658, 1963.

J. Mrlina, H. Kämpf, C. Kroner, J. Mingram, M. Stebich, A. Brauer, W.H. Geissler, J. Kallmeyer, H. Matthes, and M. Seidl. Discovery of the first Quaternary maar in the Bohemian Massif, Central Europe, based on combined geophysical and geological surveys. *J. Volcanol. Geotherm. Res.*, 182/1-2:97–112, 2009. doi: 10.1016/j.jvolgeores.2009.01.027.

H. Neunhöfer and A. Hemmann. Earthquake swarms in the Vogtland/Western Bohemia region: Spatial distribution and magnitude-frequency distribution as an indication of the genesis of swarms? *J. Geodyn.*, 39/4:361–385, 2005. doi: 10.1016/j.jog.2005.01.004.

H. Neunhöfer and T. Meier. Seismicity in the Vogtland/Western Bohemia earthquake region between 1962 and 1998. *Stud. Geophys. Geod.*, 48:539–562, 2004. doi: 10.1023/B:SGEG.0000037471.18297.07.

F. Panzera, J.D. Zechar, K. S. Vogfjörd, and D. A. J. Eberhard. A Revised Earthquake Catalogue for South Iceland. *Pure and Applied Geophysics*, 173/1: 97–116, 2016. doi: 10.1007/s00024-015-1115-9.

R. Pedersen, F. Sigmundsson, and P. Einarsson. Controlling factors on earthquake swarms associated with magmatic intrusions; Constraints from Iceland. *J. Volcanol. Geotherm. Res.*, 162:73–80, 2007. doi: 10.1016/j.jvolgeores.2006.12.010.

B. Růžek and J. Horálek. Three-dimensional seismic velocity model of the West Bohemia/Vogtland seismoactive region. *Geophys. J. Int.*, 195/2:1251–1266, 2013. doi: 10.1093/gji/ggt295.

K. Sæmundsson and P. Einarsson. Notes on the Tectonics of Reykjanes. *Report No. ÍSOR-2014/003, ÍSOR, Reykjavík*, 2014.

J. Sólnes, R. Sigbjörnsson, and J. Elíasson. Probabilistic seismic hazard mapping of Iceland. Proposed seismic zoning and de-aggregation mapping for EUROCODE 8. *3th World Conference on Earthquake Engineering, Vancouver, B.C., Canada, August 1-6, 2004, Paper No. 2337*, 2004.

R. Stefánsson, R. Böðvarsson, R. Slunga, P. Einarsson, S. S. Jakobsdóttir, H. Bungum, S. Gregersen, J. Havskov, J. Hjelme, and H. Korhonen. Earthquake prediction research in the South Iceland seismic zone and the SIL project. *Bull. Seismol. Soc. Am.*, 83/3:696–716, 1993.

P. R. Stoddard and M. T. Woods. Master event relocation of Gorda Block earthquakes: Implications for deformation. *Geophys. Res. Lett.*, 17/7:961–964, 1990. doi: 10.1029/GL017i007p00961.

T. Thordarson and Á. Höskuldsson. Postglacial volcanism in Iceland. *Jökull*, 58: 197–228, 2008.

F. Thouvenot, L. Jenatton, D. Scafidi, C. Turino, B. Potin, and G. Ferretti. Encore Ubaye: Earthquake Swarms, Foreshocks, and Aftershocks in the Southern French Alps. *Bull. Seismol. Soc. Am.*, 106/5:2244–2257, 2016. doi: 10.1785/0120150249.

A. Tryggvason, S. T. Rögnvaldsson, and Ó. G. Flóvenz. Three-dimensional imaging of the P- and S-wave velocity structure and earthquake locations beneath Southwest Iceland. *Geophys. J. Int.*, 151:848–866, 2002. doi: 10.1046/j.1365-246X.2002.01812.x.

E. Tryggvason. Seismicity, earthquake swarms, and plate boundaries in the Iceland region. *Bull. Seismol. Soc. Am.*, 63/4:1327–1348, 1973.

T. I. Urbancic, C. I. Trifu, J. M. Long, and R. P. Young. Space-time correlations of b-values with stress release. *Pure and Applied Geophysics*, 139/3-4:449–462, 1992. doi: 10.1007/BF00879946.

T. Utsu, Y. Ogata, and R. S. Matsu'ura. The centenary of the Omori formula for a decay law of aftershock activity. *J. Phys. Earth*, 43:1–33, 1995. doi: 10.4294/jpe1952.43.1.

V. Vavryčuk. Non-double-couple earthquakes of 1997 January in West Bohemia, Czech Republic: Evidence of tensile faulting. *Geophys. J. Int.*, 149/2:364–373, 2002. doi: 10.1046/j.1365-246X.2002.01654.x.

V. Vavryčuk. Principal earthquakes: Theory and observations from the 2008 West Bohemia swarm. *Earth Planet. Sci. Lett.*, 305/3-4:290–296, 2011. doi: 10.1016/j.epsl.2011.03.002.

V. Vavryčuk and D. Kühn. Moment tensor inversion of waveforms: a two-step time-frequency approach. *Geophys. J. Int.*, 190:1761–1776, 2012. doi: 10.1111/j.1365-246X.2012.05592.x.

J. E. Vidale and P. M. Shearer. A survey of 71 earthquake bursts across southern California: Exploring the role of pore fluid pressure fluctuations and aseismic slip as drivers. *J. Geophys. Res.*, 111/B5, 2006. doi: 10.1029/2005JB004034.

K. S. Vogfjörd, G. Nolet, W. J. Morgan, R. M. Allen, R. Slunga, B. H. Bergsson, P. Erlendsson, G. Foulger, S. S. Jakobsdóttir, B. Julian, M. Pritchard, and S. Ragnarsson. Crustal profiling in Iceland using earthquake source arrays. *AGU Fall meeting, Abstract S61C-1161, San Francisco, California, 6-10 December, 2002*, 2002.

G. A. Wagner, K. Gögen, R. Jonckheere, I. Wagner, and C. Woda. Dating of Quaternary volcanoes Komorní Hůrka (Kammerbühl) and Železná Hůrka (Eisenbühl), Czech Republic, by TL, ESR, alpha-recoil and fission track chronometry. *Z. Geol. Wiss.*, 30:191–200, 2002.

F. Waldhauser. A computer program to compute double-difference hypocenter locations. *U.S. Geol. Surv. Open File Rep.*, 01-113:1–25, 2001.

F. Waldhauser and W.L. Ellsworth. A double-difference earthquake location algorithm: Method and application to the northern Hayward fault, California. *Bull. Seismol. Soc. Am.*, 90/6:1353–1368, 2000. doi: 10.1785/0120000006.

WEBNET, 1991. Institute of Geophysics, Academy of Sciences of the Czech Republic (1991): West Bohemia Local Seismic Network. International Federation of Digital Seismograph Networks. Other/Seismic Network. DOI 10.7914/SN/WB.

N. R. W. Weir, R. S. White, B. Brandsdóttir, P. Einarsson, H. Shimamura, and H. Shiobara. Crustal structure of the northern Reykjanes Ridge and Reykjanes Peninsula, southwest Iceland. *J. Geophys. Res.*, 106/B4:6347–6368, 2001. doi: 10.1029/2000JB900358.

S. Wiemer and M. Wyss. Minimum magnitude of completeness in earthquake catalogs: Examples from Alaska, the western United States, and Japan. *Bull. Seismol. Soc. Am.*, 90/4:859–869, 2000. doi: 10.1785/0119990114.

S. Wiemer, S. R. McNutt, and M. Wyss. Temporal and three-dimensional spatial analyses of the frequency-magnitude distribution near Long Valley Caldera, California. *Geophys. J. Int.*, 134/2:409–421, 1998. doi: 10.1046/j.1365-246x.1998.00561.x.

J. Woessner and S. Wiemer. Assessing the Quality of Earthquake Catalogues: Estimating the Magnitude of Completeness and Its Uncertainty. *Bull. Seismol. Soc. Am.*, 95:684–698, 2005. ISSN 0037-1106. doi: 10.1785/0120040007.

M. Wyss, K. Shimazaki, and S. Wiemer. Mapping active magma chambers by b values beneath the off-Ito volcano, Japan. *J. Geophys. Res.*, 102/B9:20413–20422, 1997. doi: 10.1029/97JB01074.

T. Yamashita. Pore creation due to fault slip in a fluid-permeated fault zone and its effect on seismicity: generation mechanism of earthquake swarm. *Pure and Applied Geophysics*, 155/2-4:625–647, 1999. doi: 10.1007/s000240050280.

Y. Yukutake, H. Ito, R. Honda, M. Harada, T. Tanada, and A. Yoshida. Fluid-induced swarm earthquake sequence revealed by precisely determined hypocenters and focal mechanisms in the 2009 activity at Hakone volcano, Japan. *J. Geophys. Res.*, 116/B4, 2011. doi: 10.1029/2010jb008036.

List of Figures

List of Tables

List of Abbreviations

DC	double-couple
GR	Gutenberg-Richter
hypoDD	Double difference localization code
IMO	Icelandic Meteorological Office
MAR	Mid-Atlantic Ridge
ME	master-event
MFD	magnitude-time distribution
MT	moment tensor
NK	Nový Kostel
NLLoc	Non-Linear Location code
REYKJANET	Reykjanes seismic network
RP	Reykjanes Peninsula
SISZ	South Iceland Seismic Zone
SIL	South Iceland Lowland (regional seismic network)
WB2005	West Bohemian velocity model by Málek et al. (2005)
WB2013	West Bohemian velocity model by Růžek and Horálek (2013)
WEBNET	West Bohemia seismic network

J Seismol
DOI 10.1007/s10950-015-9502-3

ORIGINAL ARTICLE

The 2011 West Bohemia (Central Europe) earthquake swarm compared with the previous swarms of 2000 and 2008

Hana Čermáková · Josef Horálek

Received: 6 November 2014 / Accepted: 14 June 2015

Abstract This paper presents the basic characteristics of the 2011 West Bohemia/Vogtland earthquake swarm and compares it with the swarms in 2000 and 2008. All these swarms occurred in the Nový Kostel focal zone. Up to 25,000 $M_L \leq 3.7$ events with depths between 6 and 10 km were detected in the 2011 swarm. Utilizing WEBNET data, we analysed the cumulative seismic moment, magnitude-frequency and interevent time distributions, space-time distribution of foci and typical focal mechanisms. For this purpose, we improved the formula for estimating the local magnitude M_L used by WEBNET. The 2011 swarm exhibited much higher rapidity than the swarms of 2000 and 2008. The magnitude-frequency distributions of all the three swarms are similar, having the b-value close to 1.0. However, the events of higher magnitudes, roughly $M_L \sim 3.0+$, depart markedly from the general trend of the weaker events. The probability density functions of the interevent times of all the swarms comply with power law $\propto T^{-1.4}$, which points to Omori law-like mainshock-aftershock activity. All swarms exhibit a pronounced focal migration; however, no regularity was found. The spatial distribution of the 2011 foci indicates two active fault segments which differ from the segment triggered in the swarms of 2000 and 2008. Furthermore, we analysed the spatial distribution of the mini-swarm of 2013 and found that it complements the swarm of 2011. The prevailing focal mechanisms in the 2011 swarm are of both oblique-normal and oblique-thrust types and correspond closely to the geometry of the activated fault segments. Our analyses indicate that the Nový Kostel area is more complex than was believed to be.

Keywords West Bohemia/Vogtland · Local seismicity · Earthquake swarm · Relative locations · Focal mechanism estimation

1 Introduction

The region of West Bohemia (Czech Republic) and Vogtland (Saxony, Germany) is one of the most seismically active areas in Europe (Fig. 1). Typically, intraplate earthquake swarms occur in this region. The seismic activity covers an area of more than 3000 km^2, roughly delimited by 49.8° – 50.7° N and 12° – 13° E.

The region is located in the western part of the Bohemian Massif, where three Variscan tectonic units merge: the Saxothuringian, the Teplá-Barrandian and the Moldanubian (Babuška et al. 2007). The most striking geological features are the Eger Rift (NE-SW) and Mariánské Lázně fault (NNW-SSE). Another

H. Čermáková · J. Horálek
Institute of Geophysics, Academy of Sciences of the Czech Republic, Prague, Czech Republic
e-mail: jhr@ig.cas.cz

H. Čermáková (✉)
Institute of Geophysics CAS, v. v. i., Boční II/1401, 14131, Prague, Czech Republic
e-mail: cermakova@ig.cas.cz

Published online: 10 July 2015

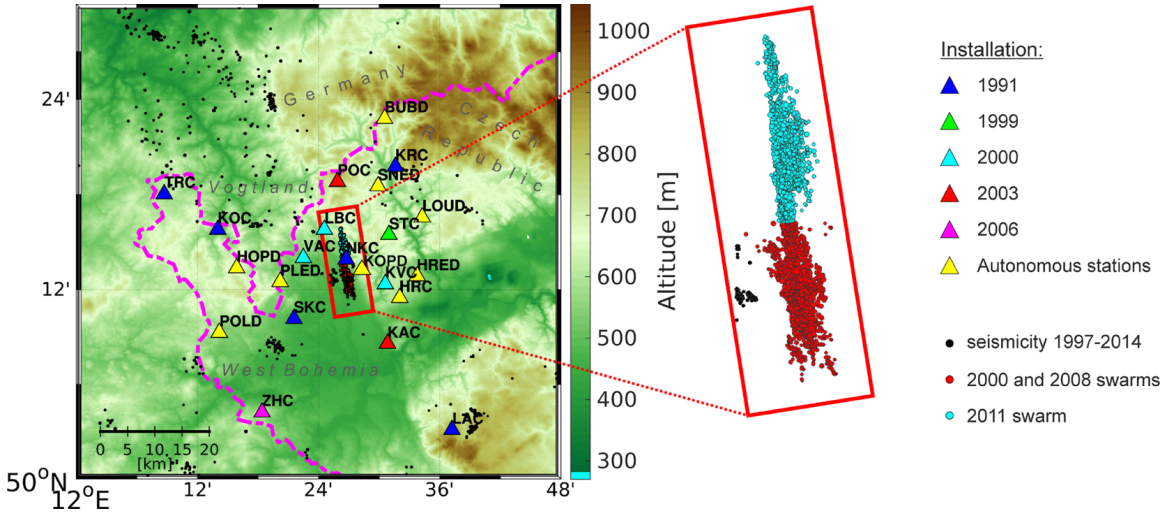

Fig. 1 Map of the central part of the West-Bohemia/Vogtland seismogenic region with the earthquake epicenters and stations of the WEBNET network. The Nový Kostel focal zone is denoted by a *red rectangle*. *Triangles* indicate WEBNET stations, different colors indicate different years of installation. *Dots* indicate seismicity, different colors indicate different time periods; the *zoomed rectangle* shows location of the 2011 swarm relative to the swarms of 2000 and 2008. *The purple dashed line* indicates the Czech-German border

fault system, which was described by Bankwitz et al. (2003), is the Počátky-Plesná zone (N-S). The seismicity is usually attributed to subsiding Quaternary volcanism. Two extinct volcanoes, Komorní Hůrka and Železná Hůrka, and Mýtina Maar are situated at only about 20 km from the main epicentral zone (Mrlina et al. 2009).

Seismicity in the area is relatively shallow with foci located at depths of 5–15 km (Horálek and Fischer 2010). Magnitudes M_L are mostly lower than 4.0, larger events are rather exceptional. The seismic potential of the region is assessed to correspond roughly to a single event of local magnitude $M_L \approx 5.5$ (Fischer et al. 2010).

Seismicity is spread out over the whole West Bohemia/Vogtland region. However, 95 % of the total seismic moment released during the last 30 years is related to the Nový Kostel (NK) focal zone (Fig. 1). Besides numerous microswarms, the most significant swarms were in 1985/1986 ($M_{Lmax} = 4.6$), 1997 (moderate, $M_{Lmax} = 3.0$), 2000 (medium, $M_{Lmax} = 3.3$) and two large ones in 2008 ($M_{Lmax} = 3.8$) and 2011 ($M_{Lmax} = 3.7$). In 2013, weak swarm activity occurred ($M_{Lmax} = 2.3$), which complemented the 2011 swarm. In 2014, exceptionally intense non-swarm activity took place here. The three dominating earthquakes can be characterised as mainshocks, accompanied by a large number of aftershocks; the strongest event was of magnitude $M_L = 4.5$, the other mainshocks of magnitudes $M_L = 3.6$ and $M_L = 3.5$.

Recently, the area has been thoroughly studied from various perspectives: the space-time distribution of events and the fault geometry in this zone (Fischer and Horálek 2003; Horálek et al. 2009; Fischer et al. 2010; Bouchaala et al. 2013); source mechanisms and stress field (Horálek et al. 2002; Vavryčuk 2002, 2011; Horálek and Šílený 2013); triggering mechanisms and driving forces (Hainzl and Fischer 2002; Hainzl and Ogata 2005; Fischer and Horálek 2005).

A comparison of the three intense West Bohemian swarms presents a challenge to reveal their common features. Therefore, the aim of our paper is to show the basic characteristics of the 2011 swarm, compare that swarm with the 2000 and 2008 swarm activities, and get more comprehensive information about the nature of West Bohemia. This involves presenting the basic statistical characteristics, precise hypocentre locations, space-time distribution of foci and preliminary focal mechanisms.

2 Data

The 2011 swarm was recorded by stations of the WEBNET network (Fischer et al. 2010), which consists of 13 telemetred and 9 autonomous stations. Seismograms are proportional to the ground velocity

in the frequency band of 0.5–80 Hz for the telemetred stations and 1.0–80 Hz for the autonomous stations. The sampling rate of all the stations is 250 Hz. For coordinates and instrumentation of the individual stations, we refer to Fischer et al. (2010). Apart from the study of focal mechanisms, we used data from the telemetred stations only. Data of the 2000 and 2008 swarms came from the WEBNET network as well. The station configuration of the 2008 and 2011 swarms is the same, for the station configuration of the 2000 swarm, we refer to Horálek et al. (2000).

First, we created the 2011 catalogue using the automatic algorithm of Fischer (2003). A total of about 23,000 events were detected down to magnitude $M_L = -0.25$. We used this catalogue for estimating magnitude-frequency distribution, interevent time distribution and cumulative seismic moment.

For the event locations, we used manually picked P- and S-wave arrival times from ten selected stations which ensure good azimutal coverage and show clear P- and S-wave onsets. The central station NKC is situated practically above the 2011 hypocentres. Five stations surround the NK focal zone at distances less than 10 km (KVC, SKC, VAC, LBC and STC), and four stations at distances from 13 to 24 km (KRC, KOC, POC and LAC). The P-wave onsets were picked at the vertical component with the accuracy of ±4 ms, the S-wave onsets at the horizontal components with an accuracy of $\pm 8 - 12$ ms.

3 Method

3.1 Calibration of the WEBNET magnitudes

Since 1992, the local magnitude M_L of the WEBNET observations has been estimated by the following formula:

$$M_{Li} = \log A_{Smax} - \log 2\pi + a \cdot \log R_i + C_i + K, \quad (1)$$

where M_{Li} is the local magnitude for each station, A_{Smax} is the absolute value of the maximum total amplitude of the S-wave ground velocity measured in μm/s, a is a constant involving intrinsic attenuation and scattering of the S wave, R_i is the hypocentral distance of the station in kilometre, C_i is the station correction and K is a calibration constant. For the WEBNET network, the constants $a = 2.1$ and $K = -1.7$ have been used (the constant $K = -1.7$ calibrates M_{Li} to local magnitudes estimated from the station PRU of the Czech Regional Seismological Network) (Horálek et al. 2000).

Since M_{Li} vary depending on the S-wave radiation pattern, the final local magnitude M_L is determined as the average of magnitudes M_{Li} of all the available stations (Horálek et al. 2000). However, the M_{Li} has been estimated so far using only five stations for which the corrections were derived in the early years of WEBNET (NKC, KOC, KRC, SKC and TRC). Moreover, the data from TRC were usually available with some delay as it formerly was an autonomous station. Since then, eight more stations have been established, so we calculated new corrections C_i, and also recalculated the constants a and K to achieve a more stable estimation of M_L.

We used the $M_L \geq 0$ events from the period 2007–2013 when several thousand events occurred. The $M_L < 0$ events were omitted due to a low signal-to-noise ratio. The events appeared in a broader area of West Bohemia/Vogtland, but their largest part was concentrated in the NK zone. Because of their high percentage, using all the NK events would have caused systematic shifts of the corrections. Therefore, their number had to be reduced to cover the whole region evenly. First, we bounded the NK area by a distance of 5 km from the NKC station; second, we raised the magnitude threshold to $M_L = 1.2$; and third, we subdivided the magnitude range $M_L = 1.2 - 3.8$ into magnitude intervals of 0.2 and randomly selected three events from each interval. By these reductions, we obtained 445 uniformly distributed events for the West Bohemia/Vogtland region.

We applied the classical iterative approach suggested by T. Fischer (via personal communication). In the first iteration, we set all the station corrections to zero. For m events, we calculated the station magnitudes M_{Li}, average magnitude $M_L = \overline{M_{Li}}$ and differences $\Delta M_{Li} = M_L - M_{Li}$. For each station, we added the arithmetic mean of m differences to the previous correction and obtained a new correction. We searched for a set of C_i for which the mean of m differences is minimal. This procedure was repeated by changing the constant a to values increasing from 1.0 to 3.0 by steps of 0.1. However, the optimum value of a was confirmed to be 2.1, even for the extended set of stations. The resulting C_i and their standard deviations σ_i are listed in Table 1 ($\sigma_i < 0.28$, for i = 1 to 13 stations).

Table 1 Station corrections (C_i) and standard deviations (σ_i) for 13 permanent WEBNET stations

	KAC	KOC	KRC	KVC	LAC	LBC	NKC	POC	SKC	STC	TRC	VAC	ZHC
C_i	−0.393	−0.013	−0.128	0.103	−0.132	0.133	0.093	0.038	0.081	0.107	0.135	0.017	−0.240
σ_i	0.217	0.219	0.185	0.185	0.274	0.199	0.229	0.197	0.182	0.259	0.183	0.218	0.270

We redefined the calibration constant K as -1.2 to match magnitudes estimated by the former and new formula. Unlike Horálek et al. (2000), we did not link the new M_L to any regional station explicitly because magnitudes over suitable stations are rather scattered. Since the former formula links local magnitudes to the regional station PRU, the same link is preserved for the new formula as well.

Therefore, a refined formula for the local magnitude M_L estimation using the WEBNET stations is:

$$M_{Li} = \log A_{Smax} - \log 2\pi + 2.1 \cdot \log R_i + C_i - 1.2, \quad (2)$$

where the changes compared to the former formula (1) are in the corrections C_i and in the new constant $K = -1.2$.

To verify that none of the WEBNET stations had a predominant effect on the M_L estimation, we applied the jackknife technique. We defined various station subsets where one or more stations were omitted. For each subset, we computed magnitudes M_L and the station corrections C_i, and we checked their stability. We also tested the stability of M_L estimated using several combinations of only four or five stations, as this is common practice. The tests show that the maximum errors of M_L are of ± 0.2 of magnitude, even when only four or five stations are used. The corrections C_i are quite stable having their variations on the order of only hundredths of a magnitude throughout all the events. Such errors are significantly lower than the errors of the M_L estimation itself and can be neglected.

3.2 Hypocentre locations

We located all manually processed 2011 events by the NLLoc technique (nonlinear earthquake location; Lomax et al. 2000, 2009). We used the 1-D vertically inhomogeneous isotropic P- and S-wave velocity model of the upper crust of the West Bohemia swarm region. The model consists of ten layers with a constant v_p/v_s ratio 1.7 (modified model of Málek et al. 2005). We used 10 selected stations given in Section 2 which ensure stable solutions, when omitting one or a few stations would cause negligible shifts of hypocentres.

We refined the locations by applying the HypoDD program package (double-difference hypocenter locations; Waldhauser and Ellsworth 2000; Waldhauser 2001). The HypoDD input parametres MAXNGH, MAXSEP and MINLNK are used to constrain neighbours of each event for which the travel time differences are calculated. Optimum values of these parametres depend on the size of a particular focal cloud, on the number and density of events and on the distribution of the stations. Based on our previous tests, we associated each event with the 20 nearest neighbours within a distance of 1 km. For each event and its neighbours, at least eight phase pairs (P and S) at common stations were necessary. These parametres ensured a stable solution without outliers and with a negligible number of lost events for the whole NK zone.

To estimate location errors, we performed a number of synthetic tests. We created a few clusters of events situated in West Bohemia and relocated them with randomly perturbed data. We tested the influence of the error size and the distribution of stations. For horizontal components, the resulting errors are on the order of tens of metres, usually lower than 30 m. Regarding focal depths, the errors are slightly higher but still lower than 50 m, which is quite satisfying.

A total of 4273 events ($\sim -0.2 < M_L \leq 3.7$) in the period from 1st August 2011 to 31st January 2012 were located by the NLLoc. For the HypoDD locations, we used only events with magnitudes $M_L \geq 0$, with epicentres in a rectangle 4 x 9 km around station NKC, which were recorded by at least four stations. In this way, we selected a well constrained group of 2418 events, which were used to derive a pattern of

the spatiotemporal distribution of the 2011 swarm. In the same way, we located hypocentres of the swarms in 2000 and 2008, and of a subsequent swarm in 2013.

3.3 Estimation of focal mechanisms

To estimate the prevailing focal mechanisms in the 2011 swarm, we used the AMT code by Vavryčuk (2011). It inverts P-waves ground displacement amplitudes on the vertical component and provides the full moment tensor. The code also includes the computation of the Green's function for each event. The same velocity model as for locations is used (modified model of Málek et al. 2005).

We estimated focal mechanisms for 129 events of $M_L \geq 2.0$. We used both telemetred and autonomous stations; number of stations varies from 8 to 22 for each event. The ground-displacement peak amplitudes of the P-waves were extracted automatically by the software package Seismon (developed by J. Doubravová and J. Michálek; Doubravová and Horálek 2013), supervised by an interpreter.

Though the full moment tensors are calculated in the AMT code, we analysed only their double-couple (DC) components. Our reason was the non-DC parts are greatly sensitive to the accuracy of the P-wave amplitudes and the Green's functions, and to the distribution of stations; Horálek and Šílený (2013) have shown such a susceptibility regarding the 2000 swarm. Some focal mechanisms may be biased by errors which are hardly recognizable in the semiautomatic focal-mechanism retrieval, so our results are preliminary. Nevertheless, a statistically significant set of focal mechanisms can give sufficient information about rupturing in the swarm.

4 Basic characteristics

The swarms of 2008 and 2011, together with the non-swarm activity in 2014, are the most intense activities in West Bohemia/Vogtland since the intense swarm in 1985/1986. The less than 3-year time period between the swarms is unusually short. It is characterised by relative inactivity until January 2011, when small background seismicity appeared only.

In the last 100 years, the rapid succession of the activities in 2000, 2008, 2011 and 2014 has been exceptional in the West Bohemia/Vogtland region. It is reminiscent of the large activity at the turn of the nineteenth and twentieth centuries, when a series of intense swarms occurred in 1896/1897, 1903 and 1908/1909.

The 2011 swarm encompassed more than 25,000 $M_L \geq -0.5$ events. Most appeared during the first two weeks, which caused an overlapping of individual swarm phases. Nevertheless, we can distinguish five apparent swarm phases, which are characterised by an abrupt revival of activity (Fig. 2).

Accordingly, a brief scenario of the 2011 swarm was as follows. The 2011 swarm started abruptly on 24th August by a series of $M_L \geq 2.0$ events, two of them with $M_L \geq 3.0$ (phase P1). The most intense phase P2 arose during the evening of 25th August. At the beginning, the strongest $M_{Lmax} = 3.7$ occurred, followed by four $M_L \geq 3.0$ and seven $M_L = 2.6-2.9$ earthquakes within the next 6 days. A short, relatively weak phase P3 with six $M_L \geq 2.0$ events was followed by the second strongest phase P4, which erupted on 2nd September and lasted about 8 days. During this phase, one $M_L = 3.5$, three $M_L = 3.0$ and seven $M_L = 2.6 - 2.9$ earthquakes occurred. Unusually long phase P5 lasted more than 4 months and was characterised by an intermittent swarm-like seismicity. During the period between 10th September and 30th November, the seismicity was weak comprising only of $M_L \leq 2.0$ microearthquakes. On 30th November, the activity increased reaching magnitudes of up to $M_L = 2.6$. During December 2011, three more activity periods occurred with $M_{Lmax} = 2.0 - 2.3$. At the turn of 2011/2012, the swarm ended.

In total, 10 $M_L \geq 3.0$ earthquakes (see Table 2) and 155 $M_L \geq 2.0$ earthquakes occurred during this swarm. The maximum values of ground motions were observed at the NKC station: 10.1×10^{-3} m/s for the ground velocity, 2.1×10^{-4} m for the displacement and 0.68 m/s^2 for the acceleration. These values are comparable to those in the 2008 swarm and roughly three times higher than those in the 2000 swarm (see Table 3). We estimated the scalar seismic moment using the Horálek and Šílený (2013) empirical formula which relates the moment M_0 to the local magnitude M_L:

$$\log M_0 = 1.12 \cdot M_L + 9.78, \quad (3)$$

where M_0 is measured in Nm. The seismic moments of the two largest events are 8.4×10^{13} Nm ($M_L = 3.7$) and 5.0×10^{13} Nm ($M_L = 3.5$).

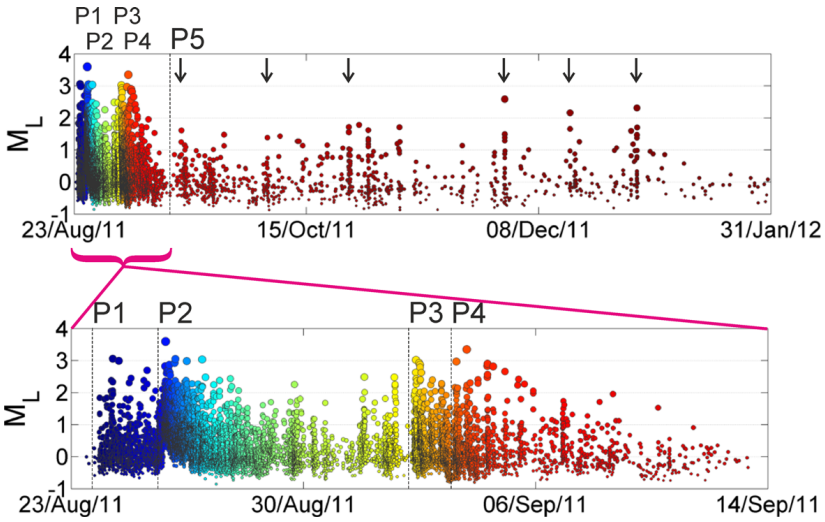

Fig. 2 Magnitude-time course of the 2011 swarm. The colour coding is proportional to time. *Top:* The time period 23rd August 2011 to 31st January 2012 with phase numbers marked on top. The individual phases (P1 to P5) are characterised by an abrupt increase of activity. A sudden revival of activity during the last phase P5 is indicated by *arrows*. Note that phases P2 and P4 are obviously dominated by mainshocks with magnitudes $M_L = 3.7$ and 3.5. *Bottom:* The magnitude-time plot for the main part of the 2011 swarm (the period 23rd August to 14th September 2011)

About 95% of the total seismic moment was released within just the first 2 weeks which indicates a significant rapidity of the swarm. The 10 events with $M_L \geq 3.0$ (Table 2) and 150 events (from 155 in total) with $M_L \geq 2.0$ occurred in that time. But during the previous swarms, a comparable amount of energy was released during a much longer time span: 70 days (2000 swarm) and 22 days (2008 swarm) (Fig. 3). Moreover, based on the results of Fischer et al. (2010), we imply that the 2011 swarm was also more rapid than the 1997 and 1985/1986 swarms.

The cumulative seismic moment released during the 2011 swarm is about 9.2×10^{14} Nm compared to 11.8×10^{14} Nm in 2008 and about 5.1×10^{14} Nm in 2000 (Fig. 3).

The magnitude-frequency distribution (MFD), also called the Gutenberg-Richter law (GR law), is the basic scaling relationship in earthquake statistics:

$$\log N = a - bM,$$

where N is the number of events having a magnitude $\geq M$; a and b are constants. It expresses the relation

Table 2 Ten largest events with magnitudes $M_L \geq 3$

Date	Origin time UTC	Latitude [°N]	Longitude [°E]	depth [km]	M_L
2011-08-24	07:23:48.760	50.230	12.441	8.61	3.1
2011-08-24	12:01:06.770	50.234	12.438	8.64	3.0
2011-08-25	23:33:23.061	50.240	12.441	9.52	3.7
2011-08-26	06:54:06.240	50.238	12.442	9.34	3.2
2011-08-26	15:27:25.211	50.243	12.445	9.78	3.0
2011-08-27	03:13:42.180	50.242	12.446	9.79	3.0
2011-09-02	21:16:26.420	50.248	12.437	7.95	3.0
2011-09-02	23:36:01.539	50.250	12.440	8.22	3.0
2011-09-04	03:52:29.381	50.248	12.440	8.25	3.0
2011-09-04	11:47:45.910	50.245	12.439	8.33	3.5

Table 3 Maximum observed ground motions and the maximum seismic-moment estimation of the 2000, 2008 and 2011 swarms

Swarm	Origin time UTC	M_L	v_{max} [mm/s]	d_{max}[mm]	a_{max}[m/s^2]	M_0[Nm $\times$ 10^{-13}]
2000	Nov 11, 22:07:20	3.2	2.4 (NKC)	0.081 (NKC)	0.26 (KVC)	2.4
2008	Oct 28, 08:30:11	3.8	9.5 (STC)	0.260 (STC)	0.65 (STC)	10.8
2011	Aug 25, 23:33:23	3.7	11.0 (NKC)	0.210 (NKC)	0.68 (NKC)	8.4

v_{max}-maximum velocity (at the station where observed); d_{max}-maximum displacement (station); a_{max}-maximum acceleration (station); M_0-estimation of seismic moment.

between the size of earthquakes and the frequency of their occurrence for a particular earthquake activity, region or time period. The *b*-value signifies the rate of smaller to larger events, the constant *a* is the logarithm of the number of events with $M_L \geq 0$ which implies the earthquake productivity in a particular swarm.

Computation of the MFD is not difficult; however, its analysis and interpretation require some care, in particular in the following points: (i) a reliable *b*-value can be obtained by applying the MFD analysis only to a complete catalogue of events with magnitudes $M_L \geq M_C$, where M_C is the magnitude of completeness (theoretically defined as the lowest magnitude at which 100 % of events in a particular space and time are detected); (ii) the M_L range of the analysed events should be at least over 2.5 magnitudes; (iii) different scaling between seismic moment M_0 and magnitude *M* can exist depending on the definition of the magnitude. Consequently, a comparison of the *b*-values derived using differently estimated magnitudes may be misleading.

We computed a standard cumulative MFD where the completeness magnitude M_C was estimated using the maximum curvature technique (MAXC; Wiemer and Wyss 2000). This approach is based on defining the point of the maximum curvature by computing the maximum value of the second derivative of the magnitude-frequency curve. In practice, this fits the magnitude bin with the highest frequency of events in the non-cumulative MFD (Fig. 4a). We used this approach for all the three swarms (2000, 2008 and 2011). We obtained $M_C = -0.25$ for the 2011 swarm and $M_C = 0.25$ for both swarms of 2000 and 2008. Such a low M_C for the 2011 swarm was achieved thanks to the automatic event detection, which identifies more small events than manual processing. As we used manually processed data for the swarms in 2000 and 2008, their M_C is higher. To keep the comparability of the MFDs, we used the same $M_C = 0.25$ for all the swarms.

As can be seen in Fig. 4a, the MFD of the three swarms shows the *b*-values close to 1 ($b = 0.97$ for the 2000 swarm, 0.96 for the 2008 swarm and 0.93 for the 2011 swarm). Because the same value has been also found for the swarm in 1997 (Fischer et al. 2010), it seems to be typical for West Bohemia earthquake swarms. By substitution of M_L in the MFD

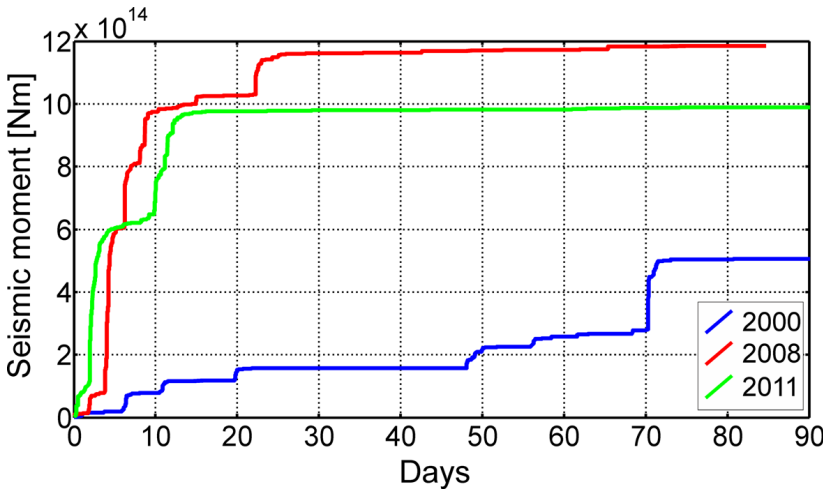

Fig. 3 Cumulative seismic moment released during the swarms of 2000 *(blue)*, 2008 *(red)* and 2011 *(green)*

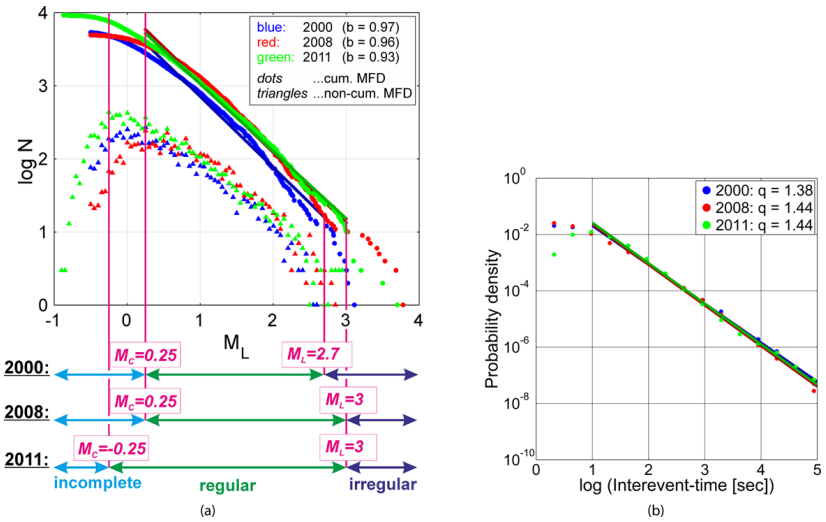

Fig. 4 Cumulative and non-cumulative magnitude-frequency distribution (**a**) and probability-density function of the interevent times (**b**) for the swarms of 2000 *(blue)*, 2008 *(red)* and 2011 *(green)*. Note that MFD of each swarm obeys the Gutenberg-Richter law (GR) within the limits of the completeness magnitude M_C and the upper magnitude 2.7–3.0 (regular part). Above this limit, in the irregular part, events diverge from the GR law. The PDF of the interevent times is computed for events with magnitudes $M_L > M_C$. Interevent times of all the swarms correspond to T_w^{-q}. For the swarms of 2000 and 2008, we obtained $M_C = 0.25$, whereas for the swarm 2011 $M_C = -0.25$. However, to maintain comparability, in both GR law and interevent time distribution we used a common $M_C = 0.25$ for all the swarms. Note that the M_C determined by the non-cumulative distribution acceptably fits the completness of events indicated in the MFD

$\log N = a - 0.93M_L$ for that from Eq. 3, one gets the power-law size distribution $N \propto M_0^{-0.85}$ for the 2011 swarm, and similarly $N \propto M_0^{-0.86}$ for the 2008, and $N \propto M_0^{-0.87}$ for the 2000 swarms. This implies that there will be about a sevenfold decrease in the number of events for every one-order rise in seismic moment of swarm events.

Constant a is usually disregarded but in our case it provides relevant information about event productivity for each individual swarm; number of $M_L \geq 0$ events is roughly 5800 for the 2011, 4400 for the 2008 and 3900 for the 2011 swarm. We can see that the event productivity of the 2011 and 2008 swarms was similar, whereas in the 2000 swarm, it was about one-third lower. The majority of the 2011 events correspond to the GR law with b-value$\sim$1; however, the strong events with magnitudes $\sim M_L > 3.0$ apparently depart from that (Fig. 4a). Besides, there is a noticeable magnitude gap between the two strongest events ($M_L = 3.7$ to 3.5) and the following weaker events. Similar changes of the slope of the MFD curve are observed also for the swarms of 2000 and 2008. Even a more pronounced magnitude gap between the strongest and weaker events is obvious in the MFD of the 2008 swarm, which has been discussed in Fischer et al. (2010).

In these aspects, the MFD features of the three swarms point to the characteristics of the mainshock-aftershock sequences. So, it implies that the swarms may be comprised of overlapping aftershock sequences, each of them dominated by a mainshock. This idea is supported by the findings of Hainzl and Fischer (2002) who showed that the 2000 swarm can be represented by such aftershock sequences. Such behaviour may be physically explained by (i) finiteness of the seismogenic layer or elongated aspect ratio of the rupture area; (ii) brittle/ductile rheology of the fault due to high crack density and abundance of fluids; (iii) lubrication of the fault by pore pressure increase.

To compare the distribution of the interevent times T_w (waiting times between consecutive earthquakes) in the three swarms, we computed their probability density functions (PDF) for the $M_L \geq M_C$ events. The Fig. 4b shows that PDFs are similar, particularly those between 3.0×10^1 and 3.0×10^3 s. They comply with the power law $\propto T_w^{-q}$, where $q = 1.38$ for the 2000, 1.44 for the 2008 and 1.44 for the 2011 swarm.

According to Utsu et al. (1995), such waiting time distribution points to the Omori-like mainshock-aftershock activity, which is represented by the modified Omori law:

$$\lambda \approx (c+t)^{-p},$$

where λ is the rate of aftershocks being associated with a main shock, t is the time elapsed since the main shock, p is close to 1 and c is a time constant; the relation between exponents p and q is given by $p = 2 - 1/q$.

The deviation of the interevent times shorter than 4 s (Fig. 4b) is caused by loosing events hidden in the waveforms of the former, often stronger ones. More detailed analysis of the interevent time distribution is beyond the scope of this paper, nevertheless, it is an issue worth in-depth investigation.

5 Space and time distribution of the swarm events

As mentioned above, the 2011 earthquake swarm occurred in the same NK focal zone as the swarms of 1985/1986, 1997, 2000 and 2008. The hypocentres were located north of those of the 2000 and 2008 swarms at depths between $\sim$ 6.5 and 9.8 km (see Fig. 1). All the swarms form a continuous focal belt which indicates a hidden fault, about 8 km long, striking in the north-south direction. In this context, we use the terms fault and fault plane in a general sense; fault segment and the smaller patch are parts of the fault delimited by hypocentres.

The space and time distribution of the 2011 swarm events is depicted in Fig. 5a. As can be seen from the vertical cross-section plot, the distribution of the foci is corner-like in shape. It cannot be approximated by a single plane as with the 2000 and 2008 swarms, when only one fault segment was activated (segment A in our notation; see Fig. 6). It is obvious that the 2011 foci form the two separately dipping clusters of narrow width which points to their planar character (segments B and C in our notation). The plane striking approximately 351° and dipping to about 72° eastwards fits segment B best, whereas the plane striking 171° and dipping 63° westwards fits segment C best. The size of both segments is similar, roughly 4.0 x 2.0 km.

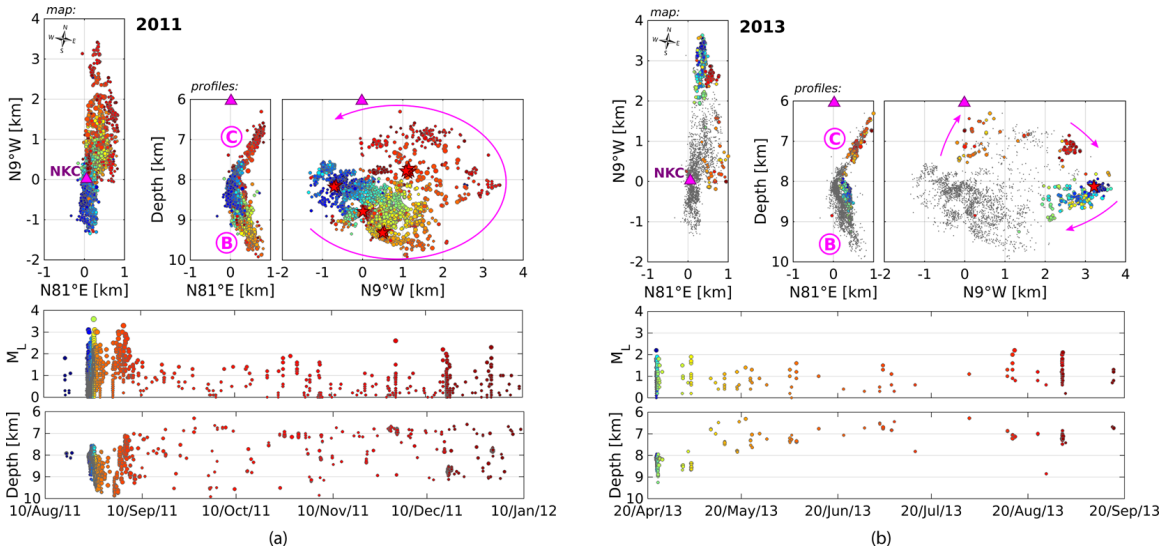

Fig. 5 Spatiotemporal distribution of events in the 2011 swarm (**a**), and its complementary swarm in 2013 (**b**). Colour coding is proportional to the origin time. *Top:* Distribution of hypocentres (coloured dots) represented by the map view (*left*) and two depth sections, across (*middle*) and along the focal belt (*right*). B and C denote the fault segments which are bounded by the two major hypocentre clusters. The *lines with arrows* denote a prevailing trend of the focal migration. The *red stars* show locations of the 10 $M_L \geq 3$ events for the 2011 swarm, and the largest event of $M_{Lmax} = 2.3$ for the 2013 swarm. The horizontal coordinates are rotated by 9° clockwise (i.e., by an angle that equals the strike of the focal belt). The axes are scaled in kilometre, the origin of the horizontal axes corresponds to the location of the central WEBNET station NKC which is marked by a *purple triangle* (latitude $\approx$ 50.23° N, longitude $\approx$ 12.45° E). The colour coding in (**a**) is consistent with that in Fig. 2. *Pale-gray dots* in (**b**) mark the 2011 hypocentres. *Middle:* Time course of the swarm activity in the magnitude-time plot. *Bottom:* Distribution of depths in time. Note that the 2013 swarm complements the 2011 swarm since it activated quiet segments from 2011. See also an alignment of the strongest events from 2011 in segment B

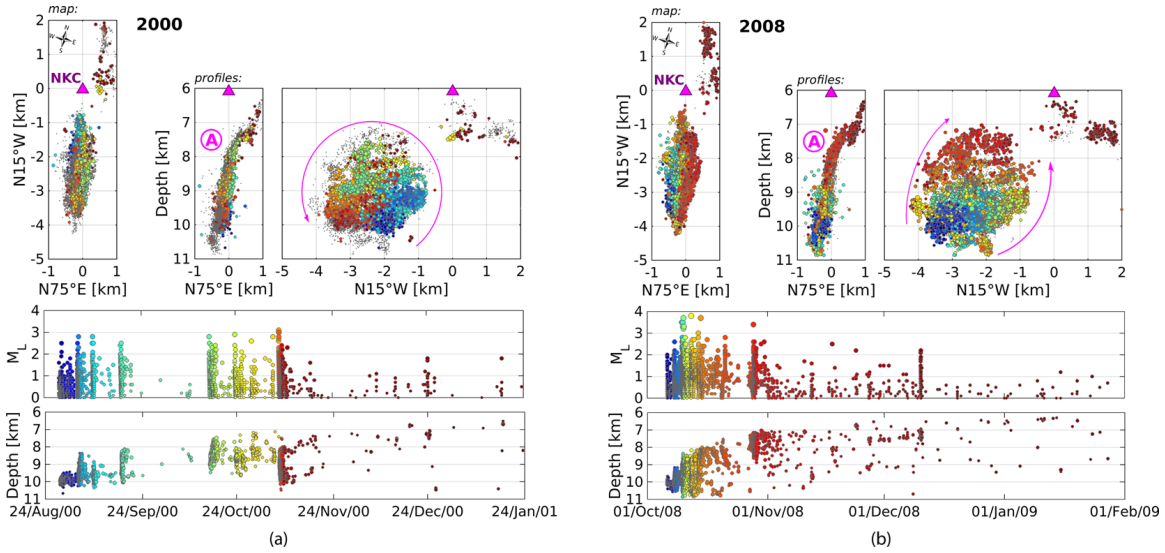

Fig. 6 Spatiotemporal distribution of events in the swarms of 2000 (**a**) and 2008 (**b**). For the figure arrangement, projection and colour coding see Fig. 5; the small difference is only in the rotation of horizontal coordinates, and is 15° clockwise here. A – the fault segment delimited by the 2000 and 2008 hypocentres

The swarm activity initiated on the boundary of the B and C segments at the depths between 8.0 and 8.5 km. Seismicity in phase P1 took place on a patch of about 1 km in diameter (dark-blue dots in Fig. 2). During phases P2 and P3, the seismicity migrated along fault segment B to the north and downwards; the majority of foci in the phase P3 are located at depths between 9.0 and 9.8 km (copper-coloured dots in Fig. 2). In phase P4, the swarm activity switched onto fault segment C and tended to migrate upwards; the shallowest foci are located at depths around 6.5 km.

A comparison of the space-time distribution pattern of the 2011 events (Fig. 5a) with the events of 2000 and 2008 (Fig. 6) shows an entirely different migration behaviour: the counterclockwise migration of the 2000 swarm, a general upward migration of the 2008 swarm, and the counterclockwise downwards/upwards migration of the 2011 swarm. The first events of the 2000 and 2008 swarms occurred at the bottom of fault segment A, while the first events of the 2011 swarm were located in the middle depths where the fault segments B and C were joined. The migration rate differs in individual swarm phases, but in most intense phases it reaches up to hundreds of metres per day for all the three swarms.

6 Focal mechanisms

To assess faulting in the 2011 swarm, we determined focal mechanisms in the form of fault-plane solution (FPS) of 129 selected $M_L \geq 2.0$ events throughout the whole swarm; the AMT code of Vavryčuk (2011) was used (see Section 3.3). The stability of the resultant solutions were tested by omitting individual stations or their pairs. Only stable solutions have been taken into account.

We determined 85 focal mechanisms for segment B and 44 mechanisms for segment C (Fig. 7). One can clearly distinguish two groups of variously oriented nodal planes matching segments B and C. The focal mechanisms are the strike-slips with a weak normal (oblique-normal) or thrust (oblique-thrust) component. The oblique-thrust mechanisms are typical for the deeper segment B (Fig. 7a), while the oblique-normal mechanisms for the shallower segment C (Fig. 7b). It implies that the oblique-thrust events prevail in the swarm-phases P1 to P3, whereas the oblique-normal events prevail in the phase P4. We infer that the nodal planes striking roughly in the north-south direction, and dipping to the east for B and to the west for C segments, signify true fault planes

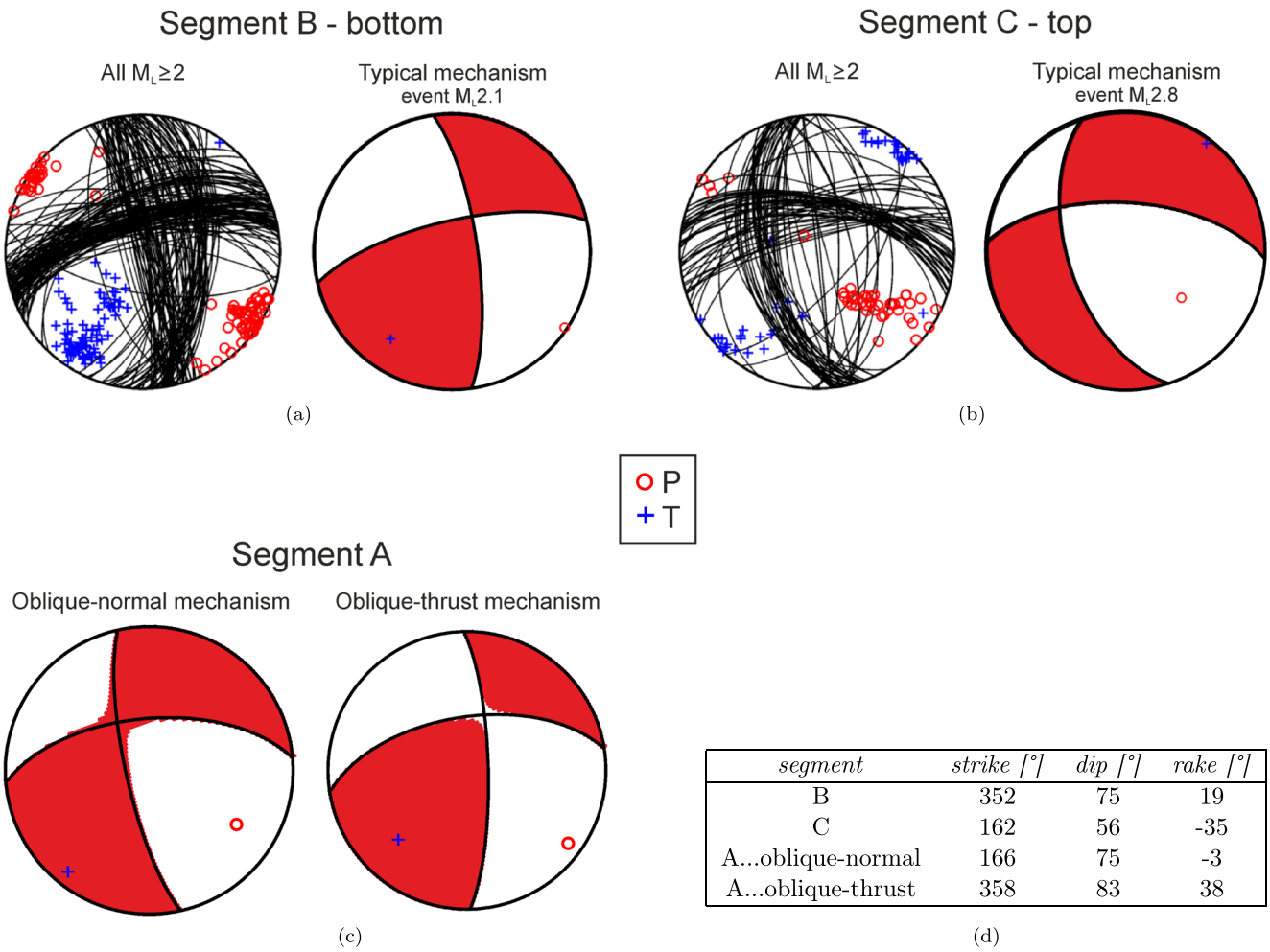

segment	*strike [°]*	*dip [°]*	*rake [°]*
B	352	75	19
C	162	56	-35
A...oblique-normal	166	75	-3
A...oblique-thrust	358	83	38

(d)

Fig. 7 Focal mechanisms of the 2011 swarm events located in fault segments B (**a**) and C (**b**). The mechanisms in **a** and **b** are displayed by a couple of plots: a graphical stack of fault plane solutions of $M_L \geq 2$ events (85 events in (**a**), 44 events in (**b**)), and a characteristic focal mechanism in the FPS representation. **c** Characteristic focal mechanisms of the 2000 and 2008 events being located in segment A which are taken from Horálek and Šílený (2013). All the FPS solutions are represented in the equal-area, lower-hemisphere projection. The principal axes *P* and *T* are marked by *red circles* and *blue crosses*. **d** The strike, dip and rake angles of the typical focal mechanisms from fault segments B, C and A

as they readily match the geometry of corresponding fault segments.

The FPS of events from C are more constrained than those from B. In segment C, the strikes vary between 160° and 180°, and dips between 50° and 80°. In segment B, the strikes vary more broadly, ranging between 330° and 20°, and the dips are similar or steeper compared to those in C.

Figure 7a (right) shows a representative mechanism of segment B (strike 352°, dip 75°). It fits the segment orientation of strike 351° and eastward dip 72°. Similarly, Fig. 7b (right) shows a representative mechanism of segment C (strike 162°, dip 56°) which nicely corresponds to the segment orientation of strike 171° and westward dip 63°. It is worth noting that the FPS of the 2000 and 2008 swarm events also show significant variability (Vavryčuk 2011; Horálek and Šílený 2013; Vavryčuk et al. 2013) which may be due to a jagged rupture pattern along the fault segment.

Figure 7 shows an obvious similarity between the focal mechanisms in the southern (A) and both northern (B, C) segments. Similar oblique-normal

mechanisms in segments A and C reflect their similar geometry. The oblique-thrust mechanisms, which prevail in segment B, were also observed in the 2000 and 2008 swarms. However, they were in a minority and occurred in rather small patches of the fault with vaguely distinguished geometry (see Fig. 11 in Fischer et al. 2014).

The FPS pattern of the 2011 events shows the P-axes in the northwest-southeast and the T-axes in the northeast-southwest directions. The P-axes are sub-horizontal and the T-axes nearly horizontal for the oblique-normal events, and slightly changed for the oblique-thrust events. This is fully consistent with the orientation of the axes indicated by the 2000 and 2008 source mechanisms (Horálek and Šílený 2013; Vavryčuk 2011), and also with the axes of the maximum (σ_1) and minimum (σ_3) regional tectonic stress in the West Bohemia/Vogtland crust (e.g. Švancara et al. 2008).

Our results confirm previous inferences that faulting during individual swarms is controlled mainly by the regional tectonic stress (Fischer et al. 2010; Horálek and Šílený 2013). However, a greater understanding of faulting and forces acting during the swarm requires an in-depth study of source mechanisms in the full moment tensor description.

7 A weak earthquake swarm of 2013

The 2013 swarm is important due to its location and time development, despite its weakness when compared to the previous swarms. This "mini-swarm" lasted about four months and comprised about 1500 events with magnitudes $M_L \leq 2.3$. Figure 5 shows that the 2013 swarm complements the 2011 swarm as it activated parts of segments B and C which were almost unbroken in 2011. The pattern of the events' space-time distribution is also basically similar, except that it was counterclockwise in 2011 and clockwise in 2013. Both activities were initiated on the boundary of the segments B and C at the depths of around 8 km, the only difference being the southern edge in 2011 and the northern edge in 2013.

In 2013, the first phase was characterised by its rapidity and downward migration along fault segment B. After about 1-week calmness, the activity recurred in segment B, switching then into segment C where it continued at a rather a low event-occurrence rate for 10 weeks. As with the 2011 swarm, the seismicity in segment C migrated upwards when the shallowest foci were located at depths around 6 km (copper-coloured dots in Fig. 5b). After 3 (in 2011) and 4 (in 2013) months of diminishing activity, both swarms were terminated by sequences of larger events.

The features of both swarms imply a gradual buildup of stress on the segments, which was released subsequently on their parts at a different time. It corresponds to the Coulomb stress changes, when the time lag was about 1.5 year.

8 Discussion

The analysis of the three successive earthquake swarms in 2000, 2008 and 2011 and of one mini-swarm in 2013 in the NK focal zone enables us to infer some more general characteristics of the West Bohemian swarms.

First, as seen in Fig. 4, the MFD of all the swarms show a noticeable similarity in the regular part of the distribution having b-value ≈ 1.0, which is bounded by a magnitude limit of about $M_L \approx 2.7$ to 3.0. Events above this limit clearly deflect from the Gutenberg-Richter law and behave irregularly. These irregularities in each swarm are totally different but they are always related approximately to the 10 to 15 largest events of the individual swarms. The irregularities are not random because they appear in all the swarms and must have some physical explanation, some of which are given in Section 4. Since this is very striking, it is worth detailed investigation.

Neunhöfer and Hemmann (2005) pointed out that strong events of the West Bohemia/Vogtland swarms cannot be characterised by the b-values of the respective MFD and solved it by introducing a bimodal MFD. Utsu (1971) modelled such discrepancy by a mixture of mainshocks and aftershocks, each having a different b-value. This idea may fittingly explain deflection of the strongest events from the 2000, 2008 and 2011 swarms from the GR law.

Second, an issue worth discussing is the focal migration in the individual swarms. Migration is often assumed to be closely connected to ascending pressurized fluids, which propagate along the fault plane in accordance with the diffusion equation (e.g. Parotidis et al. 2003; Hainzl 2004). In Figs. 5 and 6, we

demonstrate two couples of earthquake swarms which share common fault segments (2000 and 2008 the fault segment A, and 2011 and 2013 the fault segments B and C). They show similar patterns of the spatial distribution of foci, but different patterns of the focal migration. The fact that each phase of the individual swarm is dominated by one large or a few larger events suggests that the phases are mainshock-aftershock sequences (sometimes with foreshocks), or a combination of them. This behaviour evolves as a cascade of brittle failure. This agrees with the findings of Fischer and Horálek (2005) that both static and dynamic Coulomb stress changes along the fault plane due to co-seismic slip contribute significantly to triggering the swarm events. These facts indicate that migration of the earthquake swarm activity is governed by the occurrence of dominant events, space-time distribution of which differs in the individual swarms, and that the majority of the events in the phases originate due to the stress redistribution.

Third, the spatial distribution of the 2000 and 2008 swarms, as well as of microswarms and non-swarm seismicity, led us to conclude that the NK zone had a planar character signifying one fault plane (Fischer and Horálek 2003). However, the spatial distribution of the 2011 foci suggests a more complex structure. It appears more likely that the NK zone is composed of several critically loaded shorter fault segments which are activated when additional buildup of the local stress causes them to fail.

To support this claim, we cite the 1997 swarm located close to the 2011 swarm (north of the 2000 and 2008 swarms), which also showed a two-arm character (Fischer and Horálek 2000). We need only recall that the 1997 swarm is the only one earthquake activity so far in West Bohemia/Vogtland in which a significant amount of tensile-type events were indicated (Vavryčuk 2001; Horálek et al. 2002). In this paper, we do not examine the significance of the non-DC components (reasons are given in Section 3.3), which are signs of tensile earthquakes. However, such a detailed analysis would be worthwhile because tensile earthquakes likely relates to the crustal-fluid activity in the rupture process.

The 2011 swarm represents a high quality data set that could deepen our understanding of the nature of the seismic activity in the area. Our future studies will address the current pattern of the spatiotemporal event distribution in the NK zone incorporating the 2011 swarm and the recent non-swarm activity in 2014, and a detailed analysis of the 2011 source mechanisms in a full moment tensor description.

9 Conclusions

The 2011 earthquake swarm occurred from 24th August 2011 to 31st January 2012 in the Nový Kostel area of West Bohemia/Vogtland. The swarm included 10 $M_L \geq 3.0$ and 155 $M_L \geq 2.0$ events. The two largest events had magnitudes $M_L = 3.7$ and 3.5, which has made it the second most intensive swarm since the $M_L = 4.6$ swarm in 1985/1986, apart from the intense $M_L = 4.5$ non-swarm activity in May 2014. About 25,000 $M_L \geq 0.5$ events were detected using an automatic picker, a similar number to the 2008 swarm. To be consistent and for a stable magnitude estimation of events from a broader area of West Bohemia and Vogtland, we refined the parameters in the WEBNET-local-magnitude formula (1) and derived the station correction for all 13 telemetred WEBNET stations.

We analysed the 2011 swarm and compared it with the previous swarms of 2000 and 2008 from the perspective of the statistical characteristics (magnitude-frequency distribution, distribution of the interevent times and the cumulative seismic moment), spatial and temporal distribution of the swarm events, and typical focal mechanisms. The results are summarised as follows:

- The maximum ground motions in the 2011 swarm observed by the WEBNET correspond to the displacement of 0.21 mm, the velocity of 11 mm/s and the acceleration of 0.68 m/s^2, which are nearly the same as those observed in the 2008 swarm. All these maximum ground motion quantities were observed at station NKC (located inside the NK epicentral area), whereas in the 2008 swarm at station STC (located northeast of the NK area at a distance of about 6 km).
- The cumulative seismic moment released during the 2011 and 2008 swarms is comparable, of about $M_0 \approx 9.2 \times 10^{14}$ Nm and $M_0 \approx 11.8 \times 10^{14}$ Nm (estimated using the Horálek and Šílený (2013) formula), while the seismic moment released during the 2000 swarm is roughly half the size, of $M_0 \approx 5.1 \times 10^{14}$ Nm.

- The 2011 swarm was very rapid. It exhibited a much higher rate of the seismic moment release than the swarms of 2000 and 2008, when 95 % of the total seismic moment was released during just 13 days compared to 22 days in 2008 and 70 days in 2000. The magnitude-frequency distribution (MFD) of all the three swarms shows a bimodal character. For magnitudes smaller than 2.7–3.0, the MFD behaves regularly obeying the GR law with b-value ≈ 1.0. However, for higher magnitudes, the MFD is irregular, noticeably departing from the GR law. Constant a (event-productivity) gives a rough estimate of total amount of the $M_L > 0$ events, which was similar in the 2011 and 2008 swarms ($\sim$ 7000 events), and approximately one third lower in the 2000 swarm.
- Probability density functions of interevent times of these swarms are similar, complying with power law $\propto T_w^{-q}$ (q =1.38 for the 2000, 1.44 for the 2008 and 1.44 for the 2011 swarm), which points to Omori-like mainshock-aftershock activity.
- The spatiotemporal distribution of foci disclosed two fault segments (B and C in our notation), which were activated during the 2011 and 2013 swarm. In 2013, fault patches quiet in 2011 were activated. Hence, the 2013 swarm can be understood as complementary activity to the 2011 swarm. Segments B and C are different from fault segment A that hosted the 2000 and 2008 swarms. It indicates a more complex structure of the NK zone than had been known. The individual swarms investigated show quite a different migration style. It suggests that the focal migration may be a causal process associated with an occurrence of larger events in the swarm.
- Prevailing focal mechanisms are strike-slips with a weak normal (oblique-normal) or thrust (oblique-thrust) component. The oblique-thrust mechanisms are typical for the deeper segment B, while the oblique-normal mechanisms are characteristic for the shallower segment C. Both mechanism types match well the geometry of the corresponding fault segments B and C.

Acknowledgments Our special thanks belong to our colleagues Jana Doubravová and Jakub Klicpera for carefully handling the WEBNET data. We also wish to thank Alena Boušková and Martin Labuta for primary processing of the WEBNET seismograms. Tomáš Fischer is in our debt for his help with calibrations of the WEBNET magnitudes. Editor Thomas Braun devoted careful attention to this paper for which we are grateful. The two anonymous reviewers provided valuable suggestions that helped us substantially to improve the paper. The work was accomplished within the Grant Project P210–12–2336 of the Grant Agency of the Czech Republic, "Earthquake swarms and their triggering mechanisms in diverse tectonic environments (Bohemian Massif, Mid-Atlantic Ridge, Western Alps)." The monitoring system WEBNET providing earthquake data received considerable support from the Ministry of Education, Youth and Sport of the Czech Republic (Project LM201000).

References

Babuška V, Plomerová J, Fischer T (2007) Intraplate seismicity in the western Bohemian Massif (central Europe): a possible correlation with a paleoplate junction. J Geodyn 44(3–5):149–159. doi:10.1016/j.jog.2007.02.004

Bankwitz P, Schneider G, Kämpf H, Bankwitz E (2003) Structural characteristics of epicentral areas in Central Europe: Study case Cheb Basin (Czech Republic). J Geodyn 35(1–2):5–32. doi:10.1016/S0264-3707(02)00051-0

Bouchaala F, Vavryčuk V, Fischer T (2013) Accuracy of the master-event and double-difference locations: Synthetic tests and application to seismicity in West Bohemia, Czech Republic. J Seismol 17(3):841–859. doi:10.1007/s10950-013-9357-4

Doubravová J, Horálek J (2013) New interactive software for seismic data processing. Technical Computing Prague 2013 21st Annual Conference Proceedings

Fischer T (2003) Automatic location of swarm earthquakes from local network data. Stud Geophys Geod 47(1):83–98. doi:10.1023/A:1022251605990

Fischer T, Horálek J (2000) Refined locations of the swarm earthquakes in the Nový Kostel focal zone and spatial distribution of the January 1997 swarm in Western Bohemia, Czech Republic. Stud Geophys Geod 44(2):210–226. doi:10.1023/A:1022162826079

Fischer T, Horálek J (2003) Space-time distribution of earthquake swarms in the principal focal zone of the NW Bohemia/Vogtland seismoactive region: Period 1985–2001. J Geodyn 35(1–2):125–144. doi:10.1016/S0264-3707(02)00058-3

Fischer T, Horálek J (2005) Slip-generated patterns of swarm microearthquakes from West Bohemia/Vogtland (central Europe): Evidence of their triggering mechanism? J Geophys Res 110(No.B5, B05S07). doi:10.1029/2004JB003363

Fischer T, Horálek J, Michálek J, Boušková A (2010) The 2008 West Bohemia earthquake swarm in the light of the WEBNET network. J Seismol 14(4):665–682. doi:10.1007/s10950-010-9189-4

Fischer T, Horálek J, Hrubcová P, Vavryčuk V, Bräuer K, Kämpf H (2014) Intra-continental earthquake swarms in West-Bohemia and Vogtland: a review. Tectonophysics 611:1–27. doi:10.1016/j.tecto.2013.11.001

Hainzl S (2004) Seismicity patterns of earthquake swarms due to fluid intrusion and stress triggering. Geophys J Int 159(3):1090–1096. doi:10.1111/j.1365-246X.2004.02463.x

Hainzl S, Fischer T (2002) Indications for a successively triggered rupture growth underlying the 2000 earthquake swarm in Vogtland/NW Bohemia. J Geophys Res 107(B12,2338):1–9. doi:10.1029/2002JB001865

Hainzl S, Ogata Y (2005) Detecting fluid signals in seismicity data through statistical earthquake modeling. J Geophys Res 110(No.B5, B05S07). doi:10.1029/2004JB003247

Horálek J, Fischer T (2010) Intraplate earthquake swarms in West Bohemia/Vogtland (Central Europe). Jökull 60:67–87

Horálek J, Šílený J (2013) Source mechanisms of the 2000 earthquake swarm in the West Bohemia/Vogtland region (Central Europe). Geophys J Int 194(2):979–999. doi:10.1093/gji/ggt138

Horálek J, Fischer T, Boušková A, Jedlička P (2000) The Western Bohemia/Vogtland region in the light of the WEBNET network. Stud Geophys Geod 44(2):107–125. doi:10.1023/A:1022198406514

Horálek J, Šílený J, Fischer T (2002) Moment tensors of the January 1997 earthquake swarm in NW Bohemia (Czech Republic): Double-couple vs. non-double-couple events. Tectonophysics 356:65–85. doi:10.1016/S0040-1951(02)00377-3

Horálek J, Fischer T, Boušková A, Michálek J, Hrubcová P (2009) The West Bohemian 2008-earthquake swarm: when, where, what size and data. Stud Geophys Geod 53(3):351–358. doi:10.1007/s11200-009-0024-8

Lomax A, Virieux J, Volant P, Berge C (2000) Probabilistic earthquake location in 3D and layered models: Introduction of a Metropolis-Gibbs method and comparison with linear locations. In: Thurber CH, Rabinowitz N (eds) Advances in seismic event location. Kluwer, Amsterdam, pp 101–134

Lomax A, Michelini A, Curtis A (2009) Earthquake location, direct, global-search methods. In: Meyers RA (ed) Encycl complex Syst Sci, Part 5. Springer, New York, pp 2449–2473. doi:10.1007/978-0-387-30440-3

Málek J, Horálek J, Janský J (2005) One-dimensional qP-wave velocity model of the upper crust for the West Bohemia/Vogtland earthquake swarm region. Stud Geophys Geod 49(4):501–524. doi:10.1007/s11200-005-0024-2

Mrlina J, Kämpf H, Kroner C, Mingram J, Stebich M, Brauer A, Geissler W H, Kallmeyer J, Matthes H, Seidl M (2009) Discovery of the first quaternary maar in the Bohemian Massif, Central Europe, based on combined geophysical and geological surveys. J Volcanol Geotherm Res 182(1–2):97–112. doi:10.1016/j.jvolgeores.2009.01.027

Neunhöfer H, Hemmann A (2005) Earthquake swarms in the Vogtland/Western Bohemia region: Spatial distribution and magnitude-frequency distribution as an indication of the genesis of swarms? J Geodyn 39(4):361–385. doi:10.1016/j.jog.2005.01.004

Parotidis M, Rothert E, Shapiro S A (2003) Pore-pressure diffusion: a possible triggering mechanism for the earthquake swarms 2000 in Vogtland/NW-Bohemia, central Europe. Geophys Res Lett 30(20):2075. doi:10.1029/2003GL018110

Utsu T (1971) Aftershocks and earthquake statistics (III) - Analyses of the distribution of earthquakes in magnitude,time and space with special consideration to clustering characteristics of earthquake occurrence (1). Journal of the Faculty of Science, Hokkaido University Series 7, Geophysics 3(5):379–441. http://hdl.handle.net/2115/8688

Utsu T, Ogata Y, Matsu'ura R S (1995) The centenary of the Omori formula for a decay law of aftershock activity. J Phys Earth 43:1–33. doi:10.4294/jpe1952.43.1

Vavryčuk V (2001) Inversion for parameters of tensile earthquakes. J Geophys Res 106(B8):16,339–16,355. doi:10.1029/2001JB000372

Vavryčuk V (2002) Non-double-couple earthquakes of 1997 January in West Bohemia, Czech Republic: Evidence of tensile faulting. Geophys J Int 149(2):364–373. doi:10.1046/j.1365-246X.2002.01654.x

Vavryčuk V (2011) Principal earthquakes: Theory and observations from the 2008 West Bohemia swarm. Earth Planet Sci Lett 305(3–4):290–296. doi:10.1016/j.epsl.2011.03.002

Vavryčuk V, Bouchaala F, Fischer T (2013) High-resolution fault image from accurate locations and focal mechanisms of the 2008 swarm earthquakes in West Bohemia, Czech Republic. Tectonophysics 590:189–195. doi:10.1016/j.tecto.2013.01.025

Švancara J, Havíř J, Conrad W (2008) Derived gravity field of the seismogenic upper crust of SE Germany and West Bohemia and its comparison with seismicity. Stud Geophys Geod 52(4):567–588. doi:10.1007/s11200-008-0038-7

Waldhauser F (2001) hypoDD: A computer program to compute double-difference hypocenter locations. US Geol Surv Open File Rep 01–113:1–25

Waldhauser F, Ellsworth W (2000) A double-difference earthquake location algorithm: Method and application to the northern Hayward fault, California. Bull Seismol Soc Am 90(6):1353–1368. doi:10.1785/0120000006

Wiemer S, Wyss M (2000) Minimum magnitude of completeness in earthquake catalogs: Examples from Alaska, the western United States, and Japan. Bull Seismol Soc Am 90(4):859–869. doi:10.1785/0119990114

Pure Appl. Geophys.

https://doi.org/10.1007/s00024-017-1679-7

Pure and Applied Geophysics

2014 Mainshock-Aftershock Activity Versus Earthquake Swarms in West Bohemia, Czech Republic

Hana Jakoubková,[1] Josef Horálek,[1] and Tomáš Fischer[2]

Abstract—A singular sequence of three episodes of M_L3.5, 4.4 and 3.6 mainshock-aftershock occurred in the West Bohemia/Vogtland earthquake-swarm region during 2014. We analysed this activity using the WEBNET data and compared it with the swarms of 1997, 2000, 2008 and 2011 from the perspective of cumulative seismic moment, statistical characteristics, space-time distribution of events, and prevailing focal mechanisms. For this purpose, we improved the scaling relation between seismic moment M_0 and local magnitude M_L by WEBNET. The total seismic moment released during 2014 episodes ($M_{0tot} \approx 1.58 \times 10^{15}$ Nm) corresponded to a single M_L4.6+ event and was comparable to M_{0tot} of the swarms of 2000, 2008 and 2011. We inferred that the M_L4.8 earthquake is the maximum expected event in Nový Kostel (NK), the main focal zone. Despite the different character of the 2014 sequence and the earthquake swarms, the magnitude-frequency distributions (MFDs) show the *b*-values ≈ 1 and probability density functions (PDFs) of the interevent times indicate the similar event rate of the individual swarms and 2014 activity. Only the *a*-value (event-productivity) in the MFD of the 2014 sequence is significantly lower than those of the swarms. A notable finding is a significant acceleration of the seismic moment release in each subsequent activity starting from the 2000 swarm to the 2014 sequence, which may indicate an alteration from the swarm-like to the mainshocks-aftershock character of the seismicity. The three mainshocks are located on a newly activated fault segment/asperity (D in out notation) of the NK zone situated in the transition area among fault segments A, B, C, which hosted the 2000, 2008 and 2011 swarms. The segment D appears to be predisposed to an oblique-thrust faulting while strike-slip faulting is typical of segments A, B and C. In conclusion, we propose a basic segment scheme of the NK zone which should be improved gradually.

Key words: West Bohemia/Vogtland, earthquake swarms, mainshock-aftershock sequence, total seismic moment, statistical characteristics of earthquake activities, HypoDD locations, focal mechanism estimation.

1. Introduction

Earthquake swarms represent sequences of seismic events closely clustered in space and time, with a few dominant, similarly strong events occurring throughout the whole swarm (Mogi 1963). These attributes distinguish earthquake swarms from ordinary mainshock-aftershock sequences when one dominant event occurs at the beginning of the activity. The mainshock has a magnitude of one or more magnitude units higher than those of aftershocks, so a major part of seismic energy is released through it (Båth 1965).

Earthquake swarms appear at the boundaries as well as in the inner parts of tectonic plates (interplate and intraplate swarms). Their occurrence is usually related to volcanic activity (Hill 1977; Pedersen et al. 2007; Farrell et al. 2009), but quite often they are of pure tectonic origin (Horálek et al. 2015; Jenatton et al. 2007; Ibs-von Seht et al. 2008). Typical swarm-like areas involve volcanic regions, geothermal fields and ocean ridges (Horálek et al. 2015). Intraplate swarms are mainly related to Quaternary-volcanism areas, where another phenomena such as diffuse degassing or geothermal anomalies are also present.

Earthquake swarms and mainshock-aftershock sequences usually occur either in dissimilar seismogenic areas or in the same area but independently of each other (e.g., Bourouis and Cornet 2009; Courboulex et al. 2013). Their causality was observed when an earthquake swarm preceded the mainshock-aftershock sequence (e.g., Chiaraluce 2012) or was triggered by the mainshock (e.g., Ohmi et al. 2002), each activating separate parts of a common fault.

[1] Institute of Geophysics of the Czech Academy of Sciences, v. v. i., Boční II/1401, 14131 Prague, Czech Republic. E-mail: hanaj@ig.cas.cz

[2] Faculty of Science, Charles University, Prague, Czech Republic.

Published online: 25 November 2017

However, both types of seismicity in one common focal zone occur rather rarely. Their coexistence was observed in the Ubaye Valley of the French Alps where a striking seismicity having attributes of both earthquake swarms and mainshock-aftershock sequences (two dominant mainshocks) occurred in 2012 and 2015 (F. Thouvenot, personal communication). The West Bohemia/Vogtland (a border area between western Bohemia and Saxony, Germany) is a well-known European intraplate earthquake swarm region connected somehow with extinct Quaternary volcanism. Earthquake swarms there have been well documented since the beginning of the 19th century (see Credner 1876; Neunhöfer and Hemmann 2005; Fischer et al. 2014).

However, in 2014 this typical swarm-like character was disrupted by an unexpected, obviously non-swarm sequence of earthquakes with a dominant shock of local magnitude of M_L4.4. This activity represents probably the first more intense non-swarm sequence of a classical mainshock-aftershock character observed in the region during the last 100 years (Neunhöfer and Meier 2004; Fischer and Horálek 2003; Horálek and Fischer 2010; Fischer et al. 2014). Hainzl et al. (2016) recently dealt primarily with the triggering mechanism of the 2014 sequence of aftershocks following the M_L4.4 mainshock. They concluded this was a result of the combined action of tectonic stress, Coulomb stress change due to the mainshock rupture, and migration of over-pressurized fluids along the preexisting fault planes.

In this paper, we present an analysis of the entire 2014 sequence comprising cumulative seismic moment, statistical characteristics, temporal evolution of the activity, precise event locations and focal zone geometry, and source mechanisms of the three mainshocks. We also compare the 2014 characteristics with those of the previous swarms. The paper should raise these questions:

- What is the nature of the West Bohemia/Vogtland earthquake swarms?
- Why has the character of seismicity in one common focal zone changed from earthquake swarms from 2000 to 2013 to the mainshock-aftershock sequence in 2014?
- Do earthquake swarms in the meaning of their general definition, and classic mainshock-aftershock sequences represent end members of a wide range of seismic activity which may occur in West Bohemia/Vogtland?

2. *West Bohemia/Vogtland Seismogenic Area and Previous Swarms*

The West Bohemia/Vogtland seismogenic region (latitude ≈ 49.8 to 50.7° N, longitude ≈ 12 to 13°E) is situated in the western part of the Bohemian Massif where three principal tectonic units, Saxothuringian, Moldanubian and the Teplá–Barrandian, are connected. The region is intersected by an ENE-WSW trending neotectonic structure called the Eger rift and by the NNW-SSE striking Mariánské Lázně fault (Fig. 1). Quaternary volcanism is manifested by two extinct volcanoes (Komorní Hůrka and Železná Hůrka, estimated age 0.3 Ma; Wagner et al. 2002) situated only 15 and 20 km apart from the main epicentral zone, by two maar structures (Mrlina et al. 2009) and by massive degassing of CO_2 from a deep source (Bräuer et al. 2005).

Most of the seismic energy has been released there in the form of reoccurring earthquake swarms comprising a series of thousands $M_L > 0$ events, mostly with magnitudes of $M_L < 4$; their duration is from several days to three months. To date, the largest instrumentally recorded earthquake occurred in the 1985/86 swarm (M_L4.6, e.g., Vavryčuk 1993) and in May 2014 (M_L4.4). Fischer et al. (2010) assessed the seismic potential of the region to correspond roughly to a single event of local magnitude $M_L \approx 5.5$. The swarm-like seismicity clusters in a number of small epicentral zones scattered in an area of about 40 km by 60 km. However, larger earthquake activities ($\sim M_L > 2.5$) cluster predominantly in focal zone Nový Kostel (NK) which dominates the recent seismicity of the whole region; since 1991, it produced more than 90% of the total seismic moment released in the whole seismogenic area. Notable earthquake swarms in NK, the main focal zone, during the last 30 years occurred in 1985/86 ($M_{L\max}$4.6), 1997 ($M_{L\max}$3.0), 2000 ($M_{L\max}$3.3), 2008

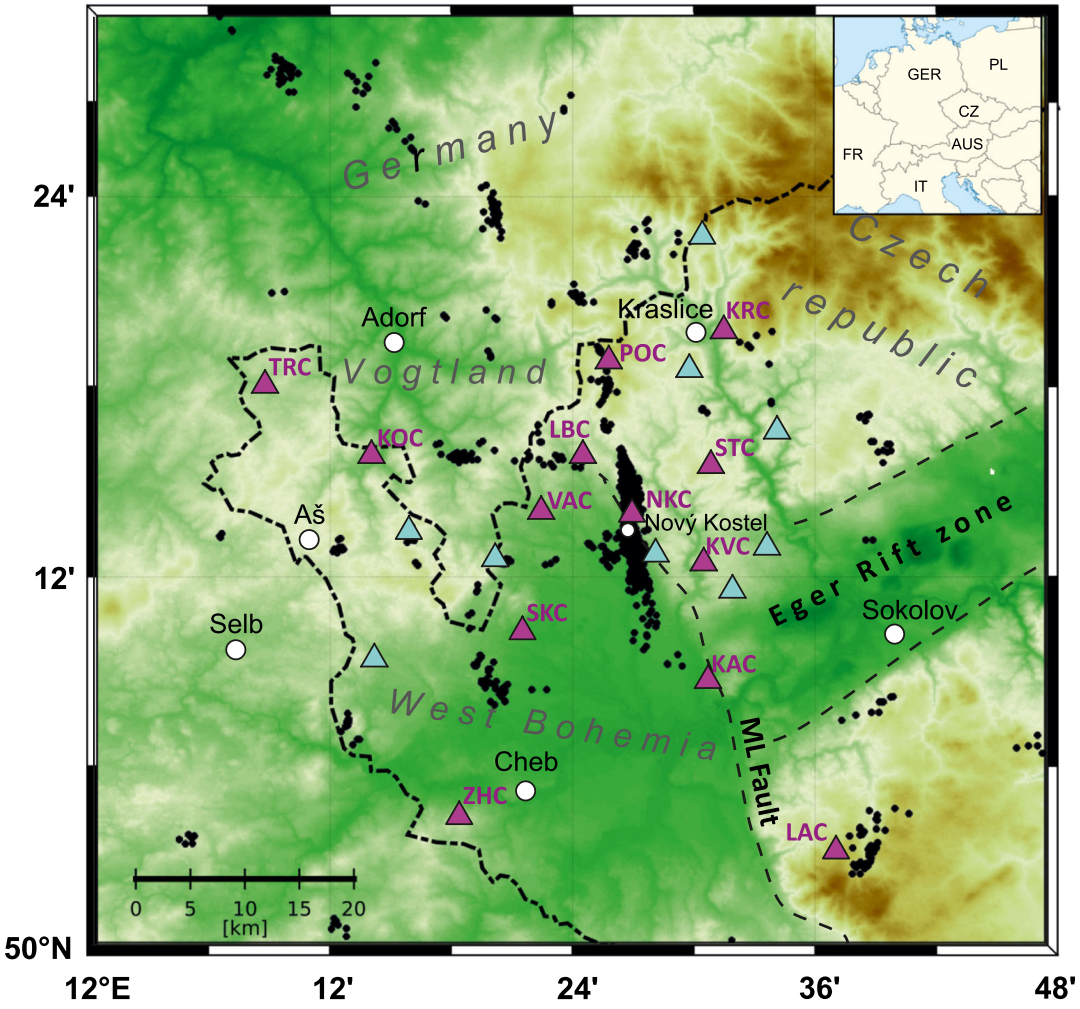

Figure 1

Map of the seismically active area in the West Bohemia/Vogtland region with stations of the WEBNET network. Violet triangles—online stations, light blue triangles—offline stations. Black dots—seismic events of $M_L \geq 0$ from the time period 1997–2015. Larger white circles—towns. Smaller white circle—village of Nový Kostel. Dashed lines mark dominant tectonic structures in the region: the Mariánské-Lázně fault (ML) and the Eger Rift. Dot-dashed line denotes the Czech-German border. Note that station NKC is located in the middle of the main epicentral area of Nový Kostel (NK)

($M_{L\max}$3.8) and 2011 ($M_{L\max}$3.7). During the past 100 years, the rapid succession of swarms in 2000, 2008, 2011 and the 2014 activity was exceptional in the West Bohemia/Vogtland region, a similarly large activity occurred there at the turn of the 19th and 20th centuries (e.g., Grünthal 1989). (For details about recent swarms compared with the 2014 sequence, see Table 1 and Fig. 2.)

The individual swarms have been thoroughly studied from various perspectives: the space-time distribution of events and the fault geometry in this zone (Fischer and Horálek 2000, 2003; Horálek et al. 2009; Fischer et al. 2010; Bouchaala et al. 2013;

Table 1

Basic characteristics of the earthquake swarms in the last 20 years (1997, 2000, 2008 and 2011) and the 2014 activity

Swarm	Duration (days)	$M_{\max}$	Num. of ev. ($M_L \geq 0$)	Segment
1997	10	3.0	530	Part of B
2000	90	3.3	3800	A
2008	70	3.8	4400	A
2011	30	3.7	5700	B, C
2014	90	4.4	2800	mainshocks: D aftershocks: A, B, C, D

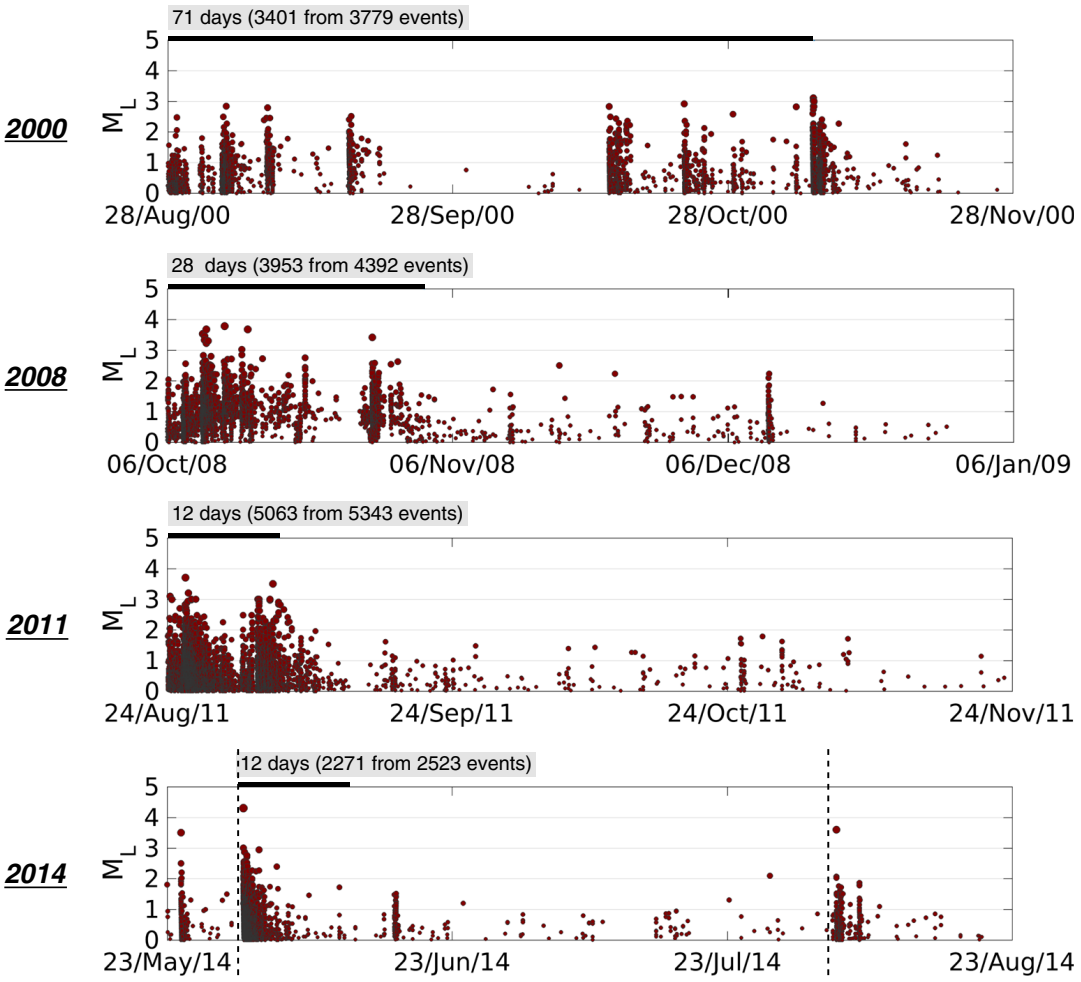

Figure 2
Magnitude-time course of the swarms 2000, 2008, 2011 and the 2014 sequence. The dataset I is used. Numbers on gray rectangles—number of days during which 90% of events, which were recorded within three months, occurred. For the 2014 sequence time interval covers only the M_L4.4 aftershocks (two months indicated by the dashed black lines). Note different patterns of individual swarms and the 2014 activity exhibiting a character of three mainshock-aftershock sequences

Čermáková and Horálek 2015); source mechanisms and stress field (Horálek et al. 2002; Vavryčuk 2002, 2011; Horálek and Šílený 2013); triggering mechanisms and driving forces (Hainzl and Fischer 2002; Hainzl and Ogata 2005; Fischer and Horálek 2005; Hainzl et al. 2012, 2016).

The results obtained can be briefly summarised as follows. Typical focal depths are between 7 and 12 km. The earthquake activity in the NK zone shows a distinctly episodic character, migrating hypocentres and the reactivation of previously ruptured patches on a fault. The individual swarms are composed of a number of swarm phases. The NK zone shows a big complexity when each swarm activates one or more fault segments. Events are not associated with any identifiable mainshock, but rather several dominant events of similar magnitude occur. The region is well known by its crustal fluid activity, therefore, the ongoing magmatic processes and related transport of fluids and their interaction with tectonic structures are presumed responsible for generating earthquake swarms.

3. *Basic Characteristic of the 2014 Seismic Activity*

The 2014 activity has been exceptional in West Bohemia/Vogtland due to its non-swarm character and a relatively large magnitude of the strongest mainshock. Swarm earthquakes occurring there since the extraordinarily intense $M_{L\max}$4.6 swarm of 1985/86, were much weaker, the strongest of them

with M_L3.8 and 3.7 took place during the swarm of 2008 and 2011. This makes the 2014 activity the most significant since the strong swarm in 1985/86 ($M_{L\max}$4.6) and also in 1908 ($M_{L\max} \approx 5.0$, estimated in catalogues).

As with the previous swarms, the 2014 sequence took place in Nový Kostel, the main focal zone, and consisted of three episodes, each with a dominant mainshock. The first M_L3.5 mainshock appeared on May 24, 2014. It occurred unexpectedly, without weaker preceding events except for the M_L1.8 event one day before. The M_L3.5 earthquake was followed by 177 events (M_L0 to 2.5), after that the activity calmed down. On May 31, after a week of tranquility, the second M_L4.4 mainshock stroke the area. It was almost immediately followed by one event of M_L3.0, and within only five days 2205 events with M_L ranging from 0 to 2.9 were detected. Low seismicity persisted for two months with about 250 events (M_L0 to 2) (Fig. 2). The activity returned on August 3 with the third M_L3.6 mainshock; seismicity lasted for three days and consisted of 294 events with a magnitude ranging from 0 to 2.0. Then the activity ceased.

Aftershocks following the three mainshocks are of the maximum magnitudes of M_L2.5 (after the M_L3.5 mainshock), M_L3.0 (after the M_L4.4 mainshock) and M_L2.1 (after the M_L3.6 mainshock). Accordingly, the magnitude difference between the individual mainshocks and their aftershocks is $\triangle M_L$1.0 for the M_L3.5 mainshock, $\triangle M_L$1.4 for the M_L4.4 mainshock, and $\triangle M_L$1.5 for the M_L3.6 mainshock. These $\triangle M_L$ exceed substantially the $\triangle M_L$ values typical for earthquake swarms and point to the three-phase mainshock-aftershock character of the 2014 activity.

4. Data and Methods

We used data recorded by WEBNET, a local network in our analysis of the 2014 sequence. In 2014, it comprised 13 online and 9 offline three-component seismic stations, which covered an area of about 900 km^2 (Fig. 1). The records are proportional to the ground velocity in a frequency band of 0.5–80 Hz for the online and 1.0–80 Hz for the off-line stations. The sampling rate is 250 Hz at all stations. (For coordinates and instrumentation see Fischer et al. 2010; for details about the network see WEBNET 1991 and Horálek et al. 2000).

The station configuration in the 2014 activity is identical to that in the 2008 and 2011 swarms. For station configuration during the 2000 swarm we refer to Fischer and Horálek (2003). In case of the M_L4.4 event three stations, NKC, KVC and STC, situated in or near the 2014 epicentral area, were clipped by S-waves. Shown in Fig. 3 are P-wave waveforms (vertical components) of the three mainshocks in the ground velocity and ground displacement representation, and the ground-displacement spectra from the "epicentral" station NKC, near station STC, and two more distant stations POC and KRC. We analysed the 2014 seismic activity together with the swarms of 1997, 2000, 2008 and 2011 and created two datasets. Dataset I was to determine the cumulative seismic moment, magnitude-frequency and interevent time distributions, and the rate of activities. The 2000 and 2008 swarms of this dataset had been processed manually from triggered records and count about 5400 and 5000 $M_L \geq -0.5$ events for the 2000 and 2008 swarm. Seeking to make the 2011 and 2014 parts of the dataset complete, we processed continuous records with an automatic event detector comparable to that of Fischer (2003). By this means we collected 8700 events for the 2011 and 5600 events for the 2014 activity (both $M_L \geq -0.5$).

Dataset II was used to locate events and afterwards for analysing their space-time distribution. This dataset was acquired by manually picking the P- and S-waves arrival times with the accuracy of $\pm$4 ms for the P-wave onset and $\pm$8–12 ms for the S-wave onset. The number of events for each activity was about 5500 (2000 swarm), 5000 (2008 swarm), 4300 (2011 swarm) and 2800 (2014 sequence).

The absolute event locations were performed by the NLLoc algorithm (Non-Linear Earthquake Location; Lomax et al. 2000, 2009) in a 1-D velocity model of the area's upper crust (modified model of Málek et al. 2005). We used P- and S-wave arrival times of ten selected stations which are at epicentral distance less than 10 km (NKC, KVC, SKC, VAC, LBC and STC) and between 13 and 24 km (KRC, KOC, POC and LAC). The locations attained by NLLoc were then refined by the HypoDD program (Double-Difference Hypocenters Location;

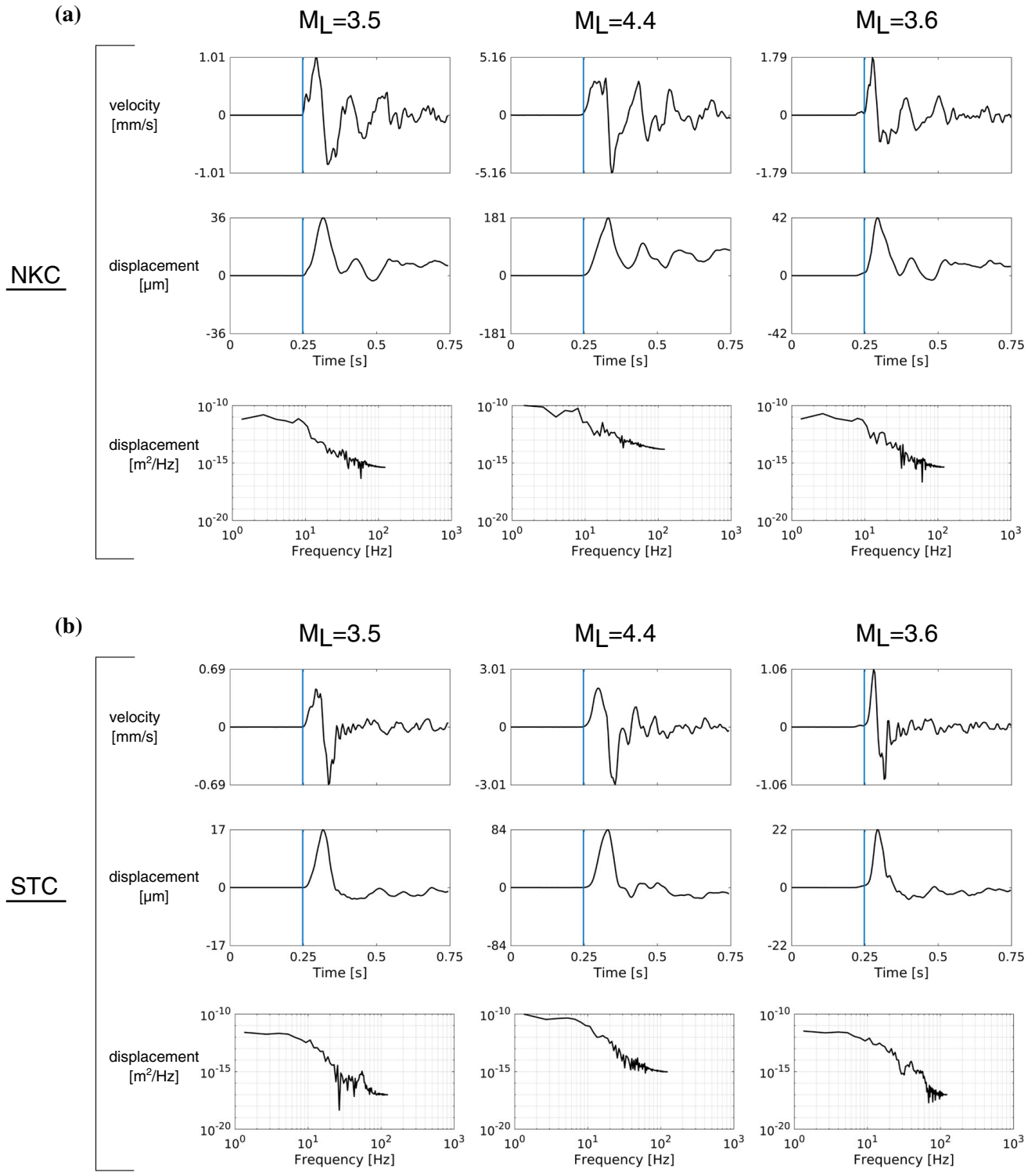

Figure 3
Vertical components of P-wave waveforms of the three mainshocks at station NKC (**a**), STC (**b**), POC (**c**) and KRC (**d**). Top—ground velocity in m/s; Middle—ground displacement in μm; Bottom—ground-displacement spectra in m^2/Hz. Blue solid lines—onsets of the P-waves

Waldhauser and Ellsworth 2000; Waldhauser 2001). (For further details about the HypoDD algorithm and setting its parameters, see Čermáková and Horálek 2015). For relative locations we used only events of magnitude $M_L \geq 0$ recorded at least on a set of 5 stations ensuring good azimuthal coverage of the

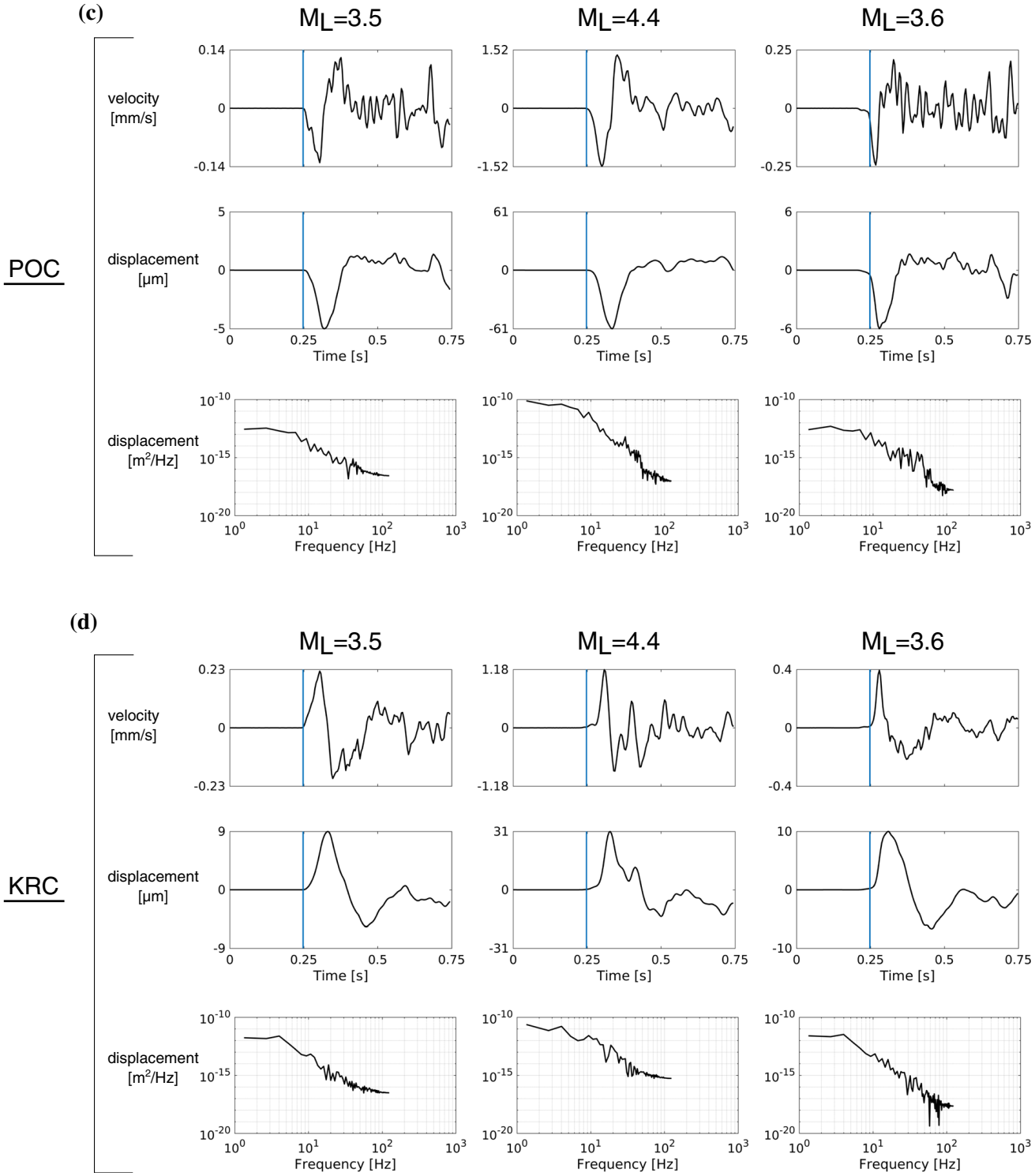

Figure 3
continued

area. In this way we got a set of 8957 precisely located events, namely for each activity: 338 (1997), 2037 (2000), 2729 (2008), 2522 (2011), and 1331 (2014).

To estimate focal mechanisms of the three mainshocks, we processed data from both online and offline WEBNET stations and we used the AMT code by Vavryčuk (2011) which inverts the P-waves

ground displacement amplitudes on the vertical component for full moment tensor. The code includes also the computation of Green's function for each event. We used the same velocity model as for locations, i.e., the modified model of Málek et al. (2005). The ground displacement peak amplitudes of the P-waves were picked automatically by the software package Seismon (developed by J. Doubravová and J. Michálek) and supervised by an interpreter.

5. *Cumulative Seismic Moment and Statistical Characteristics—A Comparison with Previous Swarms*

In our paper Čermáková and Horálek (2015), we used the empirical formula of Horálek and Šílený (2013), based on the moment tensor retrieval of the 2000 swarm, to estimate cumulative scalar seismic moment of the 2011 swarm. However, there are two more different empirical M_L-M_0 scaling relations proposed by Hainzl and Fischer (2002) and Michálek and Fischer (2013) based on the moment tensors of the 1997 swarm events and the source spectrum analysis of the 2000 and 2008 swarm events, respectively.

Figure 4 indicates that these scaling relations differ significantly when the seismic moments reported in the two latter papers exceeds those by Horálek and Šílený (2013) by more than one order. This inconsistency may be due to a different methodology of determining the M_0 but it is not a subject of this study. The 2014 activity makes it possible to verify the three M_L vs. M_0 scaling relations and, if necessary, to improve them.

The scalar seismic moments for 15 selected events in the M_L range of 2–4.4 were determined by V. Vavryčuk (personal communication). He applied the waveform inversion to P-wave displacement records in the time domain, using Vavryčuk and Kühn (2012)'s algorithm. The resultant mechanisms show seismic moments ranging between 2.0×10^{12} and 8.0×10^{14} Nm which correspond to moment magnitudes M_w 2.1 ($\sim M_L$2.0) and 3.9 ($\sim M_L$4.4). Note that the moment magnitude of the M_L4.4 mainshock is quite similar to M_w3.8 reported by the U.S. Geological Survey (USGS) based on regional stations.

An important finding is that the seismic moments of all the 15 events determined by V. Vavryčuk are quite close to those estimated using the Horálek and Šílený (2013) relation $\log_{10} M_0 = 1.12 \cdot M_L + 9.78$. Although they differ slightly in the absolute level (the seismic moments by V. Vavryčuk being larger in all but two cases), the slopes of the $\log_{10} M_0$ vs. M_L dependences are quite similar (see Fig. 4).

Since the Horálek and Šílený (2013) relation gives a bit smaller seismic moment (3.9×10^{14} Nm, $M_w = 3.7$) than that determined by USGS (6.16×10^{14} Nm, $M_w = 3.8$), and is based on a rather narrow M_L range between 1.7 and 3.1, we modified this scaling relation to fit data of the 2014 activity, in particular those of stronger events ($M_L \geq 2.5$, Fig. 4). Linear regression of the $\log_{10} M_0$ vs. M_L data yields a relation between the WEBNET local magnitude M_L and the seismic moment M_0:

$$\log_{10} M_0 = 1.10 \cdot M_L + 10.09, \qquad (1)$$

where M_0 is measured in Nm. This formula has been used to evaluate seismic moments released during the 2014 activity and the previous earthquake swarms.

By calculating the cumulative seismic moment of $M_L \geq 0$ events we found that the total seismic moment $M_{0\text{tot}}$ released during the entire 2014 activity is $M_{0\text{tot}} \approx 1.58 \times 10^{15}$ Nm which corresponds to a M_L4.6+ single event. It is comparable to total seismic moments of the 2000, 2008 and 2011 swarms being $M_{0\text{tot}} = 9.50 \times 10^{14}$, 2.15×10^{15} and 1.86×10^{15} Nm, and that corresponds to single events with M_L4.4, 4.8 and 4.7, respectively. The three 2014 mainshocks (M_L3.5, 4.4 and 3.6) and the M_L4.4 mainshock itself represent 66 and 54% of the total seismic moment released, respectively. Fig. 5a shows that practically the whole seismic moment of the 2014 activity was released in three short-time episodes, the majority in the second episode.

Seismic moment released in other periods is insignificant because only few events of a rather small magnitude occurred out of the three episodes. This distinguishes the 2014 activity from the swarm-like seismicity in which the cumulative seismic moment increases gradually with several considerable steep increases corresponding to main swarm

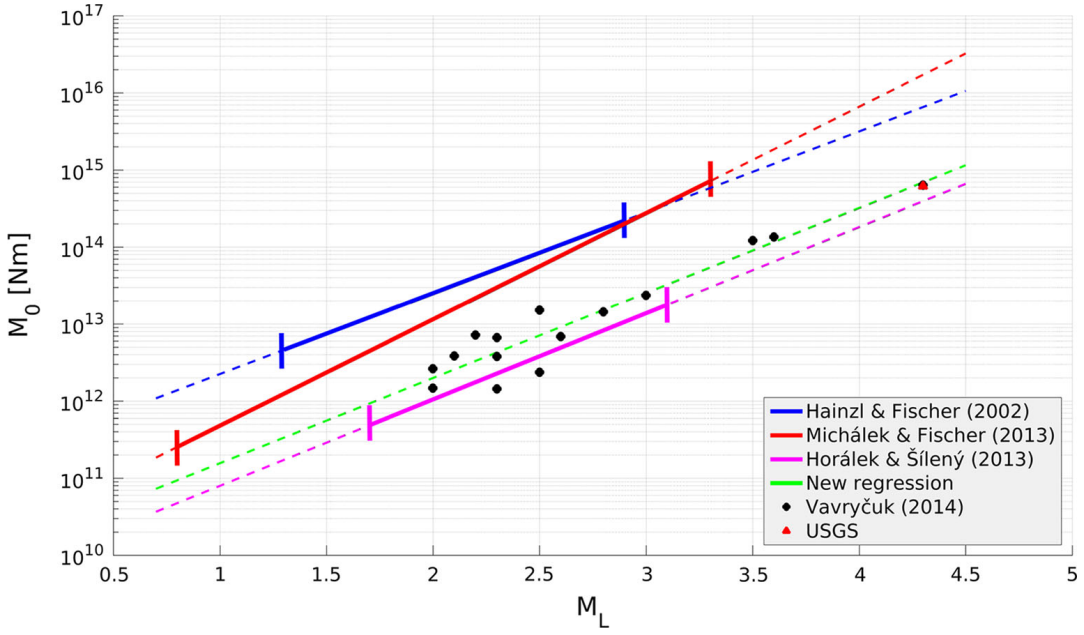

Figure 4
Scalar seismic moment M_0 versus the WEBNET local magnitude M_L for the scaling relation based on the 2014 events (dashed green line), and for the prior relations by Horálek and Šílený (2013) (violet line), Michálek and Fischer (2013) (red line), and Hainzl and Fischer (2002) (blue line). Black dots: M_0-M_L relation of 2014 events used for the M_0-M_L linear regression. Red triangle: $M_0 = 6.16 \times 10^{14}$ Nm ($\sim M_w = 3.8$) reported by USGS for the M_L4.4 mainshock. Solid parts of the blue, red and violet lines indicate the magnitude range of the events used to derive the corresponding relations

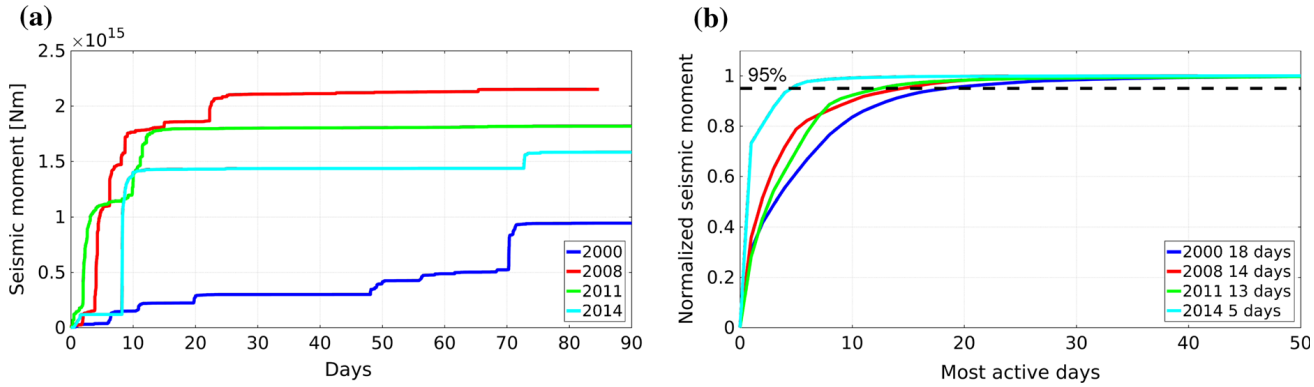

Figure 5
a Cumulative seismic moment of $M_L \geq 0$ events; **b** normalised cumulative seismic moment by the total seismic moment, sorted based on its daily amount in a descending order. Swarms 2000 (blue), 2008 (red), 2011 (green), and activity 2014 (light blue). The dashed black line in (**b**)—95% of total seismic moment. Number of days in (**b**)—time necessary to release 95 % of total seismic moment

phases. Figure 5a also shows a similar seismic moment release during the dominant phase of the 2008, 2011 and 2014 activities being about 1.2×10^{15} Nm, which corresponds to a single event of $M_L \approx 4.5$ (or $M_w \approx 4.0$). In fact, this is the maximum M_0 released in individual phases of the West Bohemian/Vogtland activities in the last 30 years.

Moreover we analysed the rate of the seismic moment release of the 2014 activity and swarms of 2000, 2008 and 2011. For this purpose we normalised the cumulative seismic moment per day by the total seismic moment, sorted these daily values in descending order, and then calculated their cumulative distribution (Fig. 5b). As a result, in Fig. 5b, the

days with the most intense activity are at the beginning while the days with weak activity are at the end of the individual diagrams. As is evident, the total seismic moment release accelerated in each subsequent activity starting from the 2000 swarm to the 2014 sequence. In other words, each new sequence was faster than the previous one leaving the 2014 activity the most rapid. It is also demonstrated by a decrease of the characteristic period during which 95% of total seismic moment was released. This period lasted for 18 days in 2000, 14 days in 2008, 13 days in 2011, and 5 days in 2014. The only deviation appears in the 2008 and 2011 swarms where the release of about 80% seismic moment was faster in 2008.

The increasing rate of seismic sequences is also apparent from Fig. 2 showing the time distribution of events of each sequence. Obviously a time period in which most of the events of each sequence are accumulated shortens with time. This indicates that the increasing rate of the seismic moment release could be connected with a transition from the swarm-like to the mainshock-aftershock character of the 2014 seismicity.

Furthermore, we calculated statistical characteristics: magnitude-frequency and interevent time distribution of the 2014 activity, and compared them with those of the previous swarms. The magnitude-frequency distribution (MFD) complying with the Gutenberg–Richter (G–R) law $\log_{10} N = a - bM$ (where N is the number of events having higher magnitude than magnitude M) gives information about the total number of the $M_L > 0$ events (event productivity a) and the ratio of smaller to larger events (b-value). The distribution of interevent times (waiting times between consecutive earthquakes) provides information about the event rate of a given activity.

However, reliable evaluation of both MFD and interevent time distribution requires the completeness of the dataset over a few orders of magnitude or they are questionable. To this end, we estimated the magnitude of completeness M_C using the maximum curvature method (MAXC; Wiemer and Wyss 2000) in which M_C corresponds to the maximum of the second derivative of the MFD. In fact, this point consists with the maximum of the non-cumulative MFD. We used this algorithm to determine M_C for the catalogues of both the 2014 sequence and previous swarms. We found that the completeness magnitude of the 2011 and 2014 catalogues (produced automatically) is $M_C = -0.25$ for the 2011, and $M_C = -0.50$ for the 2014, while that of the 2000 and 2008 swarms (obtained by manual picking) is much higher, $M_C = 0.25$ for both, and for the 1997 swarm it is higher as well being $M_C = -0.15$. To get comparable results we set M_C for all the activities to be $M_C = 0.25$.

The MFD for the activities in question are depicted in Fig. 6a. Even though the different character of the 2014 activity (three mainshock-aftershock episodes) and the earthquake swarms, the b-value is close to 1 for both swarms and mainshock-aftershock sequences. The MFD of the whole 2014 activity in particular complies quite well with the G–R law of $b = 1$ in the magnitude range of M_L0.25 to 3.0, and the three mainshocks are clearly away from the G–R law curve. A minor irregularity of MFD at magnitudes around M_L2.5 is probably due to the absence of the $M_L > 2.3$ aftershocks of the M_L3.5 and 3.6 mainshocks. Such size of the b-value is not exceptional; earthquake swarms showing b-value 1 also occur in other swarm areas in the world (Horálek et al. 2015). It should be noted that the higher value of b shown in Hainzl et al. (2016) ($b = 1.2$) is caused using the maximum likelihood estimator (MLE) where the authors used higher cutoff magnitude ($M_L \geq 1.0$) and ignored the probable incomplete recordings directly after the M_L4.4 mainshock.

The MFDs of the swarms and the 2014 aftershock sequences show a different shape at the highest magnitude level. In particular, the swarms are missing dominant events thus deflecting from the linear trend downwards, the MFDs being cut-off. On the contrary, the 2014 MFD shows an L-shape at the highest magnitude level caused by the single M_L4.4 mainshock. Being aware of the smaller significance of this observation caused by low sampling numbers for the largest magnitudes, we note that the different MFD shape of swarms and mainshock-aftershock sequences is inherent for them.

The event productivity a of the 2014 activity (the number of events with $M_L > 0$) is significantly lower than that of previous swarms. It increased from the

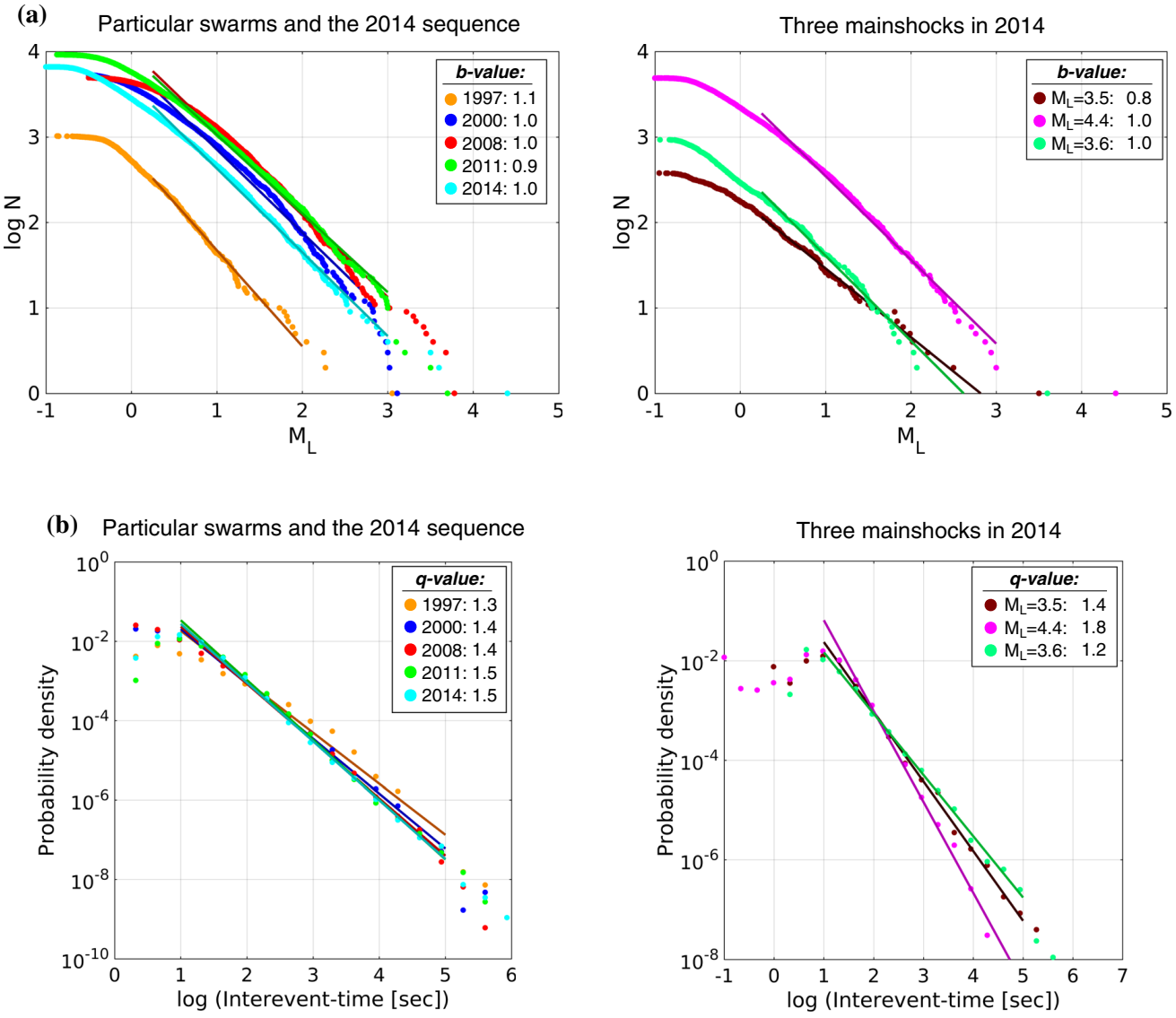

Figure 6
a Cumulative magnitude-frequency distribution (MFD), **b** probability density function of interevent times. For both (**a**) and (**b**): Left—the swarms of 1997 (orange), 2000 (blue), 2008 (red), 2011 (green) and the non-swarm activity 2014 (light blue); Right—the aftershock sequences of the 2014 mainshocks of M_L3.5 (brown), M_L4.4 (violet) and M_L3.6 (light green)

2000 to 2011 swarms (Čermáková and Horálek 2015) but decreased substantially in the 2014 non-swarm activity to 2800 $M_L \geq 0$ events. The reason is that about 66% of the 2014 total seismic moment were released in three mainshocks (M_L3.5, 4.4 and 3.6), and remaining 34% in the series of the $M_L \leq 3.0$ events. This issue is discussed in more detail in Sect. 9.

Combining formulas (1) and MFD we get the power law size distribution $N \sim M_0^{-\beta}$, where N is the number of events with seismic moment equal or larger than M_0, and $\beta = b/1.1$. The linear scale for N enables counting the total seismic moments within different moment bins M_{0i} as $N_i * M_{0i}$. This leads to $N_i * M_{0i} \sim M_0^{1-\beta}$ which gives a physical significance to the exponent β. In other words, $1-\beta$ describes the ratio of seismic moments released by small and large events. The coefficient β is equal for swarms of 2000 and 2008, the whole 2014 sequence, and for the M_L4.4 and 3.6 episodes separately ($\beta = 0.91$), and differs slightly for 1997 and 2011 swarms ($\beta = 1.0$ and 0.82) and a bit more so for the M_L3.5 episode

($\beta = 0.72$). The power law size distribution is unlike the b-value magnitude-scale independent.

The PDFs of the interevent times T_w were computed for the same datasets as the MFDs. The results are presented in Fig. 6b. The PDFs of both swarms and complete 2014 activity comply nicely with power law $\propto T_w^{-q}$ having the q-value $= 1.3$ to 1.5. This means the event rate of swarms and 2014 aftershocks is nearly the same. However, it does not meet the event rate of the individual 2014 aftershock episodes which show significant differences in the q-value being 1.4 for the M_L3.5 (May 24), 1.8 for the M_L4.4 (May 31), and 1.2 for the M_L3.6 (August 3) sequence. It implies that the event rate of the M_L4.4 aftershocks was much higher than that of the M_L3.5 and M_L3.6 aftershocks, and even than all the previous swarms.

Based on the Hainzl et al. (2016) paper, we can predict that the interevent times of the M_L4.4 mainshock aftershocks also correlate very well with a distribution of aftershocks delay times t_d. The rate of t_d should be $\propto t_d^{-p}$ (Omori law), where p is a fault-dependent constant. The relation between the constants p and q is given by $q = 2 - \frac{1}{p}$ (Utsu et al. 1995). Thus, the observed q-value 1.8 for the M_L4.4 mainshock-aftershock sequence fits very well with the maximum likelihood fit of Omori-decay function which yields $p = 5.1$ (Hainzl et al. 2016).

6. *Space-Time Distribution of Events*

In our previous paper (Čermáková and Horálek 2015), we analysed in detail a spatial distribution and geometry of the 2000, 2008 and 2011 swarms, and found a more complex structure of the NK zone than had been thought until then. We identified three fault segments: A, B and C in our notation. Segment A (strike = 166°, dip = 75°) located in the south of the NK zone was activated in 2000 and reactivated in 2008. Segments B (strike = 352°, dip = 75°) and C (strike = 162°, dip = 56°) located in the north of the NK zone were activated in 2011 (Figs. 7, 8). The foci of the moderate 1997 swarm ($M_{L\max}$3.0) are located on two corner-like patches (Fischer and Horálek 2000) on the edge of segment B (see Fig. 8). Regarding this we note as do the papers by Fischer et al. (2010) and Čermáková and Horálek (2015), using the terms fault and fault plane in a general sense; fault segments and smaller patches are parts of the faults delimited by hypocentres.

The location results obtained by the HypoDD code show that the three mainshocks of M_L3.5, 4.4 and 3.6 occurred in close proximity (see Table 2). They are located away from the A, B, C segments in the transition area between the southern (segment A) and northern (segments B and C) part of the NK zone. In Fig. 7, the three mainshocks are highlighted by stars, the boundary between the northern and southern NK zone is shown as a dashed line. This transition area was active only rarely, e.g., at the microearthquake level, before the 2014 activity (i.e. during the previous 25 years of West Bohemian seismic observations).

All the three mainshocks activated fault patches in both northern and southern parts of the NK zone; the space-time distribution of the individual mainshock-aftershock sequences is depicted in detail in Fig. 9. The aftershocks following the M_L3.5 mainshock first occurred on the northern edge of segment A, moving to southern edge of segment B. The focal depths vary at about the ± 300 m interval relative to the M_L3.5 event depth, most aftershocks occurred at a distance less than 500 m from the M_L3.5 event (see Fig. 9b).

The aftershock seismicity resulting from the M_L4.4 mainshock was quite large in a view of both size of events (two events of M_L3.0, seven of M_L between 2.5 and 3.0) and its extent. Immediately after the M_L4.4 mainshock the nearby patches of the A, B and C segments were activated as the aftershocks were spreading out quite uniformly northward and southward from the mainshock. After about ten hours, the activity moved predominantly to the north. In total, the aftershocks spread out up to ~2000 m in C, ~1000 m in B and ~1000 m in A segments. The focal depths varied between 7 km (in segment C) and 9.5 km (in segment A), whereas the M_L4.4 event depth is 8.7 km (Fig. 9c). Interestingly, the M_L4.4 aftershock activity reactivated some 2011 swarm patches, and also triggered nearby patches which were not yet active in both B and C segments. The pattern of M_L3.6 aftershocks is similar to that of M_L3.5; nevertheless the patch triggered on segment B is larger, affected earlier by the M_L4.4 aftershocks (Fig. 9d).

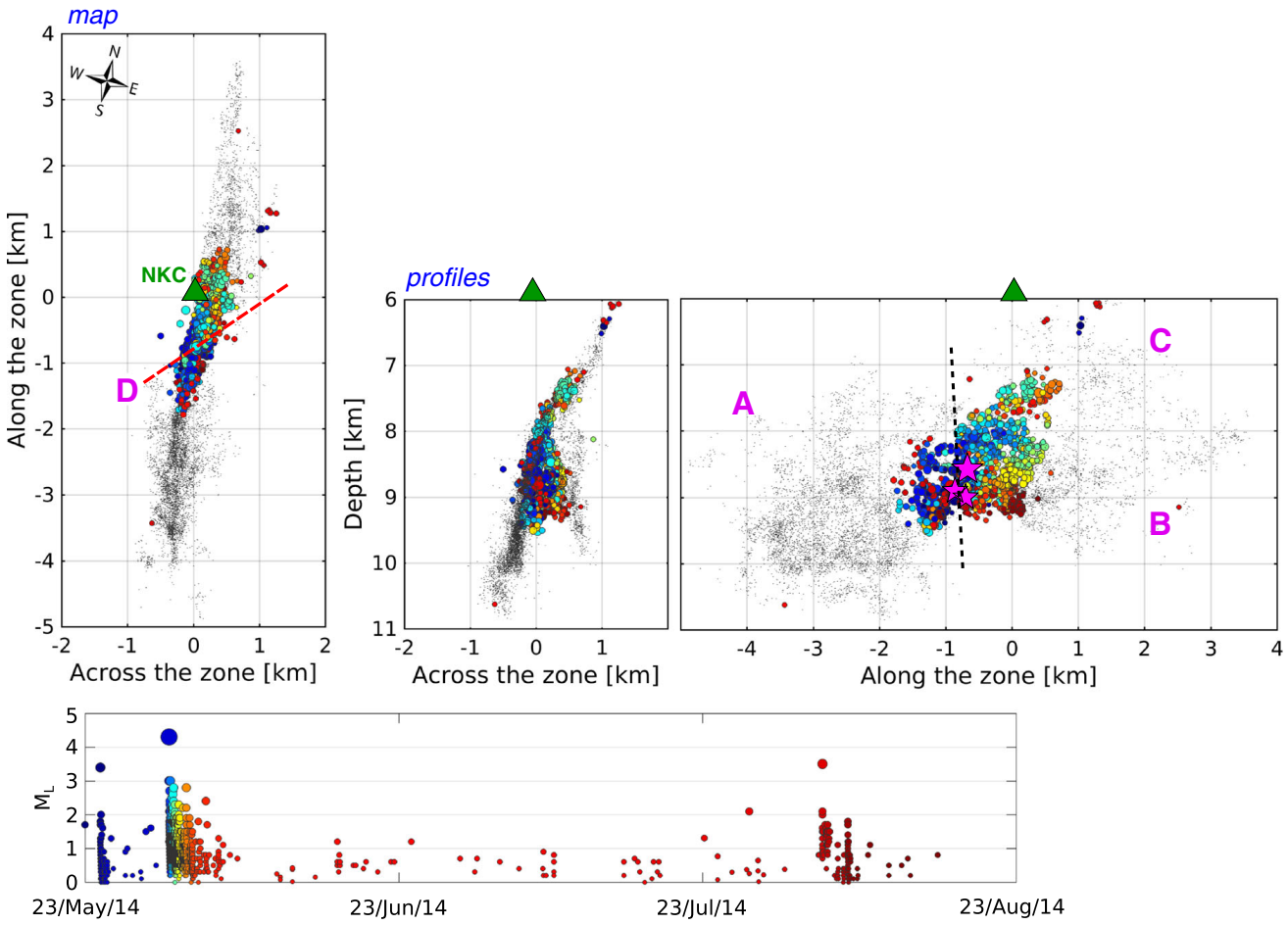

Figure 7

Spatio-temporal distribution the 2014 activity in the NK focal zone. Top: Distribution of the 2014 hypocentres (coloured dots) on a background of the 2000, 2008 and 2011 swarms (grey dots) represented by the map view (left) and two depth sections, across (middle) and along the focal belt (right). The horizontal coordinates are rotated 15° clockwise from the north, the origin corresponds to the location of the central WEBNET station NKC (green triangle). Violet stars—M_L3.5, 4.4 and 3.6 mainshocks. Black dashed line—boundary between the southern part (segment A) and the northern part of the NK zone (segments B and C). Red dashed line indicates probable orientation of the newly disclosed fault segment D inferred from focal mechanisms. Bottom: Time course of the activity in the magnitude-time plot. Colour-coding is proportional to the origin time of the events

The location of the three mainshocks is the issue. Mutual distances among them are $|M_L4.4\ M_L3.5| = 410$ m, $|M_L4.4\ M_L3.6| = 240$ m, and $|M_L3.5\ M_L3.6| = 240$ m (Fig. 9a). Figure 9b–d indicate that each mainshock is surrounded by a seismic gap without aftershocks, plausibly referring to the rupture area. To verify this idea we made a rough estimate of the rupture area based on the Madariaga (1976) formula for a circular source:

$$r = kv_rT_d, \tag{2}$$

where r is radius of the source, k is a model dependent constant, v_r is the rupture velocity and T_d is duration of the pulse of the direct P-wave. For the circular source the constant k is $k = 0.32$ for P-waves (Madariaga 1976) and the rupture velocity was assumed to be $v_r = 3000$ m/s. The duration of the P-wave pulse T_d was measured on the vertical component in the ground displacement seismograms (see Fig. 3). The pulse widths differ among individual stations, the range being 100–150 ms (M_L3.5), 120–180 ms (M_L4.4), and 100–140 ms (M_L3.6), and so T_d is an average value from all the stations used. Therefore, the radii estimated are 130 m (M_L3.5), 150 m (M_L4.4), and 120 m (M_L3.6).

We are aware of a simplified estimation of the size of the seismic source using the formula (2), however, it enables us to estimate the size of the

rupture area. The estimated radii of the ruptures of the three mainshocks were comparable to distances between the hypocentres of these events (a few hundred meters for all three distances). It implies that the mainshocks indeed served as three-step rupturing of an asperity which represents a newly disclosed significant seismogenic fault segment D in the NK focal zone. The geometry of this segment was estimated using focal mechanisms which are discussed in the next section.

Figure 8 ▶
a Spatial distribution of the earthquake swarms of 1997 (dark blue dots highlighted by yellow ellipse), 2000 (light blue), 2008 (red), 2011 (green) and 2013 (violet), and the 2014 sequence (black) in the NK zone. For the projection we refer to Fig. 7. **b** Distribution of the foci in the transition area between fault segments A, B and C represented by three horizontal sections at depths of 8000–8100 m (above the 2014 mainshocks), 8600–8700 m and 8800–8900 m (corresponding to depth of the M_L 4.4 and 3.6 mainshocks). The colour-coding matches that in (**a**). Note a fault jog (middle and right sections) separating the northern segments B and C from the southern segment A being bridged by a fault barrier D (black dots). Red line—the strike of the barrier indicated by focal mechanisms of the 2014 mainshocks. Violet dashed circle highlight a short segment which hosted the 1997 and 2011 swarms, and the 2014 activity

7. *Focal Mechanisms*

As referred to in Sect. 4, we inverted ground-motion amplitudes of the direct P-waves on the seismograms' vertical component for the source mechanism in the full moment-tensor (MT) description using the AMT code by Vavryčuk (2011). We retrieved moment tensors of the three mainshocks (M_L3.5, 4.4 and 3.6) using the P-wave data from 22 WEBNET stations which adequately cover the focal sphere (Fig. 10b). When picking the P-wave amplitudes we used a bilateral Butterworth high-pass filter with a corner frequency of 0.1 Hz to suppress low-frequency noise, a no low-pass filter was applied. Although the AMT code provides for a full moment tensor we analysed only double-couple (DC) components to avoid potential misinterpretations of non-double-couple (non-DC) components. They can be spurious, i.e., not generated inherently in the source but due to data inconsistencies (inaccurate or noisy input data, inexact location of the hypocentre and poor velocity model of the medium; for details see the tests in Horálek and Šílený 2013). That demonstrates why reliability of the non-DC components should be thoroughly verified, but such analyses are beyond the scope of this paper.

Stability of the DC components of the resultant MTs were verified by applying the jack-knife technique to the MT solutions. We computed moment tensors from the subset of the data with one or a few stations removed and observed the effect on the strike, dip, and rake angles. Resultant source mechanisms of the three mainshocks in terms of the three DC angles (strike, dip, rake) are given in Table 3, and displayed by fault-plane solution plots with nodal lines and principal axes P and T in Fig. 10b.

The source mechanisms of the three mainshocks are quite similar indicating an oblique-thrust faulting with a significant dip-slip component. Such fault plane solutions differ significantly from the predominant mechanisms in the swarms of 2000, 2008 and 2011, which are strike-slips with a weak either normal or thrust component (Fig. 10a), the former prevailed in the swarms of 2000, 2008 and in the second phase of 2011 (segments A and C), whereas the latter in the first phase of 2011 (segment B) (Vavryčuk 2011; Horálek and Šílený 2013; Čermáková and Horálek 2015). Nevertheless, source mechanisms of the oblique-thrust type with significant dip-slip components had been observed in the second phase of the 1997 swarm showing DC angles quite similar to those of 2014 (Horálek et al. 2002; Vavryčuk 2002).

To distinguish true fault planes from auxiliary ones in the mechanisms of the three 2014 mainshocks, we calculated an equation of the plane defined by the mainshocks hypocentres. In this way, we estimated the fault planes striking NE-SW and dipping $\approx 60^\circ$ to SE to be the true fault planes, which suggests geometry of segment D (ruptured asperity).

8. *Structure of the NK Focal Zone and its Complexity*

The spatial distribution of individual swarms since 1997 together with the 2014 sequence is shown in Fig. 8a. Obviously the structure of the NK zone is

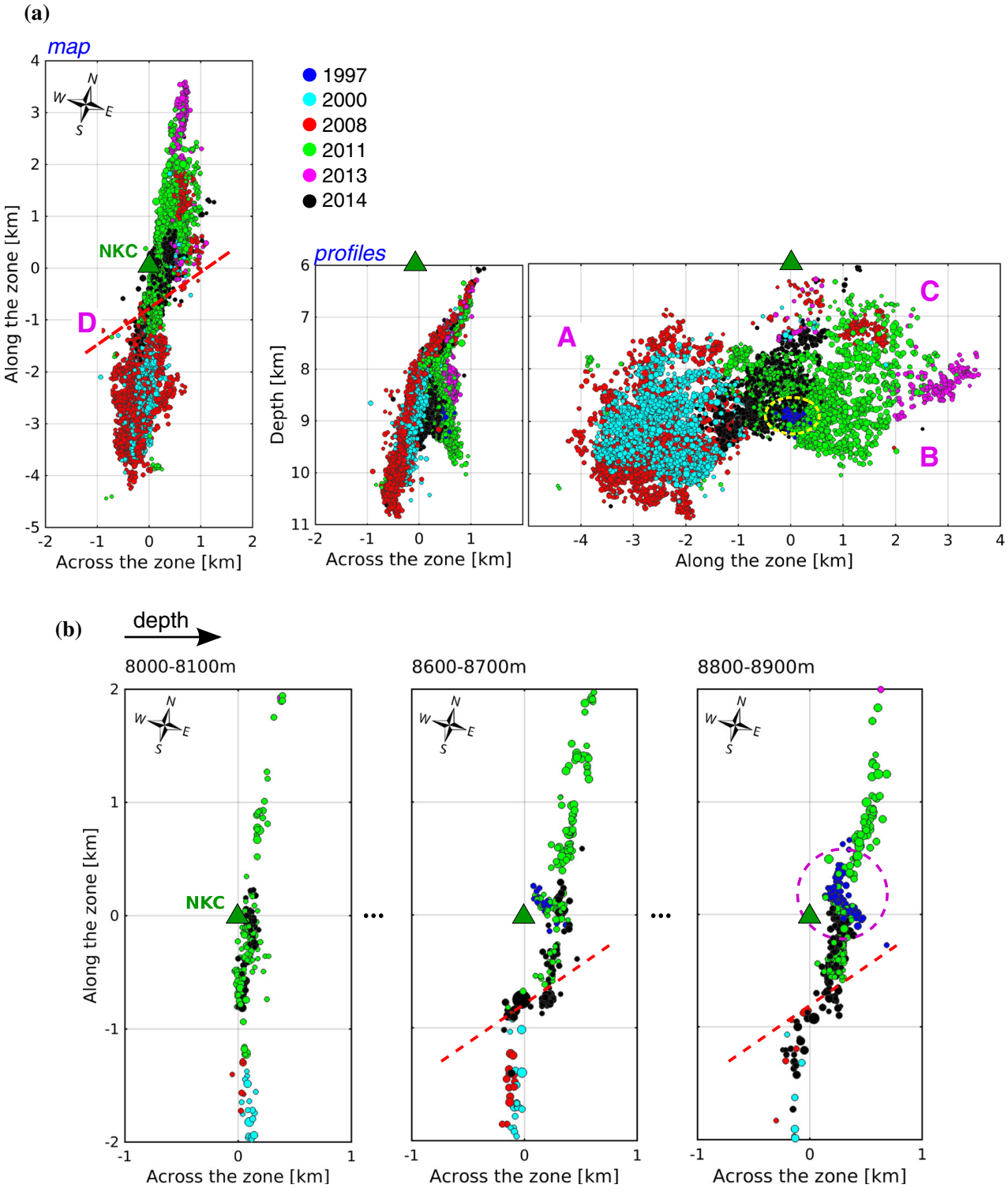

fairly complex. The individual activities are located close together and form one or two focal clusters indicating respective fault segments or patches. In practical sense, each larger local activity enhances our understanding of the structure of the NK zone. The 1997 swarm (dark blue dots in Fig. 8a, $M_{Lmax}3.0$) took place on two rather small patches being of a corner-like character (see Fischer and Horálek 2000). The 2000 swarm (light blue dots, $M_{Lmax}3.3$) activated fault segment A which was reactivated in 2008 by an

intense $M_{\mathrm{Lmax}}3.8$ swarm (red dots). The event distribution of these two swarms shows a distinctly planar character, which led us to conclude that the NK zone is composed of one fault plane striking and dipping roughly 170° and 80° (Fischer and Horálek 2003; Fischer et al. 2010). However, the spatial distribution of the 2011 (green dots, $M_{\mathrm{Lmax}}3.7$) and its complement in 2013 (violet dots, $M_{\mathrm{Lmax}}2.6$) disclosed further segments B (strike/dip ≈ 350°/75°) and C (strike/dip ≈ 160°/55°) (Čermáková and Horálek 2015). Added to that, the 2014 event locations indicate a new fault segment or rather asperity D that ruptured in the three mainshocks, while the aftershocks (black dots) are scattered in fault segments A, B, C and D. Based on the focal mechanisms of the mainshocks we conclude that the plane striking ∼ 40°E and dipping ∼ 60° to SE may be an approximation of segment D.

A notable complexity of the NK zone was found in the transition area between the fault segments A and B which is also where the 1997 swarm occurred. An analysis of the spatial distribution of the foci in this area disclosed that one of the patches activated in the 1997 swarm is located inside, on the edge of segment B (see Fig. 8). Figure 8b depicts the transition area in detail using a series of horizontal sections in depths between 8500 and 9100 m with the step of 100 m. It is clear that the area is partitioned into several segments; interestingly, some of them were repeatedly activated, namely during the swarms of 1997 and 2011 (weaker events) and the 2014 activity (aftershocks). Multiple reactivation of some patches of the 1997 swarm was reported earlier by Fischer and Horálek (2003); as mentioned above, segment A was activated first in the 2000 and then reactivated in the 2008 swarm, and a few times in between some of its patches (Fischer and Horálek 2003). The exact reason some parts were reactivated in the NK zone has not yet been determined. It could be linked to a local fast stress accumulation, a gradual strain energy release at asperities or a local pore pressure due to fluids diffusing along faults. This interesting phenomenon is worthy of extensive study.

Figure 9 ▶
a Locations of the 2014 mainshocks of $M_L3.5$ (violet), $M_L4.4$ (red) and $M_L3.6$ (green) depicted by the map view (left), depth section along the focal zone (right) and 3D view (bottom). **b–d** Space-time event distribution (colour-coded dots) for the individual $M_L3.5$ (**b**), $M_L4.4$ (**c**) and $M_L3.6$ (**d**) episodes. The spatial distribution of the foci for each episode is delineated by the depth section along the focal zone (top left), and 3D view (top right) supplemented by projection onto three perpendicular planes (light blue dots). Grey dots—foci of the 2000, 2008 and 2011 swarms; black dashed line—the boundary between the southern and northern part of the NK zone. The temporal distribution of the foci is depicted by the magnitude-time plot (bottom). The origin and rotation of the coordinate system is the same as in Figs. 7 and 8

9. Discussion

Earlier, we noted that the mainshock-aftershock character of the 2014 sequence is exceptional in the West Bohemia/Vogtland region since it is well known for its swarm-like seismicity. Similar earthquake activity had not been reported there either in papers, reports or catalogues. Hence, the data of the 2014 sequence together with those of previous swarms enabled us to gain a deeper insight into the seismic energy release in the region, particularly in the main NK focal zone.

1. A fairly good correspondence exists between the relation of $M_0 - M_L$ for the $M_L1.7$ to 3.3 events of the 2000 swarm (Horálek and Šílený 2013) and for the $M_L2.2$ to 4.4 events of the 2014 sequence, where the 2000 and 2014 seismic moments were computed by different methods. This indicates that

Table 2

Origin times, locations and local magnitudes of the three mainshocks. Note that the location is relative, therefore, it can differ from the absolute location in the order of first hundreds of meters

Mainshock	Date	Origin time (UTC)	M_L	LT (°N)	LN (°E)	D (km)	M_0 (Nm · 10^{-14})
$M_L3.5$	2014-05-24	14:35:35.49	3.5	50.225	12.451	9.04	0.87
$M_L4.4$	2014-05-31	10:37:20.99	4.4	50.226	12.450	8.66	6.60
$M_L3.6$	2014-08-03	23:58:40.38	3.6	50.224	12.451	8.81	1.10

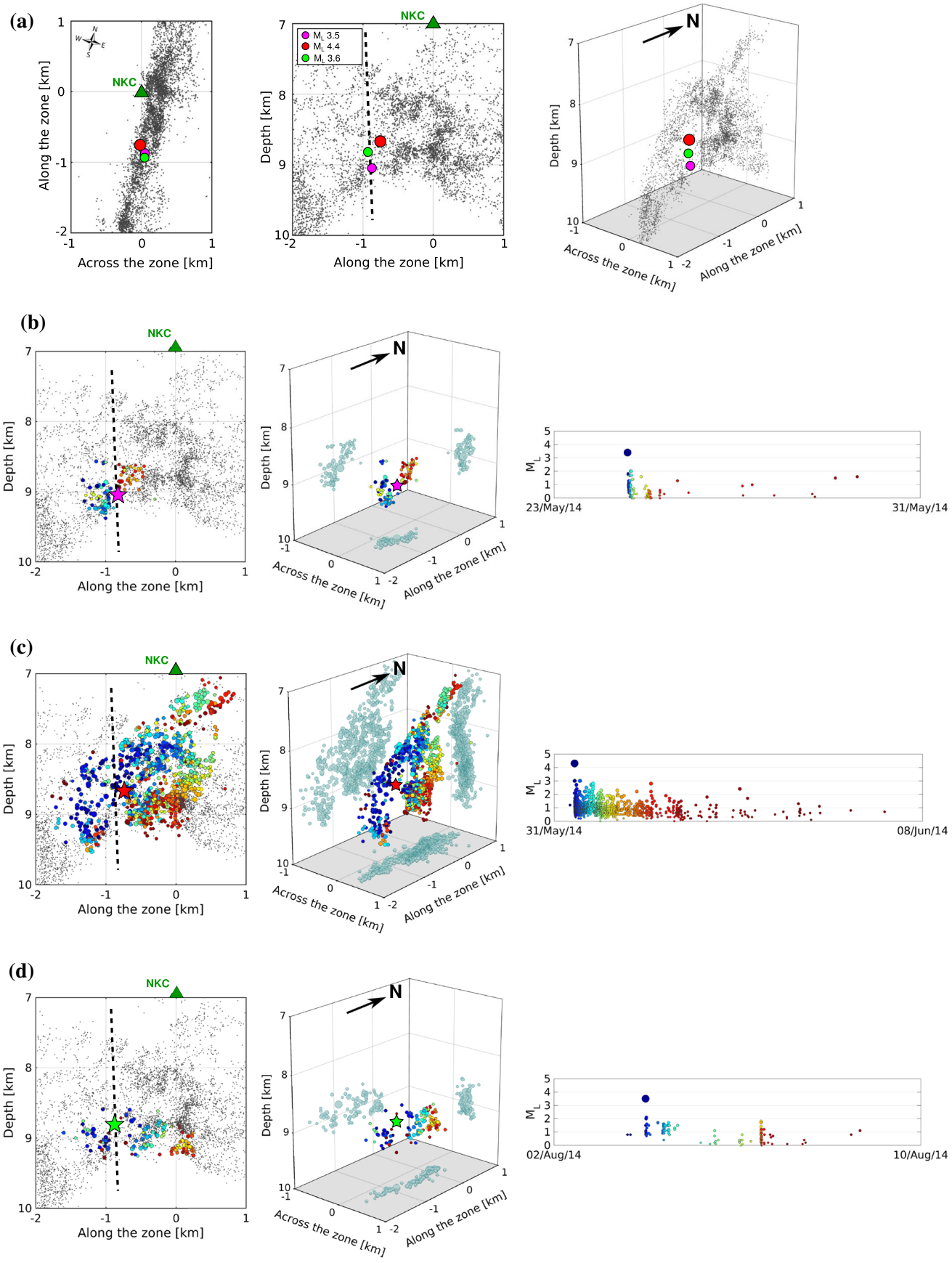
(a)
NKC
Along the zone [km]
Across the zone [km]
Depth [km]
M_L 3.5
M_L 4.4
M_L 3.6
N
(b)
(c)
(d)
M_L
23/May/14
31/May/14
08/Jun/14
02/Aug/14
10/Aug/14

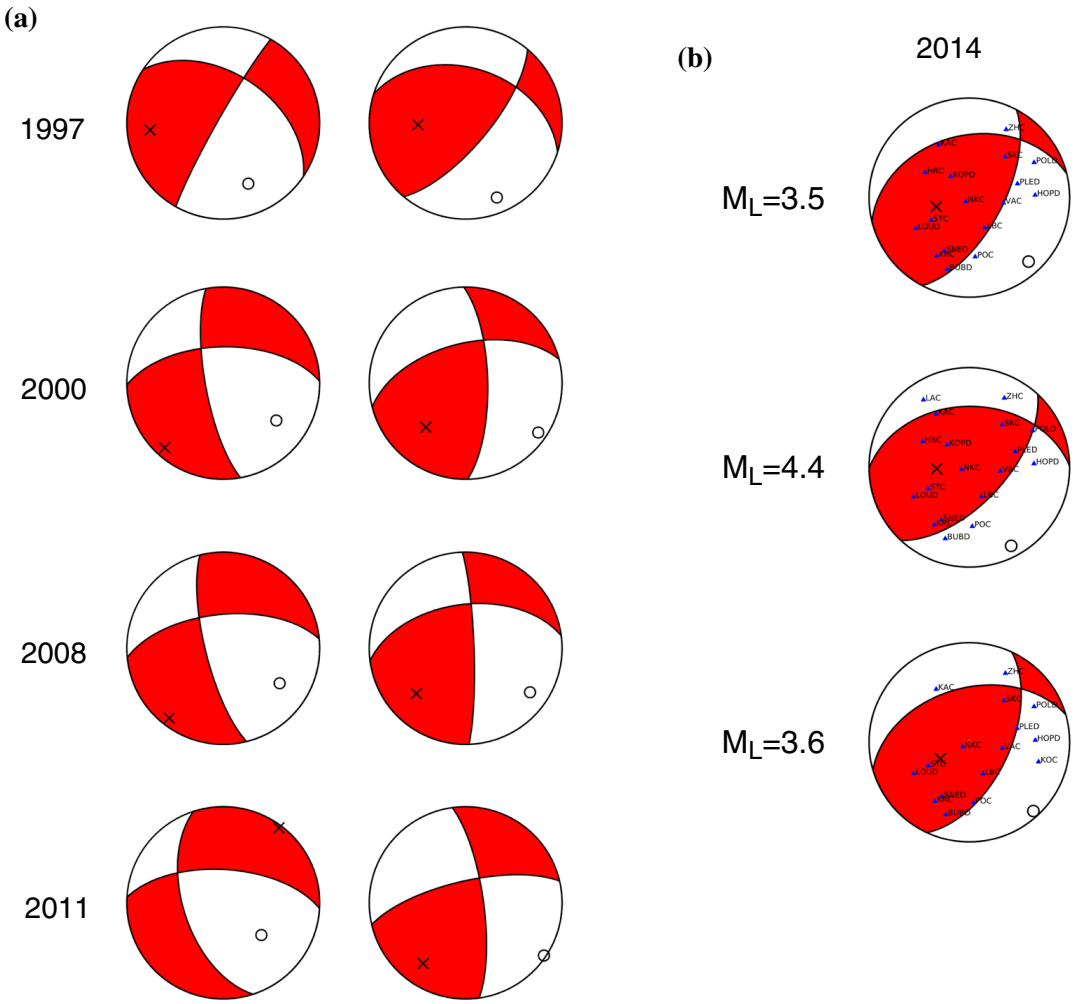

Figure 10
a Characteristic source mechanisms of the swarms of 1997, 2000, 2008 and 2011, **b** mechanisms for the three mainshocks of 2014 (left) and coverage of the focal spheres by stations used for the mainshocks mechanism retrieval (right). All the fault plane solutions are represented in the equal-area, lower-hemisphere projection. The principal axes P are marked by circles, axes T by crosses

formula (1) is proper for M_0 estimation on the basis of M_L by WEBNET. Moreover, combining formula (1) with the formula for moment magnitude $M_w = \frac{2}{3}(\log_{10} M_0 - 9.1)$ (M_0 is in Nm; Kanamori 1977) produces the relation $M_w = \frac{2}{3}(1.10M_L + 0.99)$, and thus suitable for the M_w estimate by means of M_L. This is quite useful because more and more local networks or agencies report moment magnitudes instead of local ones.

2. An issue worth discussing is the comparable amount of total seismic moments $M_{0\text{tot}}$ of the 2008 and 2011 swarms and the 2014 sequence, and also the seismic moment released in their dominant phases M_{0dom}. The reason is that: (a) $M_{0\text{tot}}$ of the most intense activities in the last 30 years (2008, 2011 and 2014) corresponds to the single events of $M_L \approx 4.6$ to 4.8, and M_{0dom} to a $M_L \approx 4.5$ event (see Sect. 5), and (b) the M_L4.6 earthquake from the swarm 1985/86 was the strongest event in West Bohemia/Vogtland in the last 100 years. This suggests that M_L4.8 is the upper limit for an earthquake in this region. Some authors refer to Kárník and Schenková (1988) and state that the strongest, instrumentally recorded earthquake in West Bohemia/Vogtland from November 1908 reached a magnitude 5.0, but that is very likely an overestimation. For example, Neunhöfer and Stelzner (1989) estimated the magnitude of this event to be only slightly higher

Table 3

Values of strikes, dips and rakes of nodal planes of the three mainshocks

Mainshock	Nodal plane 1 (°)			Nodal plane 2 (°)		
	Strike	Dip	Rake	Strike	Dip	Rake
M_L3.5	28	63	63	256	37	131
M_L4.4	43	61	63	270	39	130
M_L3.6	25	57	58	254	45	129

The error obtained by the jack-knife technique is ± 15°

Table 4

Ground motions at the stations were observed. v_{max} *maximum velocity,* d_{max} *maximum displacement,* a_{max} *maximum acceleration.* v_{large}, d_{large}, a_{large}*: in case of the* M_L4.4 *mainshock—maximum ground motions among the non-clipped stations; in case of the* M_L3.5 *and* M_L3.6 *mainshock - ground motions on the stations, which recorded maximum values among the non-clipped stations in case of the* M_L4.4 *mainshock*

Mainshock	Velocity (mm/s)		Displacement (mm)		Acceleration (m/s^2)	
	v_{max}	v_{large}	d_{max}	d_{large}	a_{max}	a_{large}
M_L3.5	4.7 (NKC)	2.5 (KRC)	0.17 (NKC)	0.14 (KAC)	0.35 (NKC)	0.33 (KAC)
M_L4.4	–	19.9 (KRC)	–	0.69 (KAC)	–	2.22 (KAC)
M_L3.6	6.4 (NKC)	3.4 (KRC)	0.21 (KVC)	0.14 (KAC)	0.42 (NKC)	0.34 (KAC)

The error obtained by the jack-knife technique is ±15°

than M_{Lmax} of the 1985/86 swarm; Neunhöfer and Hemmann (2005) reported even lower magnitude of 4.4. Moreover, there are no reports of extensive damage due to past local earthquakes. The largest macroseismic effects of intensity $I_0 = 6.5$ to 7.0 (MSK scale) were due to the strongest swarm earthquakes in 1908 and 1985 (Leydecker 2011). It supports our estimate that the maximum $M_L \approx$ 4.8 event is what can be expected in the West Bohemia/Vogtland region. This is critical for seismic risk assessment in the region, above all, of the Horka dam reservoir located close to the epicentral area of NK. Although the 2008, 2011 and 2014 activities show similar M_{0tot} and M_{0dom} in terms of size, the time course of the seismic moment release is fairly different which implies divergent number and magnitudes of strong events, and consequently differing maximum ground motions in each activity (see Table 4). This reveals that an earthquake swarm produces number of strong events to release the same seismic moment as a mainshock. For example, M_0 released in the 2014 M_L4.4 mainshock is equal to sum of all the M_L3.0–3.8 events in the 2008 swarm except the M_L3.8 event during the last swarm phase (see Table 2 in Fischer et al. 2010).

3. The 2014 non-swarm activity and the 2000, 2008 and 2011 earthquake swarms show a similar event rate (q-value) and ratio of smaller to larger events (b-value). However, the 2014 activity exhibits a substantially lower event productivity (parameter a in the MFD indicating number of $M_L \geq 0$ events) and significantly higher rate of seismic moment release which is probably due to a large portion of M_{0tot} released in the M_L4.4 mainshock. It suggests that mainshock-aftershock sequences generally comprise noticeably fewer events than earthquake swarms to release a similar seismic moment. This implication nicely correlates with the definition of a mainshock-aftershock sequence that the mainshock is significantly larger than the aftershocks. The above mentioned analysis indicate that the event productivity of the G–R law and the rate of seismic moment release could be additional criteria for distinguishing the swarm-like activity from the mainshock-aftershock-like one (in addition to the absence of one dominant event at the beginning of the activity and pronounced clustering of

events in space and time). Another important observation to note is the acceleration of the seismic moment release in each subsequent activity starting from the 2000 swarm to the 2014 sequence together with shorter time periods between subsequent activities, which resulted in redesigning the swarm-like activities as mainshock-aftershock. Accelerating activities indicate increasing stress transfer among subsequent events, which could be related to a higher stressed fault zone closer to a critical state. One possible reason for this is that fluid pressure probably increased in the years before 2014 and resulted in a strong post-seismic increase in CO_2 flow in nearby mofettes (Fischer et al. 2017).

4. Another issue worth noticing are waveforms of the mainshocks. Figure 3 shows the width of the P-wave pulses of all the mainshocks (M_L3.5, 4.4 and 3.6) which are similar at all depicted seismograms, other stations located at various epicentral distances around the NK area also share this peculiarity. In Sect. 6 our rough estimate of the radii of the ruptured area (assuming a circular source) of the M_L3.5, 4.4 and 3.6 mainshocks is 130, 150 and 120 m. But the estimated seismic moment of the M_L4.4 event is much higher than those of M_L3.5 and 3.6 ($\approx 8.0 \times 10^{14}$ Nm vs. $\approx 9.0 \times 10^{13}$ Nm and $\approx 1.1 \times 10^{14}$ Nm). One explanation is a much higher stress drop of the M_L4.4 mainshock than that of M_L3.5 and 3.6. While beyond the scope of this paper, an in-depth analysis of this could be the topic of a new study.
5. As indicated in Fig. 8a, a fault jog separates northern segments B and C from southern segment A. The jog is bridged by the oblique segment D where the three 2014 mainshocks occurred; note that the focal mechanisms with an approximate strike of 40° match the jog strike. We show in Fig. 11 a schematic illustration of this geometry based on the spatial distribution of the swarms of 2000, 2008 and 2011 and the non-swarm activity 2014. The small size of the mainshock ruptures matches quite well the offset of about 300 m between the northern and southern segments and justifies our model that the mainshocks acted as a link between these segments. In other words, the mainshocks activated a barrier, which was probably an area of stress concentration due to previous swarm activity on segments A, B and C.

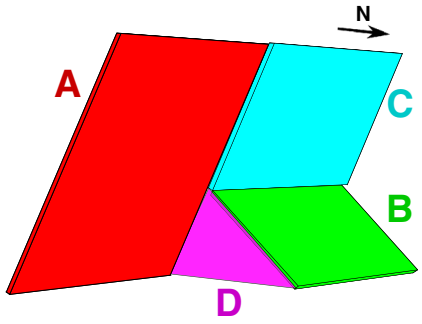

Figure 11
Basic scheme of the NK focal zone. Segment A (red) was triggered in the 2000 and 2008 swarm, segments B and C (green and light blue) in the 2011 swarm, and segment/barrier D (violet) in the 2014 sequence

A notable feature of the 2014 aftershocks is their position relative to the rupture of the mainshock. Unlike standard aftershocks that occur randomly along the edges of the mainshock rupture, the 2014 aftershocks migrated from a point in space (Hainzl et al. 2016), and occurred not on the mainshock fault but beyond it along the preexisting oblique fault segments A, B and C. This indicates that the 2014 mainshock-aftershock sequence is rather untypical in relation to common mainshock-aftershock seismicity observed at plate boundary faults.

Figure 11 is rather simplified. The scheme shows only the major fault segments where the majority of seismic moment has been released, eliminating the patches activated in the 1997 swarm and in a number of micro-swarms. We believe this scheme will be beneficial for continued broader research into the West Bohemia/Vogtland swarms.

10. Conclusions

An unusual sequence of three M_L3.5, 4.4 and 3.6 mainshock-aftershock episodes occurred in the main focal zone (Nový Kostel, NK) of West Bohemia/Vogtland in May (M_L3.5, 4.4 events) and August 2014 (M_L3.6 event). The sequence is exceptional because: (i) it is the first mainshock-aftershock-like activity observed in this typical earthquake-swarm region, and (ii) the M_L4.4 event is the second

strongest earthquake that occurred in West Bohemia/Vogtland in the last 100 years. We analysed this activity and compared it with the swarms of 1997, 2000, 2008 and 2011 from the perspective of cumulative seismic moment, statistical characteristics, space-time distribution of events, and prevailing focal mechanisms. The results are summarised as follows:

- The scaling relation between scalar seismic moment M_0 and local magnitude M_L by WEBNET that fit well the 2014 data is: $\log_{10} M_0 = 1.10 \cdot M_L + 10.09$, where M_0 is in Nm.
- Total seismic moment released in the 2014 activity, $M_{0\text{tot}} \approx 1.58 \times 10^{15}$ Nm, is equal to a single M_L4.6+ event and comparable to $M_{0\text{tot}}$ of the earthquake swarms in 2000, 2008 and 2011. About 54% of $M_{0\text{tot}}$ accounts for the M_L4.4 mainshock, 66% for all the three mainshocks (M_L3.5, 4.4 and 3.6) and 34% for aftershocks. The maximum ground motions observed at unclipped WEBNET stations are: the displacement of 0.69 mm, the velocity of 19.9 mm/s and the acceleration of 2.22 m/s^2, which are higher than maximum ground motions of previous swarms.
- Based on the analysis of M_0 released in the 2014 sequence and previous swarms, we infer that the M_L4.8 earthquake is probably the maximum expected event magnitude in the main focal zone NK.
- The 2014 sequence and the earthquake swarms show similar b-values $\sim$ 1 of the magnitude-frequency distributions (MFD), event rates indicated by PDFs of interevent times, and the ratio of seismic moments released by small and large events. However, the 2014 activity exhibits much lower event productivity (parameter a in the MFD) and a significantly higher rate of seismic moment release. This implies that mainshock-aftershock sequences generally comprise far fewer events than earthquake swarms to release similar seismic moment.
- Subsequent activities starting from the 2000 swarm to the 2014 sequence exhibit a significant increasing rate of the seismic moment release and shortening time periods between the subsequent activities, which resulted in switching the swarm-like activities to the mainshock-aftershock one.
- The M_L3.5, 4.4 and 3.6 mainshocks are located near each another, in a fault jog separating segment A in the south from B and C in the north hosting the swarms of 2000, 2008 and 2011. This new fault segment D at depths between 8.6 and 9 km deviates about 30° from the strike of the NK zone and presents a fault barrier most probably being the reason for the occurrence of the three mainshocks. Fault segment D is predisposed to oblique-thrust faulting while strike-slip faulting is typical for segments A, B and C.
- The aftershock seismicity due to the M_L4.4 mainshock was quite large in terms of both event magnitudes and its extent. Aftershocks are scattered far beyond segment D in the previously activated segments A, B and C. The M_L4.4 aftershock activity reactivated some fault patches that were active in swarms 1997 and 2011. Some patches in the NK zone were activated repeatedly, particularly those on fault segment B, which were reactivated in 1997, 2011 and 2014.

Acknowledgements

We wish to thank our colleagues Jana Doubravová and Jakub Klicpera for carefully handling the WEBNET data, and Alena Boušková, Zuzana Procházková and Martin Labuta for primary processing of the WEBNET seismograms. We are grateful also to Václav Vavryčuk for providing scalar seismic moments of strong events and for other valuable suggestions. Editor Prof. Andrzej Kijko devoted careful attention to this paper for which and to whom we express our gratitude. Our special thanks are due the reviewer, Dr. Sebastian Hainzl, who provided valuable suggestions that enabled us substantially to improve the paper. The work was accomplished through Grant Project P210–12–2336 of the Grant Agency of the Czech Republic, "Earthquake swarms and their triggering mechanisms in diverse tectonic environments (Bohemian Massif, Mid-Atlantic Ridge, and Western Alps)". WEBNET, the monitoring system, provided earthquake data receiving considerable support from the project LM2015079 CzechGeo/EPOS. The processing and management of

the WEBNET data was supported by the Project CzechGeo/EPOS-Sci (CZ.02.1.01/0.0/0.0/16_013/0001800) financed from Operational Programme Research, Development and Education.

References

Båth, M. (1965). Lateral inhomogeneities in the upper mantle. *Tectonophysics*, *2*, 483–514. https://doi.org/10.1016/0040-1951(65)90003-X.

Bouchaala, F., Vavryčuk, V., & Fischer, T. (2013). Accuracy of the master-event and double-difference locations: Synthetic tests and application to seismicity in West Bohemia, Czech Republic. *Journal of Seismology*, *17*(3), 841–859. https://doi.org/10.1007/s10950-013-9357-4.

Bourouis, S., & Cornet, F. H. (2009). Microseismic activity and fluid fault interactions: Some results from the Corinth Rift Laboratory (CRL), Greece. *Geophysical Journal International*, *178*, 561–580. https://doi.org/10.1111/j.1365-246X.2009.04148.x.

Bräuer, K., Kämpf, H., Niedermann, S., & Strauch, G. (2005). Evidence for ascending upper mantle-derived melt beneath the Cheb basin, Central Europe. *Geophysical Research Letters*, *32*. https://doi.org/10.1029/2004GL022205.

Chiaraluce, L. (2012). Unravelling the complexity of Apenninic extensional fault systems: A review of the 2009 L'Aquila earthquake (Central Apennines, Italy). *Journal of Structural Geology*, *42*, 2–18. https://doi.org/10.1016/j.jsg.2012.06.007.

Courboulex, F., Dujardin, A., Vallée, M., Delouis, B., Sira, C., Deschamps, A., et al. (2013). High-frequency directivity effect for an Mw 4.1 earthquake, widely felt by the population in Southeastern France. *Bulletin of the Seismological Society of America*, *103*(6), 3347–3353. https://doi.org/10.1785/0120130073.

Credner, H. (1876). Das vogtländisch-erzgebirgische Erdbeben vom 23. November 1875. *Z Ges Naturwiss*, *48*, 246–269.

Čermáková, H., & Horálek, J. (2015). The 2011 West Bohemia (Central Europe) earthquake swarm compared with the previous swarms of 2000 and 2008. *Journal of Seismology*. https://doi.org/10.1007/s10950-015-9502-3.

Farrell, J., Husen, S., & Smith, R. B. (2009). Earthquake swarm and b-value characterization of the Yellowstone volcano-tectonic system. *Journal of Volcanology and Geothermal Research*, *188*, 260–276. https://doi.org/10.1016/j.jvolgeores.2009.08.008.

Fischer, T. (2003). Automatic location of swarm earthquakes from local network data. *Studia Geophysica et Geodaetica*, *47*(1), 83–98. https://doi.org/10.1023/A:1022251605990.

Fischer, T., & Horálek, J. (2000). Refined locations of the swarm earthquakes in the Nový Kostel focal zone and spatial distribution of the January 1997 swarm in Western Bohemia, Czech Republic. *Studia Geophysica et Geodaetica*, *44*(2), 210–226. https://doi.org/10.1023/A:1022162826079.

Fischer, T., & Horálek, J. (2003). Space-time distribution of earthquake swarms in the principal focal zone of the NW Bohemia/Vogtland seismoactive region: period 1985–2001. *Journal of Geodynamics*, *35*(1–2), 125–144. https://doi.org/10.1016/S0264-3707(02)00058-3.

Fischer T., & Horálek J. (2005) Slip-generated patterns of swarm microearthquakes from West Bohemia/Vogtland (central Europe): Evidence of their triggering mechanism? *Journal of Geophysical Research*, *110/B05S21*. https://doi.org/10.1029/2004JB003363

Fischer, T., Horálek, J., Michálek, J., & Boušková, A. (2010). The 2008 West Bohemia earthquake swarm in the light of the WEBNET network. *Journal of Seismology*, *14*, 665–682. https://doi.org/10.1007/s10950-010-9189-4.

Fischer, T., Horálek, J., Hrubcová, P., Vavryčuk, V., Bräuer, K., & Kämpf, H. (2014). Intra-continental earthquake swarms in West-Bohemia and Vogtland: A review. *Tectonophysics*, *611*, 1–27. https://doi.org/10.1016/j.tecto.2013.11.001.

Fischer, T., Matyska, C., & Heinicke, J. (2017). Earthquake-enhanced permeability—Evidence from carbon dioxide release following the ML 3.5 earthquake in West Bohemia. *Earth and Planetary Science Letters*, *460*, 60–67. https://doi.org/10.1016/j.epsl.2016.12.001.

Grünthal, G. (1989). About the history of seismic activity in the focal region Vogtland/Western Bohemia. In: Bormann, P (Ed), Monitoring and analysis of the earthquake swarm 1985/86 in the region Vogtland/Western Bohemia, (Veröffentlichungen des Zentralinsituts für Physik der Erde; 110), Zentralinstitut für Physik der Erde, pp. 30–34

Hainzl S., & Fischer T. (2002). Indications for a successively triggered rupture growth underlying the 2000 earthquake swarm in Vogtland/NW Bohemia. *Journal of Geophysical Research107/B12*, 2338:1–9. https://doi.org/10.1029/2002JB001865

Hainzl S., & Ogata Y. (2005) Detecting fluid signals in seismicity data through statistical earthquake modelling. *Journal of Geophysical Research*, *110/B05S07*. https://doi.org/10.1029/2004JB003247

Hainzl, S., Fischer, T., & Dahm, T. (2012). Seismicity-based estimation of the driving fluid pressure in the case of swarm activity in western bohemia. *Geophysical Journal International*, *191*(1), 271–281. https://doi.org/10.1111/j.1365-246X.2012.05610.x.

Hainzl, S., Fischer, T., Čermáková, H., Bachura, M., & Vlček, J. (2016). Aftershocks triggered by fluid intrusion: Evidence for the aftershock sequence occurred 2014 in West Bohemia/Vogtland. *Journal of Geophysical Research*, *121*(4), 2575–2590. https://doi.org/10.1002/2015JB012582.

Hill, P. D. (1977). A model for earthquake swarms. *Journal of Geophysical Research*, *82*(8), 1347–1352. https://doi.org/10.1029/JB082i008p01347.

Horálek, J., & Fischer, T. (2010). Intraplate earthquake swarms in West Bohemia/Vogtland (Central Europe). *Jökull*, *60*, 67–87.

Horálek, J., & Šílený, J. (2013). Source mechanisms of the 2000-earthquake swarm in the West Bohemia/Vogtland region (Central Europe). *Geophysical Journal International*, *194*(2), 979–999. https://doi.org/10.1093/gji/ggt138.

Horálek, J., Fischer, T., Boušková, A., & Jedlička, P. (2000). The Western Bohemia/Vogtland region in the light of the WEBNET network. *Studia Geophysica et Geodaetica*, *44*(2), 107–125. https://doi.org/10.1023/A:1022198406514.

Horálek, J., Šílený, J., & Fischer, T. (2002). Moment tensors of the January 1997 earthquake swarm in NW Bohemia (Czech Republic): Double-couple vs. non-double-couple events. *Tectonophysics*, *356*, 65–85.

Horálek, J., Fischer, T., Boušková, A., Michálek, J., & Hrubcová, P. (2009). The West Bohemian 2008-earthquake swarm: When, where, what size and data. *Studia Geophysica et Geodaetica*, *53*, 351–358. https://doi.org/10.1007/s11200-009-0024-8.

Horálek J., Fischer T., Einarsson P., & Jakobsdótir S. (2015). Earthquake swarms. *Encyclopedia of Earthquake Engineering*, pp. 1–16. https://doi.org/10.1007/978-3-642-36197-5_294-1

Ibs-von Seht M., Plenefisch, T., & Klinge, K. (2008). Earthquake swarms in continental rifts—A comparison of selected cases in America, Africa and Europe. *Tectonophysics*, *452*, 66–77. https://doi.org/10.1016/j.tecto.2008.02.008.

Jenatton L., Guiguet R., Thouvenot F., & Daix N. (2007) The 16,000-event 2003–2004 earthquake swarm in Ubaye (French Alps). *Journal of Geophysical Research*, *112/B11304*. https://doi.org/10.1029/2006JB004878

Kanamori, H. (1977). The energy release in great earthquakes. *Journal of Geophysical Research*, *82*, 2981–2987. https://doi.org/10.1029/JB082i020p02981.

Kárník, V., & Schenková, Z. (1988). Comparison of the 1985/1986 events in Western Bohemia with earlier Vogtland swarms. In D. Procházková (Ed.), *Induced seismicity and associated phenomena* (pp. 324–328). Praha: Geophys Inst Czechosl Acad Sci.

Leydecker G. (2011). Erdbebenkatalog für Deutschland mit Randgebieten für die Jahre 800 bis 2008. *Geologisches Jahrbuch*, pp. 1–198

Lomax, A., Virieux, J., Volant, P., & Berge, C. (2000). Probabilistic earthquake location in 3D and layered models: Introduction of a Metropolis-Gibbs method and comparison with linear locations. In C. H. Thurber & N. Rabinowitz (Eds.), *Advances in Seismic Event Location* (pp. 101–134). Amsterdam: Kluwer.

Lomax A., Michelini A., & Curtis A. (2009). Earthquake location, direct, global-search methods. In Meyers, R.A. (ed) Encycl Complex Syst Sci, Part 5 (pp. 2449–2473). New York: Springer. https://doi.org/10.1007/978-0-387-30440-3

Madariaga, R. (1976). Dynamics of an expanding circular fault. *Bulletin of the Seismological Society of America*, *66*(3), 639–666.

Málek, J., Horálek, J., & Janský, J. (2005). One-dimensional qP-Wave Velocity Model of the Upper Crust for the West Bohemia/Vogtland Earthquake Swarm Region. *Studia Geophysica et Geodaetica*, *49*(4), 501–524. https://doi.org/10.1007/s11200-005-0024-2.

Michálek, J., & Fischer, T. (2013). Source parameters of the swarm earthquakes in West Bohemia/Vogtland. *Geophysical Journal International*, *195*(2), 1196–1210. https://doi.org/10.1093/gji/ggt286.

Mogi, K. (1963). Some discussions on aftershocks, foreshocks and earthquake swarms: The fracture of a semi-infinite body caused by an inner stress origin and its relation to the earthquake phenomena (third paper). *Bulletin of the Earthquake Research Institute University of Tokyo*, *41*, 615–658.

Mrlina, J., Kämpf, H., Kroner, C., Mingram, J., Stebich, M., Brauer, A., et al. (2009). Discovery of the first Quaternary maar in the Bohemian Massif, Central Europe, based on combined geophysical and geological surveys. *Journal of Volcanology and Geothermal Research*, *182*(1–2), 97–112. https://doi.org/10.1016/j.jvolgeores.2009.01.027.

Neunhöfer, H., & Hemmann, A. (2005). Earthquake swarms in the Vogtland/Western Bohemia region: Spatial distribution and magnitude-frequency distribution as an indication of the genesis of swarms? *Journal of Geodynamics*, *39*(4), 361–385. https://doi.org/10.1016/j.jog.2005.01.004.

Neunhöfer, H., & Meier, T. (2004). Seismicity in the Vogtland/Western Bohemia earthquake region between 1962 and 1998. *Studia Geophysica et Geodaetica*, *48*, 539–562. https://doi.org/10.1023/B:SGEG.0000037471.18297.07.

Neunhöfer, H., & Stelzner, J. (1989). Historical results from near stations. In P. Bormann (Ed.), *Monitoring and analysis of the earthquake swarm 1985/86 in the region Vogtland/Western Bohemia* (pp. 39–42). Potsdam: Akad der Wissensch der DDR.

Ohmi, S., Watanabe, K., Shibutani, T., Hirano, N., & Nakao, S. (2002). The 2000 Western Tottori earthquake—Seismic activity revealed by the regional seismic networks. *Earth Planets Space*, *54*(8), 819–830. https://doi.org/10.1186/BF03352075.

Pedersen, R., Sigmundsson, F., & Einarsson, P. (2007). Controlling factors on earthquake swarms associated with magmatic intrusions; Constraints from Iceland. *Journal of Volcanology and Geothermal Research*, *162*, 73–80. https://doi.org/10.1016/j.jvolgeores.2006.12.010.

Utsu, T., Ogata, Y., & Matsu'ura, R. (1995). The centenary of the Omori formula for a decay law of aftershock activity. *Journal of Physics of the Earth*, *43*, 1–33. https://doi.org/10.4294/jpe1952.43.1.

Vavryčuk, V. (1993). Crustal anisotropy from local observations of shear-wave splitting in West Bohemia, Czech Republic. *Bulletin of the Seismological Society of America*, *83*(5), 1420–1441.

Vavryčuk, V. (2002). Non-double-couple earthquakes of 1997 January in West Bohemia, Czech Republic: Evidence of tensile faulting. *Geophysical Journal International*, *149*(2), 364–373. https://doi.org/10.1046/j.1365-246X.2002.01654.x.

Vavryčuk, V. (2011). Principal earthquakes: Theory and observations from the 2008 West Bohemia swarm. *Earth and Planetary Science Letters*, *305*(3–4), 290–296. https://doi.org/10.1016/j.epsl.2011.03.002.

Vavryčuk, V., & Kühn, D. (2012). Moment tensor inversion of waveforms: A two-step time-frequency approach. *Geophysical Journal International*, *190*, 1761–1776. https://doi.org/10.1111/j.1365-246X.2012.05592.x.

Wagner, G. A., Gögen, K., Jonckheere, R., Wagner, I., & Woda, C. (2002). Dating of Quaternary volcanoes Komorní Hůrka (Kammerbühl) and Železná Hůrka (Eisenbühl), Czech Republic, by TL, ESR, alpha-recoil and fission track chronometry. *Zeitschrift für Geologische Wissenschaften*, *30*, 191–200.

Waldhauser, F. (2001). A computer program to compute double-difference hypocenter locations. *US Geological Survey Open File Report*, *01–113*, 1–25.

Waldhauser, F., & Ellsworth, W. (2000). A double-difference earthquake location algorithm: Method and application to the northern Hayward fault, California. *Bulletin of the Seismological Society of America*, *90*(6), 1353–1368. https://doi.org/10.1785/0120000006.

(1991). *West Bohemia Local Seismic Network*. International Federation of Digital Seismograph Networks: Other/Seismic Network. https://doi.org/10.7914/SN/WB.

Wiemer, S., & Wyss, M. (2000). Minimum magnitude of completeness in earthquake catalogs: Examples from Alaska, the western United States, and Japan. *Bulletin of the Seismological Society of America*, *90*(4), 859–869. https://doi.org/10.1785/0119990114.

(Received February 15, 2017, revised July 28, 2017, accepted September 18, 2017)